

Copyright

By

James Michael Foreman Jr.

2010

The thesis committee for James Michael Foreman Jr.
certifies that this is the approved version of the following thesis:

Controlling Cracking in Prestressed Concrete Panels

**APPROVED BY
SUPERVISING COMMITTEE:**

Richard Klingner, Supervisor

Oguzhan Bayrak

Controlling Cracking in Prestressed Concrete Panels

by

James Michael Foreman Jr., B.S.C.E.

Thesis

Presented to the Faculty of the Graduate School of

The University of Texas at Austin

in Partial Fulfillment

of the Requirements

for the Degree of

Master of Science in Engineering

The University of Texas at Austin

May 2010

Dedication

To my parents, for so much support and encouragement.

Acknowledgements

Many people deserve credit for contributing to this thesis. First of all, I am grateful for the generous support of the Texas Department of Transportation.

Additionally, I was fortunate to have three great advisors on this project. Dr. Bayrak, your genuine interest in the success of this project kept me motivated. Dr. Jirsa, thank you for making sure we always remembered to keep it simple. Dr. Klingner, your professional approach to leading this research project and reviewing this thesis has been greatly appreciated.

I am also very grateful for my research partner Stephen “in it to win it” Foster. Your patience and attention to detail made up for many of my shortcomings. Thanks for all your help and hard work. Many other students also helped out with this project in various ways. Jeremiah Fasl, Dean Deschenes, Dave Dunkman, Alejandro Avendaño, and Jason Stith, in particular, were all more than generous with their time and advice.

Finally, I need to thank the FSEL lab techs. Nothing would get done without the help of Andrew Valentine, Blake Stasney, Dennis Phillip, Mike Watson, and Eric Schell.

April 26, 2010

Controlling Cracking in Prestressed Concrete Panels

James Michael Foreman Jr., M.S.E.

The University of Texas at Austin, 2010

SUPERVISOR: Richard Klingner

Precast, prestressed concrete panels (PCPs) are used in 85% of bridges in Texas. The goal of this thesis is to reduce collinear cracking (cracks propagating parallel to strands) in PCPs. One way to reduce collinear cracking would be to reduce the initial prestress force. In design, TxDOT conservatively assumes total prestress losses of 45 ksi. Based on eight panel specimens, instrumented and fabricated at two different precast plants in Texas, actual prestress losses were measured as at most 25 ksi. This difference (about 20 ksi) is consistent with a reduction in initial prestress force from 16.1 kips per strand to 14.4 kips per strand. Another way to reduce collinear cracking would be to provide additional transverse reinforcement in the end regions of the panels. By comparing crack spacings and crack widths in current and modified panel specimens, it was found that additional reinforcement consisting of one or two #3 bars placed transverse to strands at panel ends would effectively control collinear cracking in PCPs.

TABLE OF CONTENTS

CHAPTER 1 Introduction.....	1
1.1 Background.....	1
1.2 Scope.....	2
1.3 Objectives	3
CHAPTER 2 Literature Review	4
2.1 Development Of Prestressed Concrete Panels.....	4
2.1.1 Background.....	4
2.1.2 Design Guides.....	6
2.1.3 TxDOT Specifications for Precast Prestressed Panels.....	8
2.2 Prestress Losses	10
2.2.1 Introduction.....	10
2.2.2 AASHTO	12
2.3 Bond and Stress transfer, and Strand Slip.....	15
2.3.1 Development length.....	15
2.3.2 Bond Stress	17
2.3.3 Cracks	19
2.4 Thermal Expansion of Concrete	19
2.5 Summary	20
CHAPTER 3 Introduction to Testing Program.....	21
3.1 Field Fabrication	21
3.1.1 Objectives of field fabrication and panel monitoring	21
3.1.2 General sequence of field fabrication and panel monitoring	21
3.2 Laboratory Testing.....	22
3.2.1 Objectives of laboratory testing.....	22
3.2.2 General sequence of laboratory testing.....	22
CHAPTER 4 Fabrication and Panel Monitoring at Plant A	23

4.1	Field Fabrication	23
4.1.1	Panel Design	23
4.1.2	Instrumentation	26
4.1.3	Fabrication	32
4.2	Transportation and Storage	38
4.3	Panel Monitoring	40
CHAPTER 5 Laboratory Testing of Panels Fabricated at Plant A.....		41
5.1	Objectives of testing	41
5.2	Test setup	41
5.2.1	Knife edge.....	41
5.2.2	Loading	42
5.2.3	Test specimens	42
5.2.4	Instrumentation and data acquisition	43
5.3	Testing of specimen C1	49
5.4	Testing of specimen M1.....	52
5.5	Testing of specimen C3	54
CHAPTER 6 Fabrication and Panel Monitoring at Plant B		57
6.1	Field Fabrication	57
6.1.1	Panel Design	57
6.1.2	Instrumentation	59
6.1.3	Fabrication	63
6.2	Transportation and Storage	69
6.3	Panel Monitoring	71
CHAPTER 7 Test Results.....		72
7.1	Prestress Losses	72
7.1.1	Short-Term Prestress Losses (Elastic Shortening).....	72
7.1.2	Long-Term Prestress Losses (Creep, Shrinkage, and Relaxation) ...	77
7.1.3	Estimated Losses.....	77

7.1.4	Observed Losses	78
7.2	Transverse Tensile Stresses During Release.....	87
7.3	Effectiveness of Bursting Reinforcement	89
7.4	Effects of Cracking on Prestress Losses	92
CHAPTER 8 Summary, Conclusions, and Recommendations		95
8.1	Summary of Thesis	95
8.2	Conclusions.....	96
8.3	Recommendations for Design.....	97
8.4	Recommendations for Implementation.....	97
8.5	Recommendations for Future Investigation.....	98
APPENDIX.....		99
A.1	TxDOT Plants	99
A.2	Concrete Mixture Designs	104
A.2.1	Plant A Concrete Mixture	104
A.2.2	Plant B Concrete Mixture	107
A.3	Gage Information	109
A.3.1	PMFL-60-8LT.....	109
A.3.2	VWG (Geocon’s Model 4200).....	111
A.4	Prestress Loss Predictions (AASHTO).....	117
A.4.1	2004 AASHTO	104
A.4.2	2008 AASHTO	104
A.5	Example Calculations	120
A.5.1	Percentage prestress force remaining based on measured slip	120
REFERENCES		122
VITA.....		127

LIST OF TABLES

Table 7.1 Calculated versus measured values of elastic shortening (ksi)..... 77
Table 7.2 Summary of long-term prestress losses and predictions..... 86
Table 7.3 Summary of maximum tensile stresses at panel edges during release 87

LIST OF FIGURES

Figure 2.1 TxDOT section view of typical panel	8
Figure 2.2 TxDOT plan view of typical precast, prestressed panel.....	9
Figure 2.3 Stress in strand versus time for a post-tensioned concrete girder (Tadros et al., 2003)	11
Figure 2.4 Shrinkage versus time (ACI, 1971).....	12
Figure 2.5: Prestress loss provisions of AASHTO 8 th Ed. (AASHTO, 1975).....	14
Figure 2.6: Stress transfer from strand to concrete (Cousins et al., 1990).....	16
Figure 2.7: Variation of steel stress with distance from free end of strand (Zia et al., 1977)	17
Figure 2.8 Cross-section of a strand cast in concrete (Stocker et al., 1970).....	18
Figure 2.9 Schematic representation of how the radial components of the bond forces are balanced against tensile stress rings in the concrete (Tepfers, 1973)	19
Figure 4.1 Transverse reinforcement in place at Plant A.....	24
Figure 4.2 Section view of reinforcement layout in panels M1 and M2 (modifications shown in orange).....	25
Figure 4.3 Plan view of reinforcement layout in panels M1 and M2 (modifications shown in orange).....	25
Figure 4.4 Campbell Scientific CR5000 measurement and control system	26
Figure 4.5 Gage layout and numbering scheme for Panels C1 and C2	28
Figure 4.6 Gage layout for Panels M1 and M2.....	29
Figure 4.7 Concrete embedment gage (Tokyo Sokki Kenkyujo Co.).....	30
Figure 4.8 Concrete embedment gage installed parallel to a prestressing strand	31
Figure 4.9 Set of gages completely installed on additional bars.....	32
Figure 4.10 Installing gages at Plant A.....	33
Figure 4.11 Sidewinder pouring concrete into forms and over gages at Plant A	34
Figure 4.12 Plant A's crew running a vibrating screed over the wet concrete	35

Figure 4.13 Strands being torch-released at Plant A.....	36
Figure 4.14 Panels lifted out of prestressing bed and stacked at Plant A	37
Figure 4.15 Stack of panels placed in storage area at Plant A.....	37
Figure 4.16 Panels strapped to flatbed truck.....	38
Figure 4.17 Truck driver tightening straps	39
Figure 4.18 Side view showing relative alignment of straps and dunnage.....	40
Figure 5.1 Knife edge setup to induce flexural cracks.....	42
Figure 5.2 Typical slip gage installed on a strand	44
Figure 5.3 Linear potentiometer used with metal wire to measure average strain over center strand	45
Figure 5.4 Concrete surface strain gages as applied to Specimen C1	46
Figure 5.5 Crack microscope	47
Figure 5.6 Upper components of data-acquisition system.....	48
Figure 5.7 Lower components of data-acquisition system	48
Figure 5.8 Three of the “pods” used with the data-acquisition system	49
Figure 5.9 Gage layout for top of Specimen C1	50
Figure 5.10 Gage layout for bottom of Specimen C1	51
Figure 5.11 Final distribution of cracking in central zone of Specimen C1	52
Figure 5.12 Gage layout for Specimen M1.....	53
Figure 5.13 Specimen M1 after testing (the near edge is the double-bar edge)	54
Figure 5.14 Gage locations for Specimen C3	55
Figure 5.15 Photograph of Specimen C3.....	56
Figure 5.16 Gage 26 shown with the plunger stuck in the major crack of Specimen C3.	56
Figure 6.1 Transverse reinforcement in place at Plant B.....	58
Figure 6.2 Section view of reinforcement layout in panels M3, M4, and M5 (modifications shown in orange).....	58
Figure 6.3 Plan view of reinforcement layout in panels M3, M4, and M5 (modifications shown in orange).....	59

Figure 6.4 Gage layout and numbering scheme for Panels M3, M4, C4, and C5	61
Figure 6.5 Concrete embedment gage installed parallel to a prestressing strand	62
Figure 6.6 VWG installed next to an embedment gage	63
Figure 6.7 Installing gages at Plant B	64
Figure 6.8 Vibrating screed used at Plant B	65
Figure 6.9 Sidewinder pouring concrete into forms and over gages	66
Figure 6.10 Vibrating screed being maneuvered over a panel at Plant B.....	67
Figure 6.11 Strands being torch released at Plant B	68
Figure 6.12 Stacked panels being placed in the storage area at Plant B.....	69
Figure 6.13 Plant B panels arrive at Ferguson Lab.....	70
Figure 6.14 Panels from Plant B stacked outside of Ferguson Lab	71
Figure 7.1 Stress in prestressing strands at the center of Specimen C2 during release	73
Figure 7.2 Stress in prestressing strands at the center of Specimen M1 during release ...	73
Figure 7.3 Stress in prestressing strands at the center of Specimen M2 during release ...	74
Figure 7.4 Stress in prestressing strands at the center of Specimen C4 during release	75
Figure 7.5 Stress in prestressing strands at the center of Specimen C5 during release	75
Figure 7.6 Stress in prestressing strands at the center of Specimen M3 during release ...	76
Figure 7.7 Stress in prestressing strands at the center of Specimen M4 during release ...	76
Figure 7.8 Stress in the strand at the center of Specimen C1	79
Figure 7.9 Stress in the strand at the center of Specimen C2	80
Figure 7.10 Stress in the strand at the center of Specimen M1.....	80
Figure 7.11 Stress in the strand at the center of Specimen M2.....	81
Figure 7.12 Long-term stresses in the center strand of Plant A panels as well as lump-sum code values.....	82
Figure 7.13 Stress in the strand at the center of Specimen C4	83
Figure 7.14 Stress in the strand at the center of Specimen C5	83
Figure 7.15 Stress in the strand at the center of Specimen M3.....	84
Figure 7.16 Stress in the strand at the center of Specimen M4.....	84

Figure 7.17 Stress in the strand at the center of limestone and river-gravel panels (limestone is dashed and river-gravel is solid)	85
Figure 7.18 Testing methods used to determine tensile strength of concrete (Tuchscherer, 2009)	88
Figure 7.19 Relationship between modulus of rupture and compressive strength of concrete (Tuchscherer, 2009).....	89
Figure 7.20 Edge of Specimen C3 after testing	90
Figure 7.21 Single-bar edge of Specimen M2 after testing	91
Figure 7.22 Double-bar edge of Specimen M2 after testing.....	92
Figure 7.23 Percentage of prestress force remaining in a strand vs. width of collinear crack (typical crack widths)	93
Figure 7.24 Percentage of prestress force remaining in a strand vs. the width of a collinear crack (wide cracks)	94

CHAPTER 1

Introduction

1.1 BACKGROUND

Precast, prestressed concrete panels (PCPs) are used in approximately 85% of all bridges in Texas (Merrill, 2002). Bridge decks containing PCPs can be built very efficiently, because the panels act as stay-in-place formwork and serve as the bottom portion of the final bridge deck. The panels are typically 4 in. thick and act compositely with a 4-in. overlay of cast-in-place (CIP) concrete.

Of the 4 million square feet of PCPs produced in Texas annually, a small percentage is rejected by TxDOT inspectors due to cracking parallel to the prestressing strands. The exact number is not tracked by TxDOT or fabricators. One fabricator has estimated a 7% rejection rate, while another reported having only 5 panels rejected in one year. TxDOT's bridge construction specifications indicate that any panel with a crack parallel to a strand, within 1 in. of a strand, and running more than a third of the length of panel may be rejected. Significant rejection rates result in an increased price of production.

To address this and other bridge deck-related issues, TxDOT sponsored Research Project 0-6348 ("Controlling Cracking in Prestressed Concrete Panels and Optimizing Bridge Deck Reinforcing Steel"). Cracked panels are rejected because of concerns about prestress loss. A loss in prestress force reduces the stiffness of a panel and affects performance in service. Cracking is caused by the initial prestress force and the way that force is transferred to the concrete by the strand. If the initial prestress force could be reduced, cracking should also be reduced. The amount of initial prestress force required is determined by the final prestress force desired plus the expected prestress loss. Expected prestress loss is calculated based on certain assumptions. The American

Association of State Highway and Transportation Officials (AASHTO) publishes the governing code for calculating expected prestress loss in concrete bridge members. The prestress loss calculation methods prescribed by AASHTO have been developed based on experimental data on prestressed beams. It is not clear whether or not these methods are appropriate for PCPs. However, following a conservative AASHTO provision, TxDOT's design calculations assume a lump-sum value of 45 ksi for all prestress losses in PCPs. If the actual prestress loss in a panel is significantly lower than 45 ksi, it would be possible to reduce the initial prestress force. A smaller initial prestress force should result in fewer cracks. Therefore, a major goal of this thesis is to determine the true prestress loss in PCPs.

Typically, steel reinforcing bars are used to control cracking in structural concrete elements. While TxDOT's specifications require a minimum amount of transverse reinforcement in panels to control shrinkage cracking, additional reinforcement near the edges of the panel may help control longitudinal crack propagation. The edge of the panel is the critical region for longitudinal crack formation. A secondary goal of this thesis is to determine the feasibility of controlling cracking with additional transverse reinforcement in panel edges.

1.2 SCOPE

This thesis addresses only the aspects of Project 0-6348 related to controlling cracking in PCPs. A thorough literature review is conducted. Actual prestress losses in PCPs are measured experimentally. Panels from two different precasters are fabricated and instrumented with embedded concrete strain gages. The strains in the PCPs are measured over time and prestress losses are calculated. Some panels from the two precasters are fabricated with additional transverse reinforcement at panel edges. Laboratory tests are conducted to investigate the relationship between cracking and slip of prestressing strands. Those tests also allow researchers to evaluate the effectiveness of additional edge reinforcement on crack control. Repair of cracks is not investigated.

The researchers express no opinion on whether cracked panels should be accepted by TxDOT inspectors.

1.3 OBJECTIVES

The objectives of this thesis are:

- 1) Determine possible causes of the cracking that is observed on the top surface of panels collinear to strands;
- 2) Assess the significance of that cracking;
- 3) Evaluate the feasibility of additional transverse reinforcement near panel edges to control crack propagation;
- 4) Determine the actual prestress loss in PCPs;
- 5) Recommend a new initial prestress force requirement; and
- 6) Recommend design alternatives as necessary.

CHAPTER 2

Literature Review

2.1 DEVELOPMENT OF PRESTRESSED CONCRETE PANELS

2.1.1 Background

PCPs were first used in bridge deck construction by the Illinois Toll Highway Authority in the early 1950s (Barker, 1975). Although the first PCP bridges built in Texas were opened to traffic in 1963, interest in PCPs increased rapidly in the early 70s. Many research projects were conducted by the Texas Highway Department, the Pennsylvania Department of Transportation, and the Florida Department of Transportation (Barker, 1975). Research was focused on developing connection details and determining how compositely the PCPs interacted with the CIP portion of the deck.

Design recommendations for PCP bridges were first included in the 1979 AASHTO *Standard Specification for Highway Bridges* (Deshmukh, 2004). In 1983, TxDOT specifications were revised to encourage the use of PCPs, and precast manufacturers began producing large quantities of panels. Nationally, interest in PCP bridges continued to grow; in 1988, PCI published a special report on them (Ross Bryan Associates, Inc., 1988). That report cites a 1986 survey in which twenty-one state highway departments reported specifying the use of PCPs. In 2002, approximately 85% of bridges in Texas used PCPs (Merrill, 2002). Although PCP deck systems have generally performed well in Texas, they sometimes show reflective cracking in the CIP portion of the deck.

Many PCP bridges were constructed in Florida in the 70s and 80s (Deshmukh, 2004). While investigating cracks in the decks of such bridges, researchers at the University of South Florida conducted a survey of state DOTs to determine their level of success with PCP deck construction. They used the National Bridge Inventory database

to determine which states were using PCP bridges and included only those DOT's in their survey. Their results of their investigation identified 11 states with PCP bridges at that time:

- 1) Alabama – 2 PCP bridges performing well
- 2) Arkansas – 2 PCP bridges
- 3) Florida – Many PCP bridges with various results. Some have been replaced due to serious cracking or failure of bridge deck.
- 4) Georgia – Many PCP bridges performing satisfactorily
- 5) Indiana – Many PCP bridges performing well. PCP decks are still an option for contractors, but they are not chosen very often.
- 6) Iowa – Several PCP bridges. DOT specifies 3/8th in. strands spaced at 6 in. and stressed to 16.1 kips per strand for panels 5 in. thick.
- 7) Kansas – Many PCP bridges performing satisfactorily. DOT specifies 3.15 in. panels and 7/16th in. strands stressed to 17.2 kips.
- 8) Louisiana – 12 PCP bridges
- 9) New Mexico – Several PCP bridges in early state of use, but so far performing well.
- 10) Oklahoma – Many PCP bridges.
- 11) Texas – Many PCP bridges. DOT specifies 3/8th in. strand spaced 6 in. and stressed to 16.1 kips per strand for panels 4-in. thick.

Deshmukh summarized that although most DOTs reported satisfactory results, only Texas encouraged their use (Deshmukh, 2004).

In 2008, another survey was conducted as part of TxDOT Research Project 0-4418. The researchers surveyed 121 state DOTs and tollway authorities about their usage of PCPs, specifically trapezoidal and skewed PCPs. Of the 69 agencies that responded to the survey, 29 said that they used PCPs in bridge construction (Kreisa, 2008). Surveys were also sent out to 192 different precasters. Of the 72 precast plants who responded to the survey, 27 said they had fabricated PCPs for bridge construction.

2.1.2 Design Guides

2.1.2.1 Significance of cracking

A 1988 PCI special report summarizes PCP use at the time and recommends certain practices for design and construction (Ross Bryan Associates, Inc., 1988). The bulk of that report discusses production and construction details. Chapter 4 of that report, however, provides recommendations for cracking tolerances and repair. The writers of that report claim that “the most objectionable cracks are those that would increase the strand development length with a resulting decrease in panel capacity.” They list three specific crack types which would cause such an increase in development length:

- 1) Two cracks, each occurring within 1 in. of two adjacent strands.
- 2) Corner cracks or breaks involving two or more strands.
- 3) Cracks parallel to and along more than 25% of the strands.

The writers conclude that such cracks may cause a panel to be rejected but that decisions should be decided case by case by a qualified inspector.

A 2006 PCI publication further explains that cracks which go from the surface of the panel to the strand will cause debonding of the strand and concrete (PCI, 2006). Such cracks propagate along the strand over time. The writers suggest that panels be rejected if two adjacent strands have cracks or if more than 12% of all the strands in the panel have cracks. Because TxDOT panels typically have 16 strands, a 12% limit would mean that at most two strands could show cracks anywhere on a panel.

2.1.2.2 Cause of cracking

A recent bulletin published by the FIB suggests several sources of longitudinal cracking (FIB, 2007). A similar PCI document agrees with FIB on the main three causes (PCI, 2006):

- 1) Excessive prestress force;
- 2) Inadequate transverse reinforcement; and
- 3) Improper release of prestressing strand.

The issues of excessive prestress force and inadequate transverse reinforcement are each investigated in this thesis. Precasters in Texas avoid damaging the panels during release by slowly torch cutting the strands near the bulkhead.

Additional sources of cracking identified by the FIB and PCI individually are:

- 1) Uneven or sudden lifting;
- 2) Strands too near casting pallet;
- 3) Casting concrete in hot forms;
- 4) Low release strength of concrete; and
- 5) Rapid development in epoxy strand with grit.

This secondary list of problems is mostly outside the scope of this thesis. Items related to concrete strength or handling are generally well understood by the precasting industry.

2.1.2.3 Prevention of panel cracking

To prevent cracking caused by excessive prestress force, the designer can either reduce the prestress force or specify smaller prestressing strands (FIB, 2007). PCI recommends that the average prestress acting over the end face of a panel be no more than 750 psi (PCI, 2006). For typical TxDOT panels using 3/8-in. strands, this would correspond to a limit of 18.0 kips per strand. TxDOT currently specifies an initial prestress force of 16.1 kips per strand. Although that value is less than PCI's recommended maximum, reducing it to a still lower value would further reduce panel cracking.

Because panel cracking may also be caused by inadequate transverse reinforcement, adding such reinforcement may help control cracking (FIB, 2007). PCI recommends providing transverse reinforcement both above and below the strand at panel ends (PCI, 2006). Such additional reinforcement is most effective at panel ends because that is the critical region for crack formation. In this study, panels will be manufactured with additional reinforcement and tested.

2.1.3 TxDOT Specifications for Precast Prestressed Panels

Over 40 years of research and construction, TxDOT has developed a reliable system for constructing bridges with PCP decks. The complete set of plans for PCP bridge deck construction is given on TxDOT's website (www.txdot.gov) and is also included in the Appendix (TxDOT, 2004). Basic section and plan views are included in this chapter as Figure 2.1 and Figure 2.2, respectively. The specified release strength for panel concrete is 4000 psi, and the minimum 28-day strength is 5000 psi.

2.1.3.1 Sectional view of typical TxDOT panels

Panels are typically 4-in. thick and strands are always placed at mid-depth. Several options are available for longitudinal reinforcement. The most common option is #3 reinforcing bars spaced at 6 inches or the equivalent area of steel in a welded wire mesh. In the diagram below, the transverse reinforcement is shown above the prestressing strands; TxDOT also allows it to be hung below the strands. Two different high-strength strand options are also available.

TYPICAL PANEL PLAN

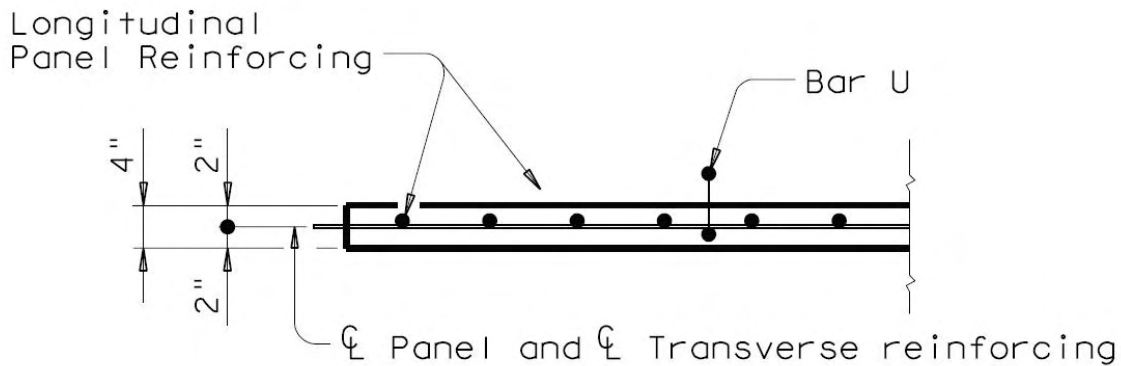


Figure 2.1 TxDOT section view of typical panel

2.1.3.2 Plan view of typical TxDOT panels

Panels are typically 8-ft long, and are allowed a maximum width of 9 ft – 6 in. For panels over 5-ft wide, prestressing strands are permitted to be 3/8 in. or 1/2 in. in diameter. They must be 270-ksi steel, and they must be stressed to an initial tension of at least 16.1 kips per strand.

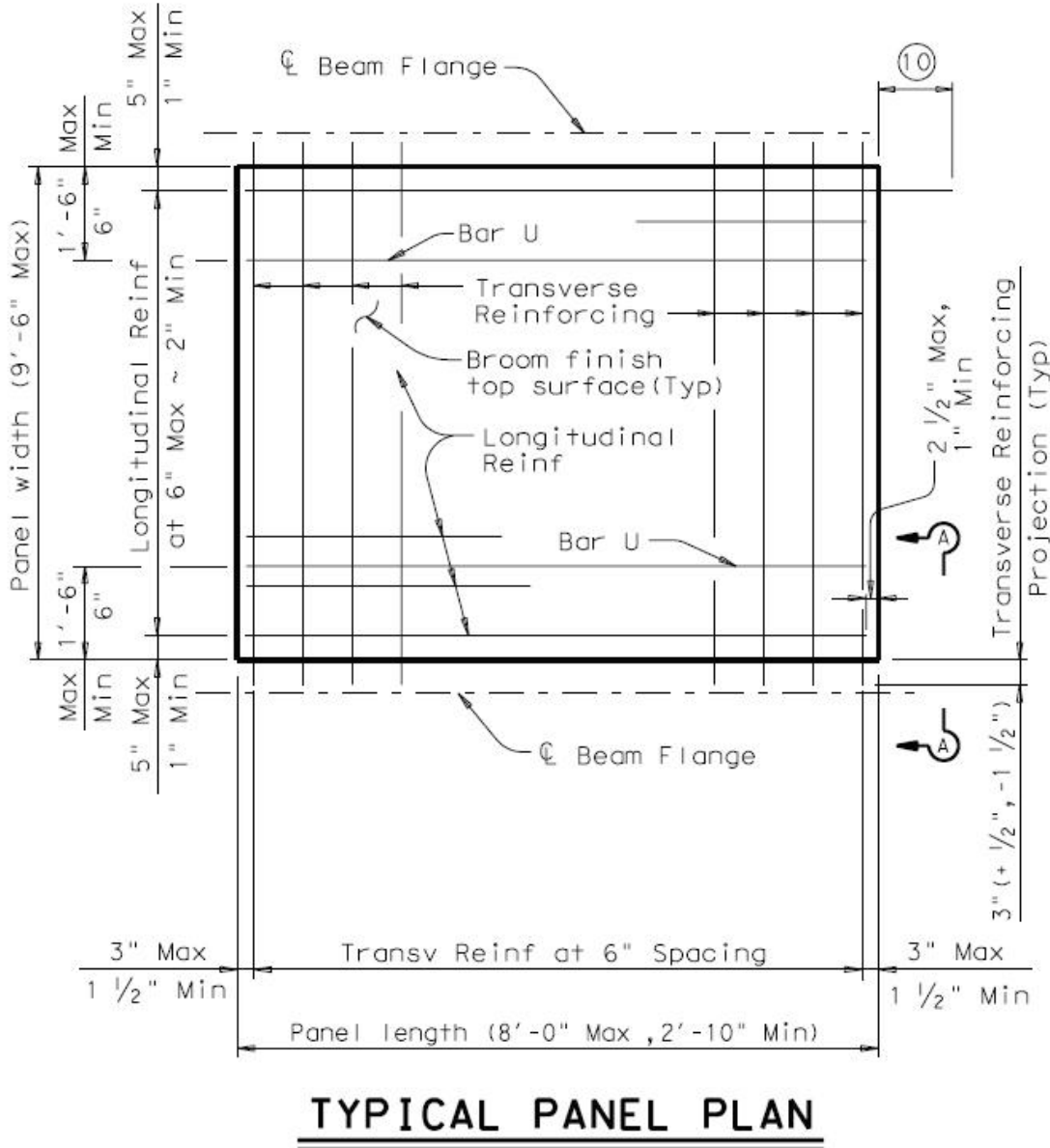


Figure 2.2 TxDOT plan view of typical precast, prestressed panel

2.1.3.3 Criteria for panel rejection

TxDOT standard specifications (TxDOT, 2004) prescribe two conditions warranting panel rejection:

- 1) Any crack extending to the reinforcing plane and running parallel and within 1 in. of a strand for at least 1/3 of the embedded strand length; or
- 2) Any transverse or diagonal crack, including corner cracks and breaks, intersecting at least 2 adjacent strands and extending to the reinforcing plane.

These criteria are clearly taken from the 1988 PCI special report (Ross Bryan Associates, Inc., 1988).

2.2 PRESTRESS LOSSES

2.2.1 Introduction

“The most representative definition of prestress loss is the loss of compressive force acting on the concrete component of a prestressed concrete section” (Tadros *et al.*, 2003). For purposes of design and of this research project, however, it is easier to think about the associated loss of tension in the prestressing strand. Figure 2.3 shows the many components of prestress loss experienced by post-tensioned girders. Since panels are pretensioned, anchorage seating losses do not apply. Only two of the components shown in that figure do apply to panel production: Section CD (elastic shortening); and Section DG (creep, shrinkage, and relaxation).

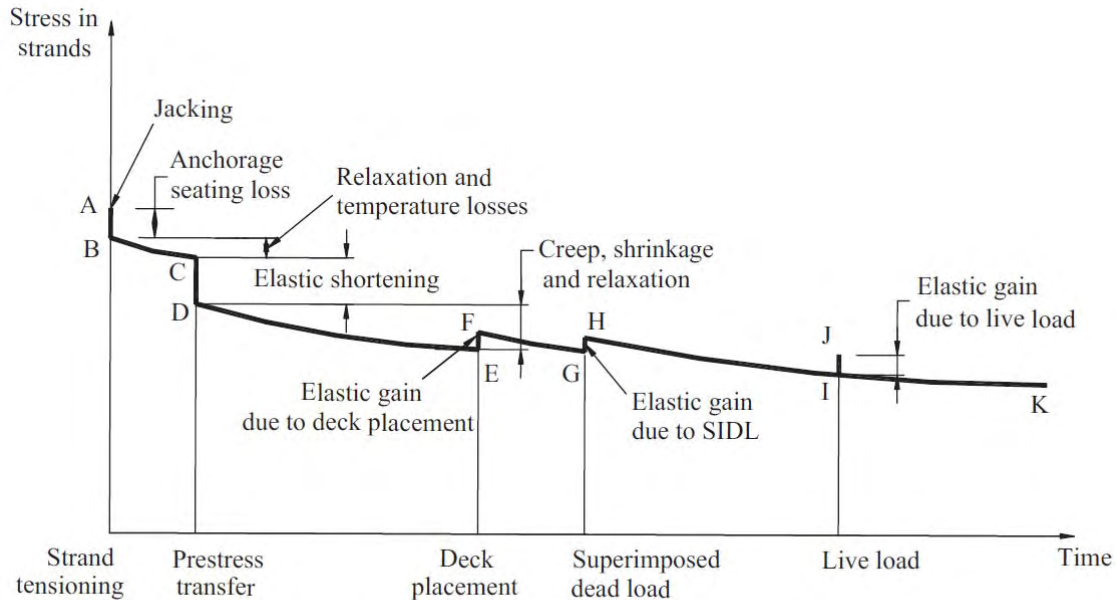


Figure 2.3 Stress in strand versus time for a post-tensioned concrete girder (Tadros *et al.*, 2003)

Elastic shortening is the immediate, short-term loss of tension in the strand after release, due to the elastic shortening of the concrete when the initial prestress force is transferred to it.

Creep, shrinkage, and relaxation are long-term losses. Creep affects materials held at a constant stress over long periods of time. When loaded in compression by the prestressing strand, the concrete panel will shorten over time. Creep is highly dependent on material properties, such as the volume content of hydrated cement paste; the relative humidity; the type and volume of aggregate; and the geometry of the member (Tadros *et al.*, 2003).

Shrinkage is the loss in volume of a concrete member over time, independent of loading. Within the concrete, it is the cement paste that actually shrinks. Shrinkage is largely dependent on aggregate type, because stiff aggregates restrain the cement from shrinking. Texas precasters typically use either crushed limestone or river-gravel for aggregate. River-gravel is stiffer than crushed limestone. Figure 2.4 shows the results of data comparing different aggregate types. The tests show 40% less shrinkage in beams

made with river-gravel than beams made with limestone aggregate. It is also shown that shrinkage stabilizes after about a year.

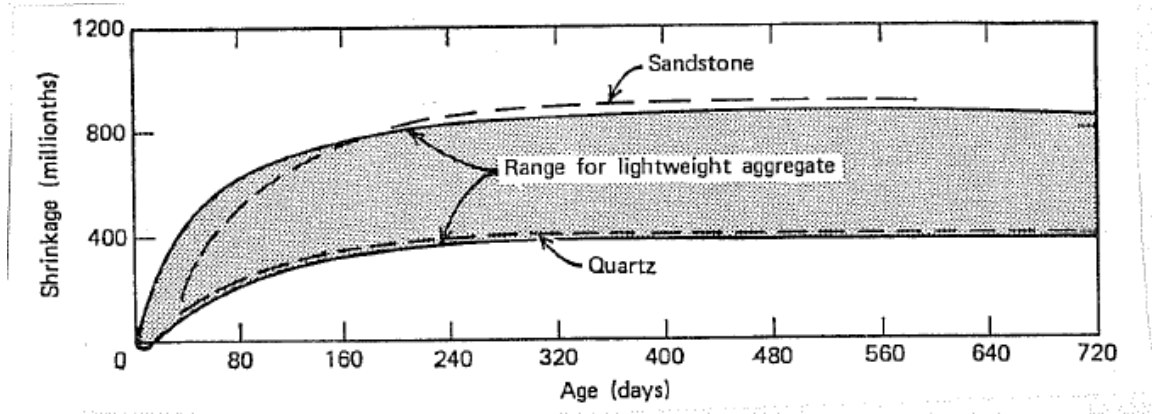


Figure 2.4 Shrinkage versus time (ACI, 1971)

When steel is held at a constant strain, the stress in the steel slowly decreases with time. This material behavior is known as relaxation. In precast concrete panels, the relaxation of the steel accounts for a small portion of the total loss in strand stress. This is especially true for the “low-relaxation” strands, which are currently the standard in precast products. Additionally, relaxation can be predicted with very good accuracy (Tadros *et al.*, 2003). The following equation is given in the AASTHO 4th Edition LRFD. The equation was taken from Tadros *et al.* (2003).

$$\Delta f_{pR1} = \left[\frac{f_{pt}}{K'_L} \frac{\log(24t)}{\log(24t_i)} \left(\frac{f_{pt}}{f_{py}} - 0.55 \right) \right] \left[1 - \frac{3(\Delta f_{pSR} + \Delta f_{pCR})}{f_{pt}} \right] K_{ia} \quad \text{C5.9.5.4.2c-1}$$

2.2.2 AASHTO

According to section 426.4 of the TxDOT *Specifications*, design of bridges in Texas is governed by the AASHTO Bridge Design Specifications (TxDOT, 2004). The first guidelines for computation of prestress losses appeared in the 8th edition of the AASHTO (then AASHO) specifications, published in 1961. At that time, the only

recommendation given was to use 35 ksi as a lump-sum estimate of total prestress losses (AASHTO, 1961). The 11th edition of AASHTO, published in 1973, was the first edition to estimate prestress loss as the summation of the main components: elastic shortening, creep, shrinkage, and relaxation. The suggested values for each component are tabulated average values, as shown in Figure 2.5.

(B) Prestress Losses

Loss of prestress due to all causes, excluding friction, may be estimated from the following method. The method is based upon the use of 270 ksi, seven-wire, stress-relieved strand and normal-weight concrete. For data regarding the properties and effects of lightweight aggregates and low-relaxation tendons, refer to documented tests or see authorized suppliers.*

(1) Pretensioned

$$\Delta f_p = SH + ES + CR_c + CR_s$$

where: Δf_p = total prestress loss, excluding friction.

(a) Shrinkage

SH = concrete shrinkage loss computed using the following average values. Select the average ambient relative humidity for the geographic area.

Average Ambient Relative Humidity (percent)	SH (psi)
100-75	5,000
75-25	10,000
25- 0	15,000

(b) Elastic Shortening

ES = $7 f_{cr}$ = elastic shortening loss, where f_{cr} = average concrete stress at the center of gravity of the prestressing steel at time of release. ES may be estimated using the following average values:

Sections with Composite Deck Slab		Sections without Composite Deck Slab	
f_{cr} (psi)	ES (psi)	f_{cr} (psi)	ES (psi)
1,000	7,000	600	4,000
1,400	10,000	800	5,500
1,800	13,000	1,000	7,000

(c) Creep of Concrete

$CR_c = 16 f_{cd}$ = loss due to creep of concrete, where f_{cd} = average concrete compressive stress at the center of gravity of the prestressing steel under full dead load. CR_c may be estimated using the following average values. These values apply to sections that are both with and without composite deck slabs.

f_{cd} (psi)	CR_c (psi)
500	8,000
800	13,000
1,200	19,000

(d) Relaxation of Prestressing Steel

$CR_s = 20,000 - 0.125 (SH + ES + CR_c)$ = loss due to relaxation of prestressing steel.

Figure 2.5: Prestress loss provisions of AASHTO 8th Ed. (AASHTO, 1975)

A major change to AASHTO's prestress-loss provisions came in the 12th edition (1977), which was the first to use equations to estimate each component of loss. Those equations are given below, with their original AASHTO equation numbers repeated. The

lump-sum option also remained, but the value was increased to 45 ksi. This development is particularly significant to TxDOT Research Project 0-6348, because 45 ksi is the value currently used for TxDOT panel design.

$$\Delta f_s = SH + ES + CR_c + CR_s \quad (9-3)$$

$$SH = 17,000 - 150RH \quad (9-4)$$

$$ES = \frac{E_s}{E_{ci}} f_{cir} \quad (9-6)$$

$$CR_c = 12f_{cir} - 7f_{cds} \quad (9-9)$$

$$CR_s = 5,000 - 0.1ES - 0.05(SH + CR_c) \quad (9-10A)$$

In the 1985 supplement to the 12th edition, an equation to predict the relaxation of low-relaxation strands was added. The methods and equations suggested in the 13th edition, published in 1975, remained in following editions, up through the 3rd edition of AASHTO LRFD (2004).

AASHTO's prestress loss provisions were significantly changed again in 2008 when the 4th LRFD edition was published. The new provisions incorporated equations recommended by Tadros *et al.* in NCHRP Report 490, and developed based on data from bridges in Connecticut, Illinois, Nebraska, New Hampshire, Ohio, Pennsylvania, Texas, and Washington.

2.3 BOND AND STRESS TRANSFER, AND STRAND SLIP

2.3.1 Development length

“In a pretensioned member, the prestressing force imparted by the strand is transferred to the concrete by bond in the end region of the member. The distance over which the effective prestress is developed in the strand is called the transfer length” (Zia *et al.*, 1977). The bond in the transfer length is commonly referred to as the “prestress

transfer bond” (Janney, 1954). When loaded, the strands in a prestressed member may develop additional bond stress due to flexure. This additional bond is referred to as “flexural bond” so as to differentiate it from prestress transfer bond. The sum of the transfer length and the flexural bond length is known as the development length of a strand. The development length is the distance on each end of a prestressing strand required to develop nominal strength of the strand. The development length of a 3/8-in. strand in a PCP was experimentally determined to be 22 in. (Jones *et al.*, 1970). The transfer length for a 3/8-in. strand in a PCP has been reported from 20 to 26 in. (PCI Bridge Committee, 1978).

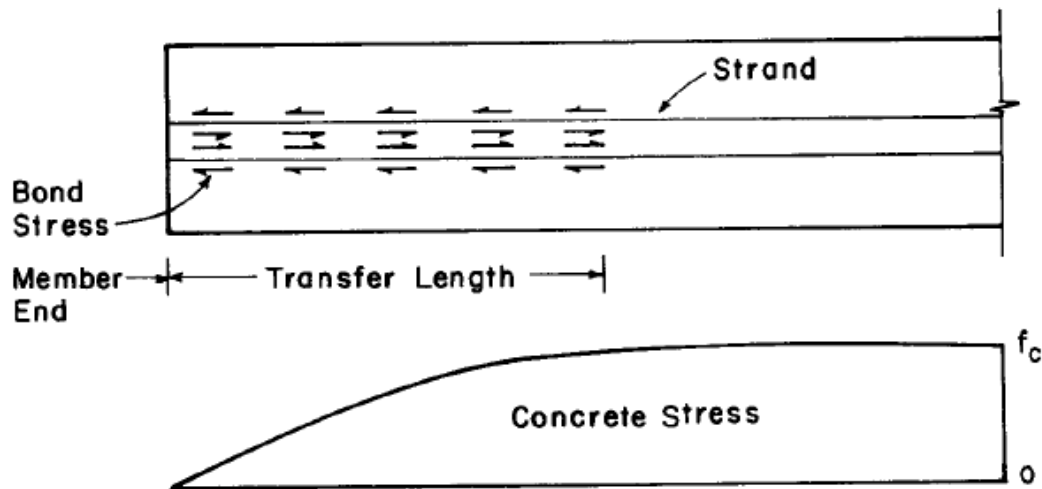


Figure 2.6: Stress transfer from strand to concrete (Cousins *et al.*, 1990)

ACI 318-08 presents the following equation to approximate development length.

$$l_d = \left(\frac{f_{se}}{3000} \right) d_b + \left(\frac{f_{ps} - f_{se}}{1000} \right) d_b \quad \text{ACI 318-08 Eq. (12-4)}$$

The first term in the equation represents the transfer length and the second term represents the flexural bond length. For a 3/8-in. strand initially stressed to 189.4 ksi and

assuming 20% prestress losses, the ACI equation predicts a transfer length of 19 in. and a flexural bond length of 44.4 in.

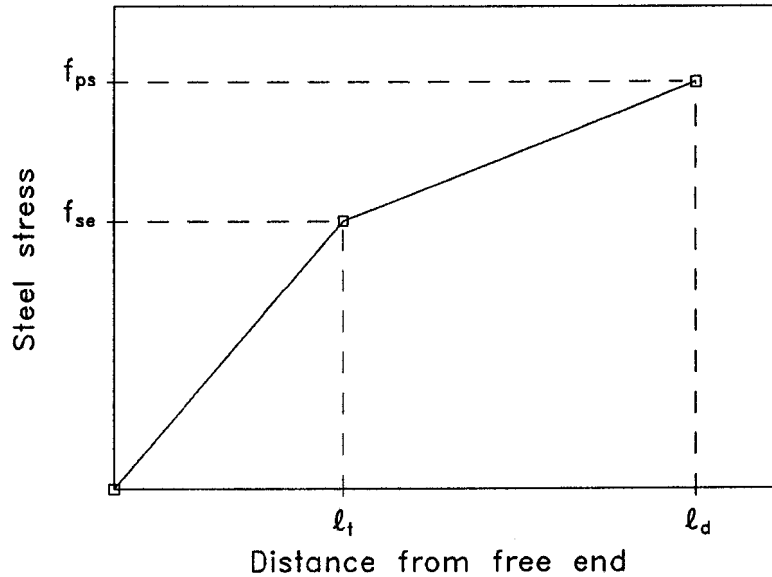


Figure 2.7: Variation of steel stress with distance from free end of strand (Zia et al., 1977)

2.3.2 Bond Stress

The main components of bond strength within the transfer length are:

- 1) Friction between the steel and the concrete;
- 2) Chemical adhesion between the two materials; and
- 3) Mechanical interlock allowed by the helical twist of the strands.

The amount of friction between the steel and the concrete depends on two factors. The first is the relative roughness of the two surfaces, generally defined by a coefficient of friction. The coefficient of friction varies with the surface characteristics of the strand and the character of the cement paste (Janney, 1954). For example, lightly rusted strands have been shown to have a higher coefficient of friction than clean strands, thereby requiring a shorter transfer length. Friction also depends on the radial pressure developed

within the concrete member. When strands are first released, they come to equilibrium with the concrete through elastic shortening. As the strands shorten, they also expand radially (Hoyer, 1939). The expansion of the strand is resisted by circumferential tension in the concrete. As long as the concrete's tensile strength is not exceeded, the concrete's confinement of the strand creates friction at the strand's surface.

Chemical adhesion between the two materials is created by the cement in the concrete. This adhesion can only be maintained, however, if there is no slip of the strand relative to the concrete. Because some slip may occur when strands are released, chemical adhesion is not relied upon in the transfer length.

In a 7-wire strand, the interior wire is slightly larger in diameter than the exterior wires. The geometry allows the void space to be filled with concrete, as shown in Figure 2.8. That, combined with the fact that prestress strands are twisted, creates a mechanical interlock between the steel and the concrete. The interlock makes the strand perform like a deformed reinforcing bar. Because longitudinal slip of the strand is resisted by the concrete paste that has penetrated into the interstices of the strand, the strand must untwist as it slips.

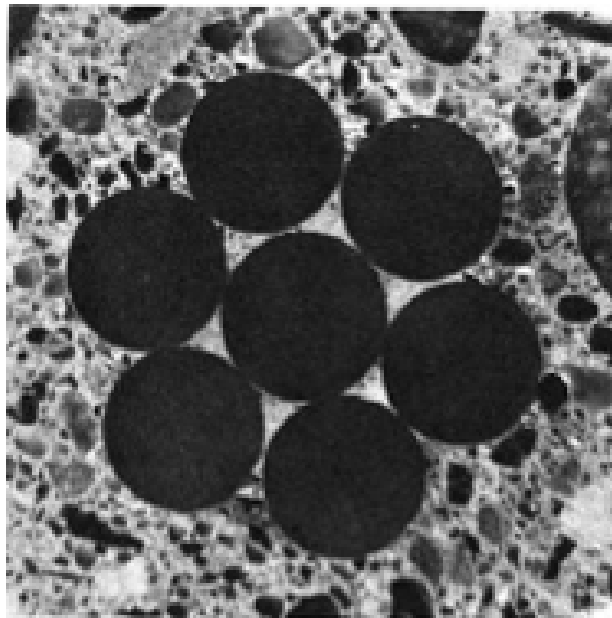


Figure 2.8 Cross-section of a strand cast in concrete (Stocker et al., 1970)

2.3.3 Cracks

As discussed in the previous section, the resultant force transmitted into concrete by the prestressing strand has a longitudinal component in the direction of the strand and a radial component, as shown in Figure 2.9. The radial component is equilibrated by circumferential tension in the concrete. If the circumferential tensile stress exceeds the tensile strength of the concrete, a crack will form in the concrete.

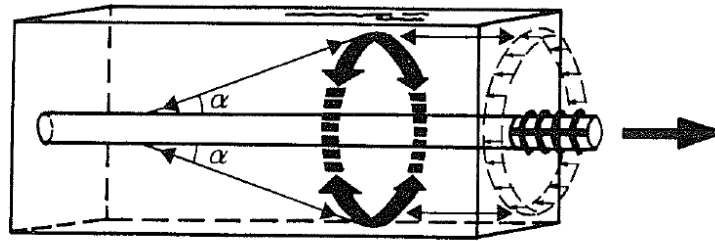


Figure 2.9 Schematic representation of how the radial components of the bond forces are balanced against tensile stress rings in the concrete (Tepfers, 1973)

The significance of collinear cracks is discussed in Section 2.1.2.1. In terms of bond stress, collinear cracks are a problem because they can decrease confinement which is part of the frictional component of bond strength. A decrease in bond strength could lead to strand slip and increased development length.

2.4 THERMAL EXPANSION OF CONCRETE

Like all materials, concrete expands when heated. This behavior is usually modeled by a linear thermal coefficient of expansion (CTE). The true CTE of concrete is not constant, and is affected most significantly by age and temperature (Berwanger *et al.*, 1976). Nevertheless, it is standard practice to model thermal expansion linearly with a constant CTE. In design, the most commonly used value for CTE of concrete is $5.5 \times 10^{-6} / ^\circ\text{C}$ (Mallela *et al.*, 2005).

CTE varies with time, temperature, and material. Many studies have published CTE data for different concrete mixtures. In one report, the CTE for a limestone-

aggregate concrete is reported as $6.125 \times 10^{-6}/^{\circ}\text{C}$ (Emanuel *et al.*, 1977). The same report lists a CTE of $7.385 \times 10^{-6}/^{\circ}\text{C}$ for gravel aggregate concrete.

2.5 SUMMARY

Many states currently have PCP bridges in service, and continue to allow PCPs as an option for bridge construction. Texas has by far the most PCP bridges of any state. Not surprisingly, TxDOT has also been a leader in PCP research. With decades of research and experience, TxDOT's PCP decks have become quite reliable.

Collinear cracks are recognized as a problem in prestressed panels. Cracks disrupt the confinement of the concrete around the strand. Confinement is considered to be a major component of the bond stress which allows the prestressing strand to transfer force into the concrete. If the bond is broken, slip may occur, reducing the prestress in the strand.

PCPs are used in bridge decks, for which AASHTO governs the design. AASHTO has developed very refined equations to estimate the prestress losses in bridge girders, which may not apply to PCPs. No research has specifically focused on determining prestress losses in concrete panels. AASHTO provides the conservative option of assuming a total prestress loss of 45 ksi in design. TxDOT uses that conservative option. An investigation of true prestress losses in PCPs may permit this initial prestress requirement to be lowered, thereby reducing of panel cracking.

CHAPTER 3

Introduction to Testing Program

3.1 FIELD FABRICATION

As a part of TxDOT Research Project 0-6348, ten panels were fabricated in Texas and monitored or tested at the Ferguson Structural Engineering Lab. Four panels were fabricated at a plant referred to here as Plant A, and six more were fabricated at a plant referred to here as Plant B.

3.1.1 Objectives of field fabrication and panel monitoring

The main purpose of fabricating and monitoring panels is to measure long-term prestress losses. For the data to be useful, it is also important that the panels be fabricated like typical TxDOT panels. Other than gages and additional transverse reinforcement installed by the researchers, the panels tested here are typical of those used in Texas for bridge deck construction.

Because several different precasters make panels in Texas, it was also important that panel specimens be fabricated at multiple plants. Similarly, precasters use different concrete mixtures in the winter than in the summer. To be able to observe the different losses associated with different mixes, it was important to have panels fabricated during different seasons.

3.1.2 General sequence of field fabrication and panel monitoring

- 1) Panels were fabricated at two different plants. At each plant, the fabrication process required two days. On the first day, gages were tied to prestressed strands and concrete was cast. On the second day, the strands were released and the panels were stacked at the precast yard.

- 2) Sometime in the following two weeks, the panels were transported by truck to the Ferguson Structural Engineering Laboratory, and were stacked in groups up to four high outside of the laboratory.
- 3) Strain data are downloaded and compiled about every month. Those data are used to estimate the prestress losses in each panel.

3.2 LABORATORY TESTING

Two of the four panels fabricated at Plant A were tested in the laboratory. One panel provided separately by Plant A, with no embedment gages installed, was also tested. Details of the experiments conducted on the panels are given in Chapter 5.

3.2.1 Objectives of laboratory testing

Laboratory tests had two main objectives. The first was to determine the relationship between longitudinal cracking and prestress loss. The other was to evaluate the effectiveness of additional transverse reinforcement in controlling collinear cracking.

3.2.2 General sequence of laboratory testing

A total of three specimens were tested. One of the specimens had additional transverse reinforcement at the edge, and the other two did not. The general sequence of testing was as follows:

- 1) A testing apparatus was designed to bend a panel about its center, parallel to the strands. The bending was intended to create flexural cracking in the center of the panel.
- 2) A panel is placed into the test set up, balancing on its centerline on a knife edge.
- 3) Slip gages (linear potentiometers) were installed on the extended ends of critical strands to measure strand retraction, an indicator of prestress loss.
- 4) Each panel was tested in flexure. While testing the panels, researchers photographed, counted, and measured cracks.

CHAPTER 4

Fabrication and Panel Monitoring at Plant A

4.1 FIELD FABRICATION

Four instrumented panels were cast at Plant A on February 18, 2009. Two of the panels were provided with additional transverse reinforcement at the edges. For the purpose of this thesis, those two panels are referred to as M1 and M2. The other two panels were not modified, and are referred to as C1 and C2.

4.1.1 Panel Design

TxDOT specifications for panel design and fabrication are summarized in Section 2.1.3 of this thesis. Those specifications allow several options for transverse reinforcement. Additionally, precasters determine their own mixture designs, within the requirements of TxDOT specifications. The relevant details of Plant A's panel design are described in Section 4.1.1.1 and Section 4.1.1.2.

4.1.1.1 Reinforcement

Plant A typically uses welded wire mesh for transverse reinforcement, as shown in Figure 4.1. D7.5 wires at 4 in. satisfy TxDOT Specification requirements for an area equivalent to that of #3 bars at 6 in. The mesh is placed directly on top of the strands. Once the strands are stressed, the mesh is tied to the strands at a few points on each panel.



Figure 4.1 Transverse reinforcement in place at Plant A

In addition to Plant A's standard mesh reinforcement, extra reinforcing bars oriented perpendicular to the strands were tied (by the researchers) at the edges of panels M1 and M2. Panels M1 and M2 each have the same reinforcement layout, shown below in Figure 4.2 and Figure 4.3. One edge of each panel (shown as the left edge in Figure 4.2) has two additional #3 bars tied 1 inch from the edge. The lower bar is tied directly to the strand, and the higher bar is tied to the lower bar with a spacer. The spacer is 5/8-inch high, leaving 3/8-in. clear cover for the top bar. The other edge of the panel (shown as the right edge in Figure 4.2) has one additional reinforcing bar tied 1 inch from the edge. The purpose of the additional reinforcement in the edge regions is to control the growth of cracks collinear to strands. The two edges of a modified panel are reinforced differently so that two different design alternatives can be evaluated.

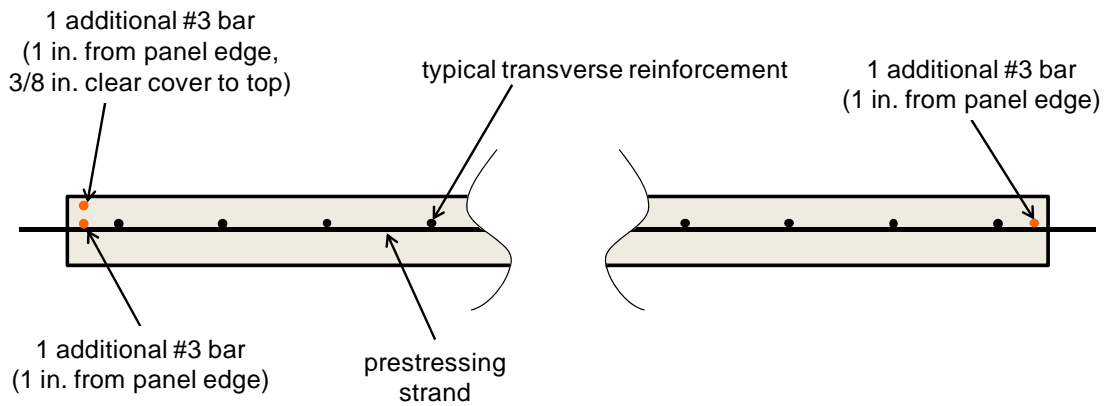


Figure 4.2 Section view of reinforcement layout in panels M1 and M2 (modifications shown in orange)

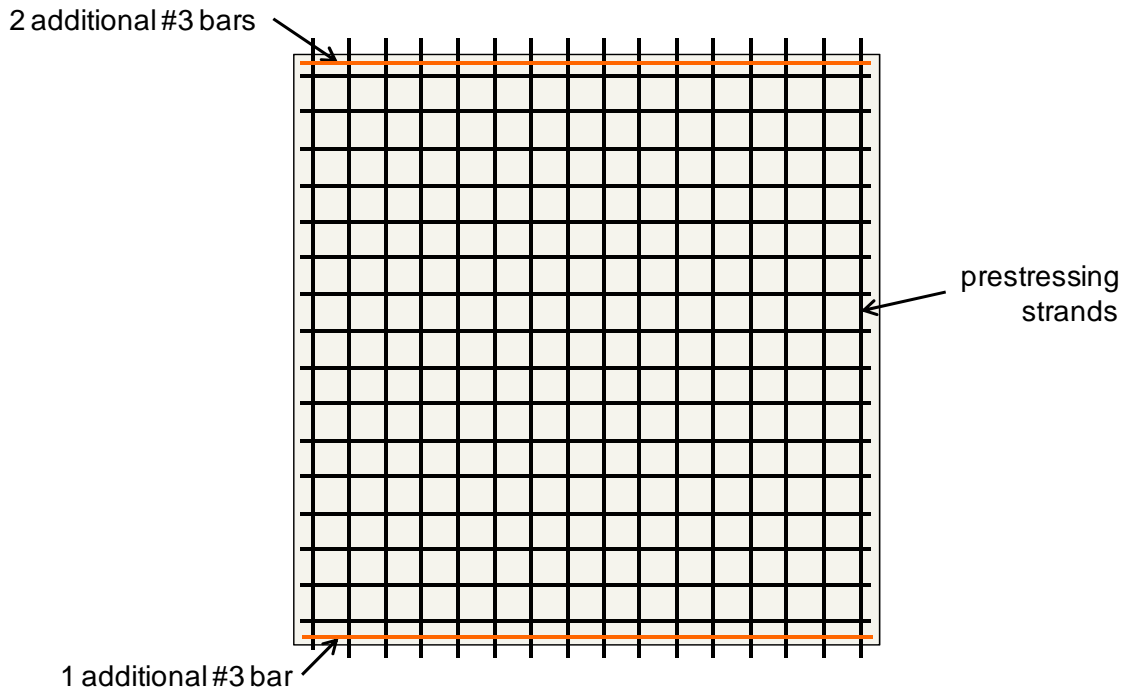


Figure 4.3 Plan view of reinforcement layout in panels M1 and M2 (modifications shown in orange)

4.1.1.2 Concrete Mixture Design

Plant A uses crushed limestone aggregate in their panel mixture. TxDOT specifies concrete with a 4000-psi compressive strength at release and a 5000-psi for design. For PCPs, Plant A uses a mixture with a 5000-psi compressive strength at release and a 9000-psi design strength. Concrete cylinder tests performed by Plant A show an average 28-day compressive strength of 11,015 psi. Details of Plant A's mixture design and material testing are given in the Appendix.

4.1.2 Instrumentation

4.1.2.1 Data Acquisition

The data acquisition systems used to monitor the panels are Campbell Scientific's, Model CR5000, shown in Figure 4.4. During fabrication, each panel was connected to its own CR5000 for the sake of mobility. However, once the panels were stored at Ferguson Laboratory, they were eventually connected to single CR5000 using multiplexers, which allow 16 new channels to be connected through just one channel on the CR5000. Without any modifications, the CR5000 can support 20 separate channels.



Figure 4.4 Campbell Scientific CR5000 measurement and control system

In the field, the CR5000's were placed inside weatherproof cases which were kept inside of plywood boxes. The boxes were painted orange to increase their visibility to operators of heavy machinery.

4.1.2.2 Strain Gages

Two different types of strain gages were installed in the panels at Plant A. Each panel was equipped with ten concrete embedment gages and ten foil reinforcing bar gages. Twenty gages were installed per panel because the CR5000 data acquisition system is designed to handle twenty channels. The locations of the gages are shown in Figure 4.5 and Figure 4.6. The embedment gage locations are the same for all four panels. However, the foil gage locations differ because the configuration of reinforcing bars differs. The foil gages were pre-installed on #3 reinforcing bars at Ferguson Laboratory, and those bars were then tied into the forms at Plant A. The embedment gages were all installed in the field.

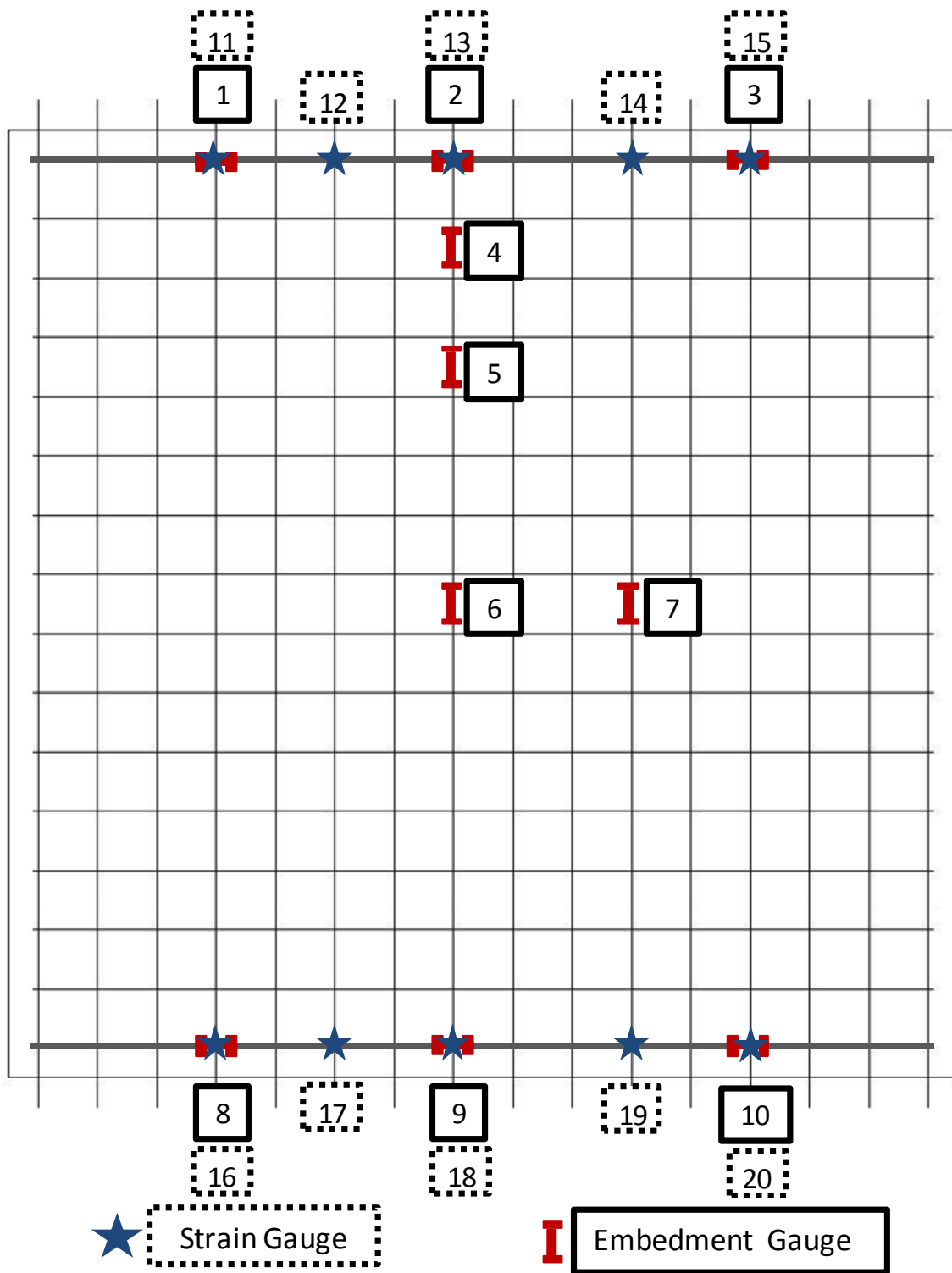


Figure 4.5 Gage layout and numbering scheme for Panels C1 and C2

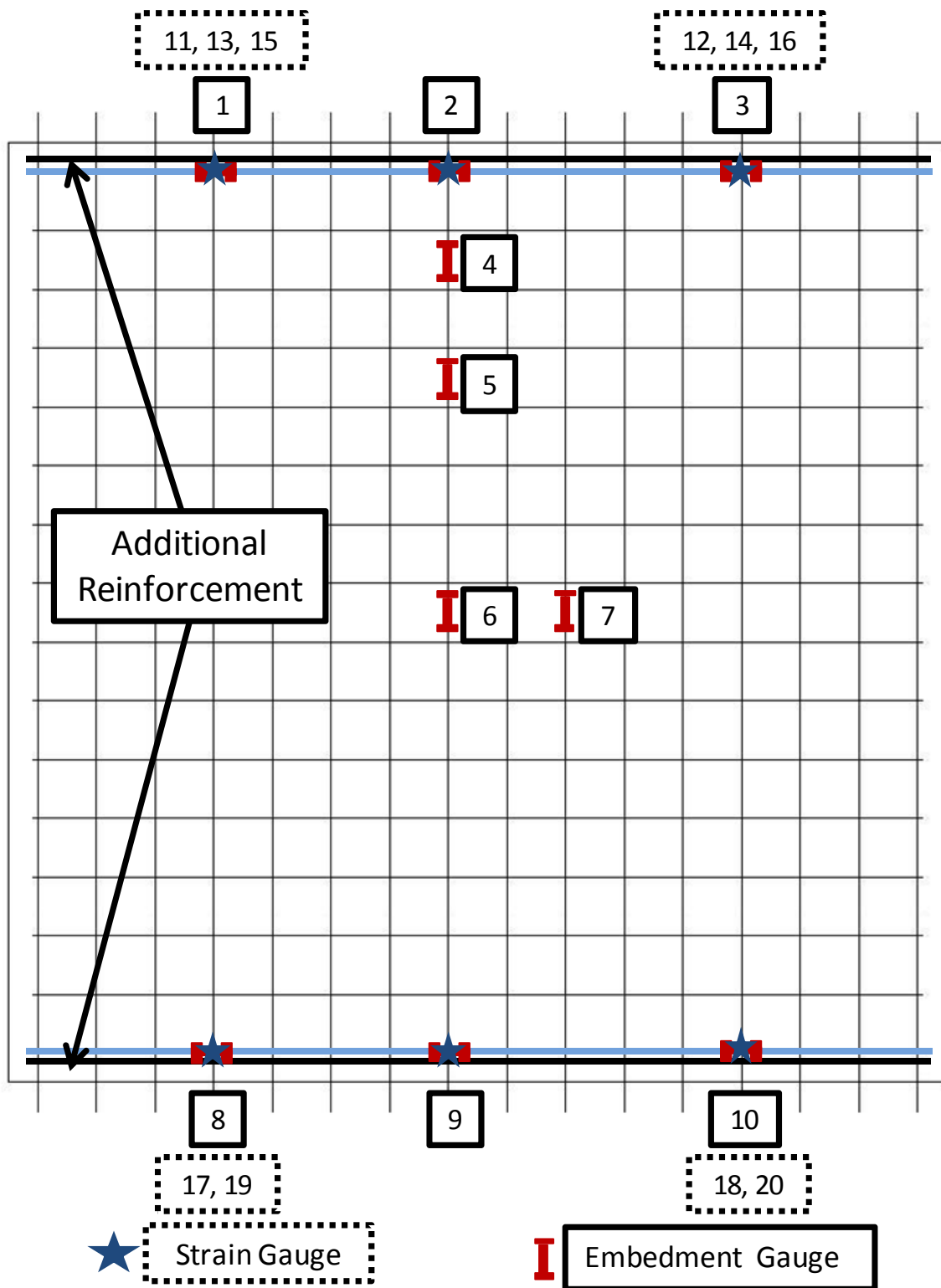


Figure 4.6 Gage layout for Panels M1 and M2

The embedment gages, shown in Figure 4.7, are the Tokyo Sokki Kenkyujo Company's Model PMFL-60-8LT. In Figure 4.5 and Figure 4.6, Gages 1 through 10 are embedment gages. The purpose of Gages 4, 5, 6, and 7 is to allow the researchers to monitor the levels of strain in a panel over time. Those four strain gages are all aligned with the prestressing strands. Since the gages were installed before the panels were cast, the strain data allow researchers to calculate and monitor prestress losses in the panel. The purpose of Gages 1, 2, 3, 8, 9, and 10 (shown in Figure 4.5 and Figure 4.6) is to indicate the transverse strains at the edge of the panels. If cracks were to form at the location of a transverse embedment gage, the strain in the concrete at that location would be of interest.



Figure 4.7 Concrete embedment gage (Tokyo Sokki Kenkyujo Co.)

The embedment gages were tied beneath the prestressing strands with plastic zip ties and Styrofoam spacers, as shown in Figure 4.8. It was important to tie the gage firmly so that it would not be dislodged or lose its orientation. However, it was also important not to put any bending stresses into the gage. Perhaps the most important requirement for gage installation was time. To minimize inconvenience to Plant A, the

selected method of gage installation needed to be fast. The use of zip ties proved to be a quick way to secure gages, and using two of them prevented the gage from twisting. It would have been slightly quicker to install the gages above the strands, but placing the gages beneath the strands was much safer.



Figure 4.8 Concrete embedment gage installed parallel to a prestressing strand

The foil gages were also manufactured by the Tokyo Sokki Kenkyujo Company (Model FLA-6-350-11-8LT). The purpose of the foil gages was to monitor the stresses in the transverse steel at edges of the panel. This is important for two reasons. The first reason is to permit a comparison between the three different reinforcement options. Panels C1 and C2 have typical transverse reinforcement. Panels M1 and M2 each have an edge with one additional bar, and an edge with two additional bars. The second reason is to permit strains in edge steel to be monitored as cracks form.

To save time in the field, the foil gages were installed on reinforcing bars at Ferguson Laboratory prior to the field work. Those bars were later tied to the prestressing strands in the field. This approach was ideal for Panels M1 and M2, because since those additional reinforcing bars needed to be placed whether or not they were instrumented. For Panels C1 and C2, the precast plant cut their typical mesh short by two bars. The mesh was still positioned in the center of the panel so that the end bar on each

side was missing. Those two bars were replaced with the bars from Ferguson Laboratory, which had strain gages already connected.

The process to install the strain gages on to the reinforcing bar is as follows:

1. Grind a 6-mm long portion of the surface of the bar just enough so the deformations are gone and surface is smooth and shiny;
2. Clean the surface of the bar with acetone and let it dry;
3. Apply glue to the dry, smooth surface and press down the gage;
4. Wrap the gage with yellow, waterproof, heat-shrink tape; and
5. Coat the tape with wax sealant.

Those steps are necessary and sufficient to protect the gage from the wet concrete. Finished gages installed on additional bars are shown in Figure 4.9.



Figure 4.9 Set of gages completely installed on additional bars

4.1.3 Fabrication

Installing the gages and routing the wires on all four panels (Figure 4.10) took about two hours.



Figure 4.10 Installing gages at Plant A

When the research team finished installing the gages, the panel crew at Plant A began casting the panels. Concrete was poured into the forms from a sidewinder concrete transporter, as shown in Figure 4.11.



Figure 4.11 Sidewinder pouring concrete into forms and over gages at Plant A

Once the concrete was in place, a crew dragged a vibrating screed over the top of the formwork, as shown in Figure 4.12. Since the embedment gages were hung below the strands and the wires were zip-tied to reinforcing bars, the screed shouldn't have damaged any of the electronics.



Figure 4.12 Plant A's crew running a vibrating screed over the wet concrete

The research team returned to Plant A the following day to observe strand release and confirm that the electronics were functioning properly. The strands were slowly released by gradual torch cutting, as shown in Figure 4.13. Unfortunately, there was a problem acquiring data from Panel C1 during release. The data acquisition system was programmed to record a strain value either every thirty minutes, or every three seconds. The system for Panel C1 was accidentally set to record every thirty minutes. The release process lasted only fifteen minutes, so there are no data for Panel C1 during that time.



Figure 4.13 Strands being torch-released at Plant A

After the strands were released, the panels were lifted by cranes and stacked four high, as shown in Figure 4.14. The data-loggers, which are housed in the orange boxes, were strapped to the top of the stack of panels. The panels were then transported by forklift to the storage area, as shown in Figure 4.15.



Figure 4.14 Panels lifted out of prestressing bed and stacked at Plant A



Figure 4.15 Stack of panels placed in storage area at Plant A

4.2 TRANSPORTATION AND STORAGE

The panels were transported to Ferguson Laboratory a week after casting. They were loaded onto a flatbed truck and secured with straps, as shown in Figure 4.16. An important detail of the strapping process is shown in Figure 4.17. The truck driver is tightening the straps by putting leverage on a long rod, which hooks into the ratchet-clamp. By doing so, he is able to get the straps very tight, which is good for keeping the panels secure to the truck, but potentially bad for introducing bending stresses into the top panel. As shown in Figure 4.18, the straps are not aligned perfectly over the top of the dunnage. Therefore, the force from the straps causes bending stresses in the top panel. The panels were inspected when they arrived at the Ferguson Laboratory, and no cracks were found.



Figure 4.16 Panels strapped to flatbed truck



Figure 4.17 Truck driver tightening straps



Figure 4.18 Side view showing relative alignment of straps and dunnage

4.3 PANEL MONITORING

Once stacked at Ferguson Lab, monitoring the panels was very simple. The CR5000 data-logger was programmed to record a strain reading from each gage in each panel every thirty minutes. Periodically, a researcher would download the data and compile it in a master file. Of the four Plant A panels, two were intended for long-term monitoring, and two were monitored short-term and then tested in the lab. One problem arose when the battery charger for the CR5000's was accidentally unplugged. The battery voltages in Panels C2 and M2 dropped below the required level, and the units shut down. A week's worth of data was lost from Panel C2, and a month of data from Panel M2. When the problem was discovered, power was restored to the units and they started working again.

CHAPTER 5

Laboratory Testing of Panels Fabricated at Plant A

5.1 OBJECTIVES OF TESTING

Laboratory tests of the panels from Plant A had two major objectives. The first was to investigate the relationship between panel cracks and loss of prestress. The second was to compare the effectiveness of crack control provided by different edge reinforcement options.

Neither of those two objectives had been completed by simply monitoring the panels. The panels were inspected at Ferguson Lab; no cracks were found; and no comparisons could be made. To accomplish the two major objectives, the panels were intentionally cracked in the lab. The most reliable way to crack a panel is to bend it, and the test setup designed to do this is described in detail in Section 5.2.

5.2 TEST SETUP

5.2.1 Knife edge

A knife edge was used to provide a controlled means of cracking the panels. The components of the setup (Figure 5.1) are structural steel shapes. The knife edge itself is simply two 6-in. angles bolted together. The load-distribution beams are two W10x15 shapes welded along the flanges. The setup is anchored to a strong floor using $\frac{3}{4}$ -in. threaded rods. One-inch holes were drilled through the load distribution beams to allow the threaded rods to pass through. The panel is placed into the setup with strands running parallel to the knife edge. It is positioned so that the center strand is directly above the knife edge, where the highest bending moment will exist.

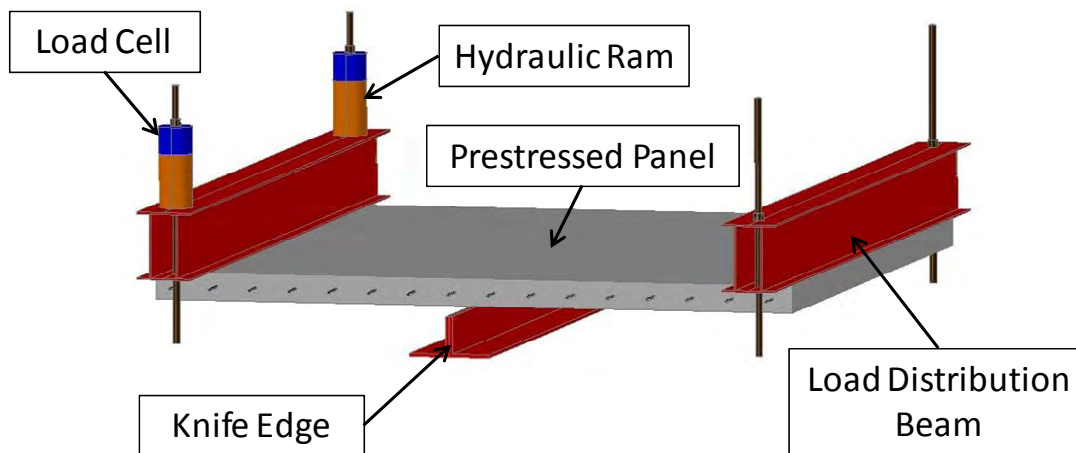


Figure 5.1 Knife edge setup to induce flexural cracks

5.2.2 Loading

The two hydraulic rams, shown as orange cylinders in Figure 5.1, were connected to a single hand pump. The hydraulic line from the hand pump divided at a manifold so that each ram would be at equal pressure. The load was increased in increments of 100 psi, inspecting the panel for cracks after at each increment. The panels were loaded until failure, which was controlled by fracture of the transverse reinforcement.

5.2.3 Test specimens

In total, three panels were tested in the laboratory, and are referred to as Specimens C1, M1, and C3. Specimen C1 is a current design panel, with internal gages located as shown in Figure 4.5. Specimen M1 is a modified design panel with internal gages and additional reinforcement located as shown in Figure 4.6. Specimen C3 is a current design panel, without gages, provided by Plant A. Specimen C1 was the first panel tested, and was used as a pilot test. The results of the test conducted on Specimen C3 are used in place of those that would have come from Specimen C1.

5.2.4 Instrumentation and data acquisition

5.2.4.1 Instrumentation

Several different external gages were connected to the test specimens. To estimate the prestress losses caused by the cracks generated during the test, slip gages (2-in. linear potentiometers) were installed on the extensions of the critical strands (Figure 5.1). They are manufactured by Novotechnik and are accurate to one ten-thousandth of an inch. They were fastened to a wood block bolted to the strand, and positioned so that the plunger of the potentiometer reacted against the side of the panel, measuring strand retraction directly.

To use this type of gage, it is very important to have the gage tightly secured to the strand, so that the gage cannot move. Unfortunately, the strand extensions of Specimen C1 had been trimmed very short to allow the specimen to fit through the lab doors. This made it very difficult to properly secure the slip gages, and is one reason that Specimen C1 was designated as a pilot specimen, and replaced by Specimen C3.

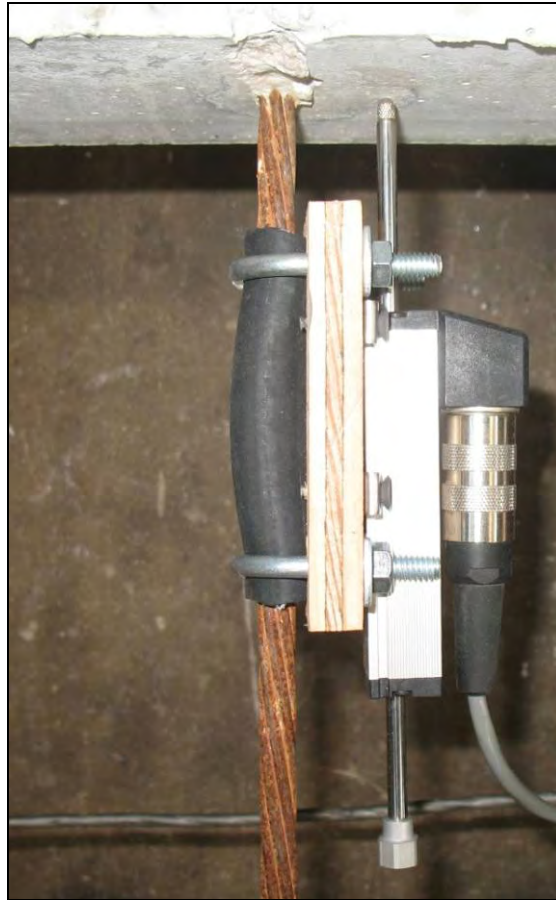


Figure 5.2 Typical slip gage installed on a strand

The same type of linear potentiometer was also used to measure the average strain transverse to the center strand. A metal wire was tied between the linear potentiometer and a fastener. The fastener and the gage were then glued to the panel, as shown below in Figure 5.3. The two components of the resulting string potentiometer were separated by a 15-in. gage length. The main use of this type of gage was to estimate average crack widths, as the total elongation of the gage divided by the number of cracks within that gage length.



Figure 5.3 Linear potentiometer used with metal wire to measure average strain over center strand

In an additional attempt to measure prestress losses, strain gages were glued to the top and bottom surfaces of Specimen C1, as shown in Figure 5.4. The surface of the panel was ground smooth and epoxy was used to fill any voids. The gages are the Tokyo Sokki Kenkyujo Company's Model PL-60-11-5LT. After testing Specimen C1, however, it was clear that these gages were not providing good data. The overall change in strain the panel associated with the amount of prestress force loss to cracking was too small for the gages to detect. Therefore, these gages were not used on the other two specimens.

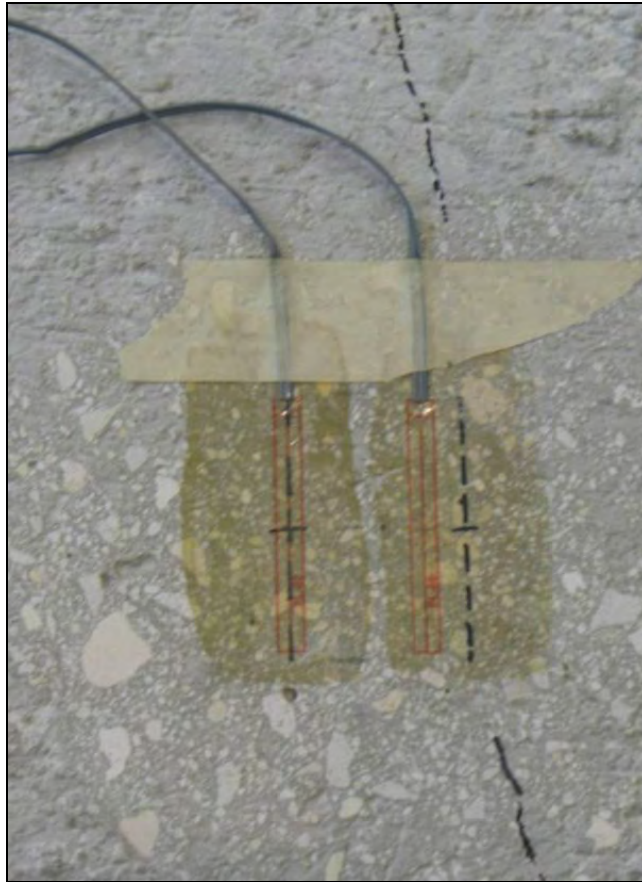


Figure 5.4 Concrete surface strain gages as applied to Specimen C1

Although many gages were attached to the specimens to record strains and displacements, crack widths were also measured and counted by hand. Initial measurements were made using a special microscope, shown below in Figure 5.5. As cracks widened further, widths were measured using crack comparators.



Figure 5.5 Crack microscope

5.2.4.2 Data acquisition system

The data acquisition system, shown in Figure 5.7 and Figure 5.7, consisted of a desktop computer, an Agilent 34980A Multifunction Switch/Measure Unit, and several “pods” containing bridge completion modules, specially made by Ferguson Lab staff. Each pod has eight channels. The channels can be set to read strain gages, displacement gages, or load cells. The total system was equipped with eight pods, so that roughly 64 channels were available. Three of the pods are shown in Figure 5.8. The system was controlled by a program written in National Instruments’ LabVIEW®.

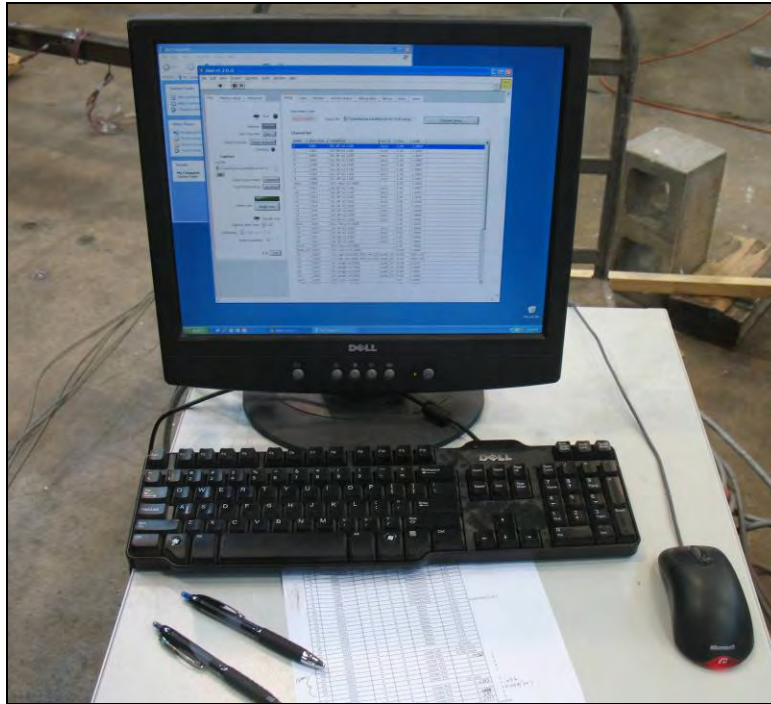


Figure 5.6 Upper components of data-acquisition system



Figure 5.7 Lower components of data-acquisition system

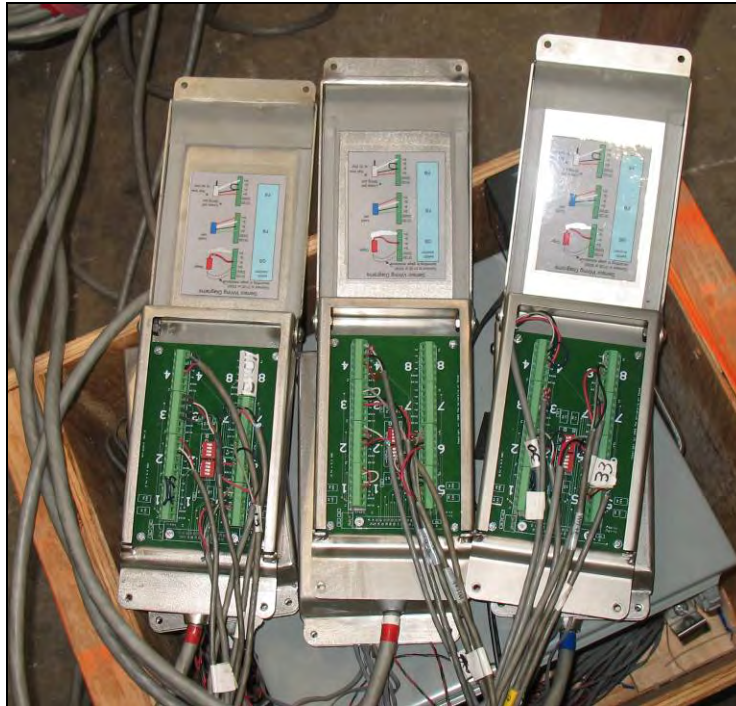


Figure 5.8 Three of the “pods” used with the data-acquisition system

5.3 TESTING OF SPECIMEN C1

Specimen C1 was tested on July 7, 2009, at an age of 109 days. The specimen was instrumented with the gages described in Section 5.2.4.1, as shown in Figure 5.9 and Figure 5.10. The gages were positioned to record the effects of what was expected to be one large crack down the center of the panel, over the knife edge. However, as the panel was being loaded, many cracks began to form over the central 5 feet of the panel, with the final distribution as shown in Figure 5.11. Due to the broad distribution of cracking in Specimen C1, many more strands were instrumented with slip gages for the other two specimens.

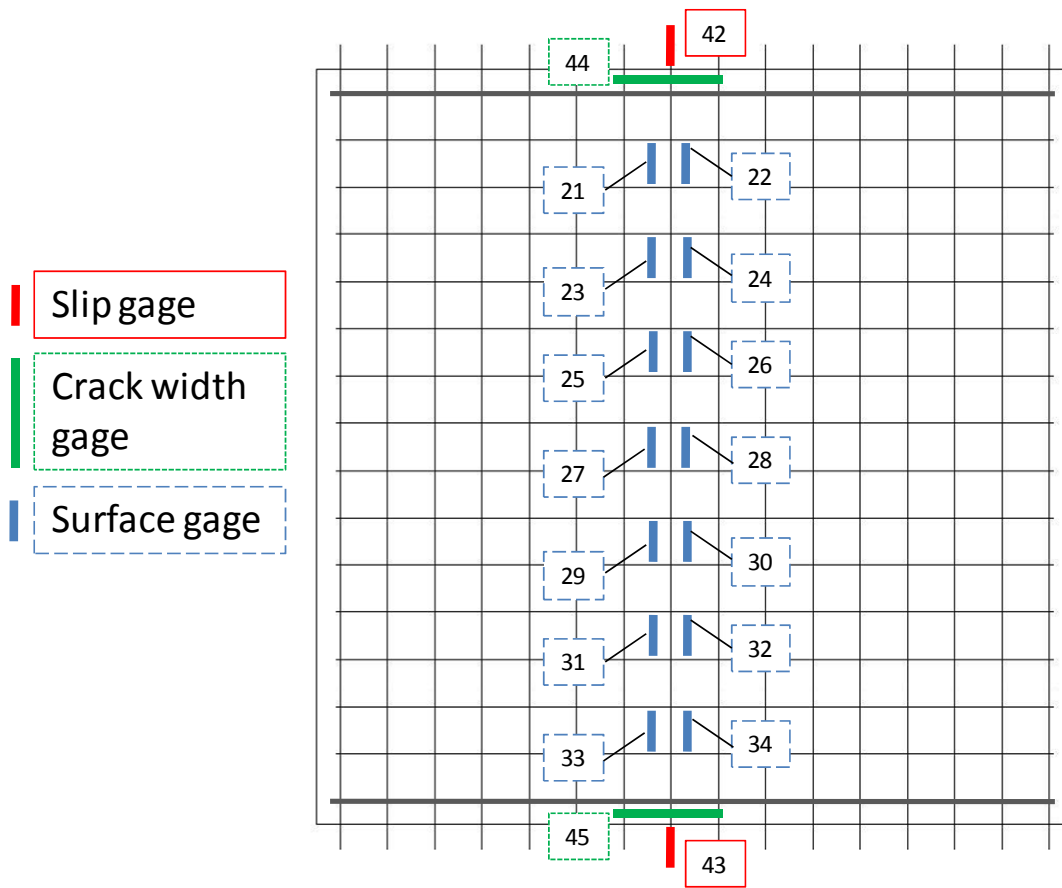


Figure 5.9 Gage layout for top of Specimen C1

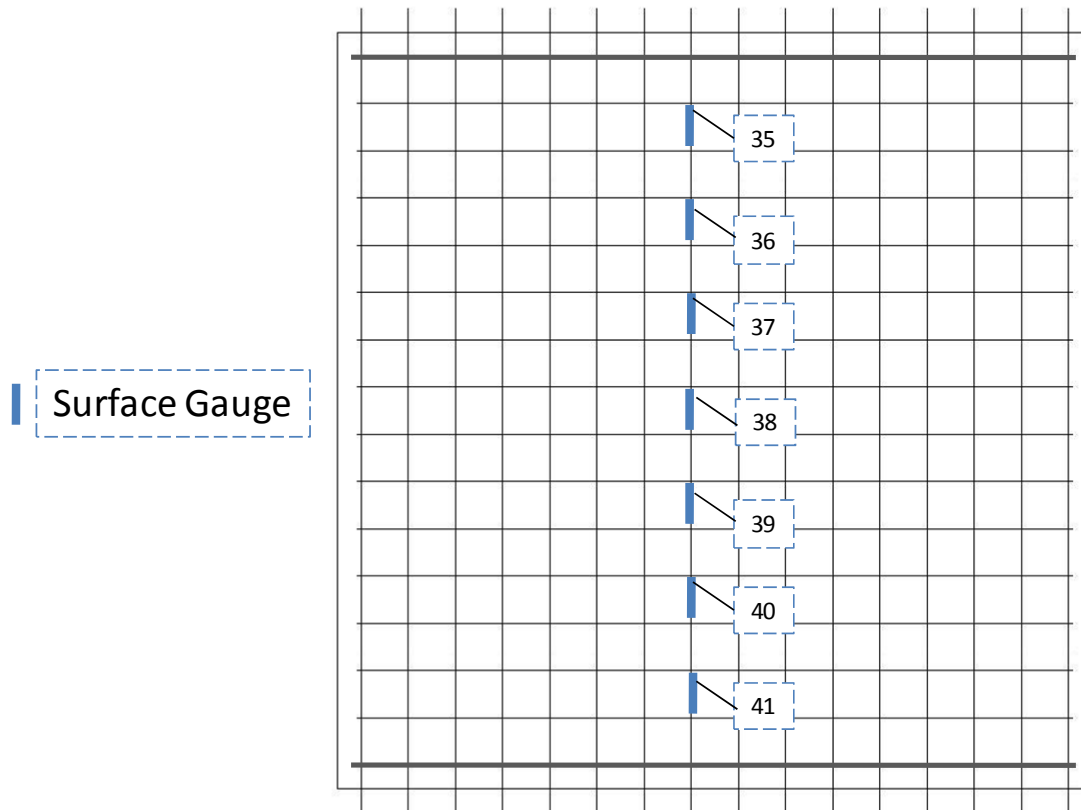


Figure 5.10 Gage layout for bottom of Specimen C1

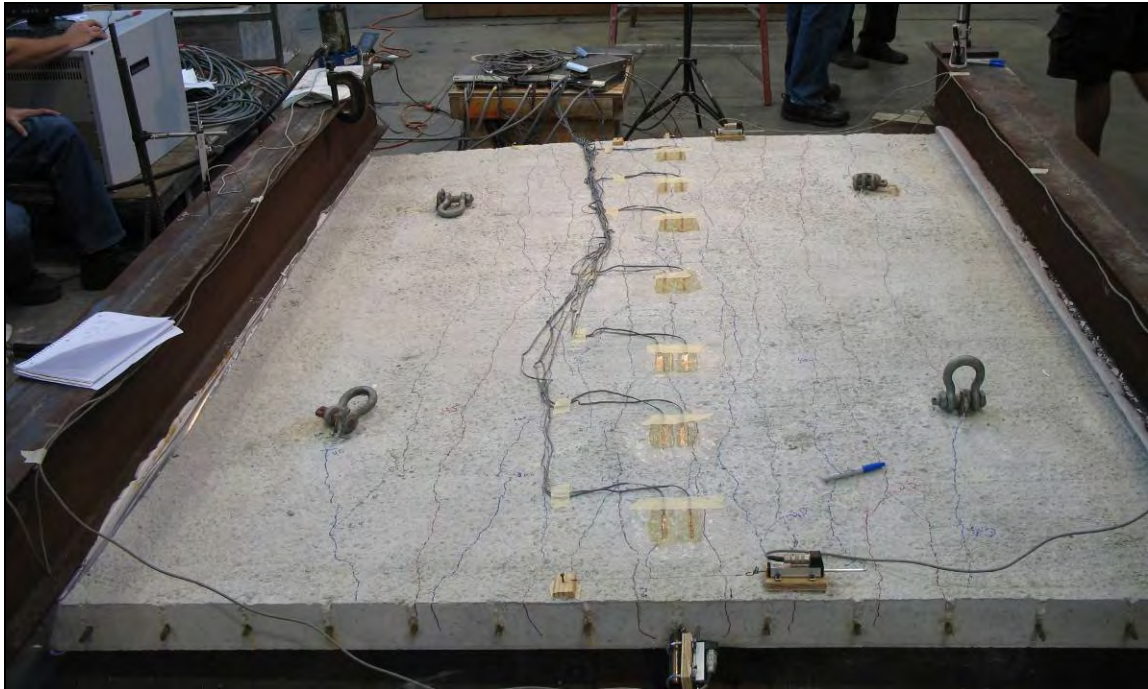


Figure 5.11 Final distribution of cracking in central zone of Specimen C1

5.4 TESTING OF SPECIMEN M1

Specimen M1 was tested on September 30, 2009, at an age of 120 days. The locations of the gages used for the test are shown in Figure 5.12. As is shown, the center six strands were instrumented with slip gages, and no concrete surface gages were used. Specimen M1 was loaded to failure, indicated by a popping sound as the transverse reinforcement ruptured. As the transverse steel was yielding, a large crack began opening up in the center of the panel. This was in contrast to Specimen C1, which was not loaded to failure. Specimen M1 after testing is shown in Figure 5.13.

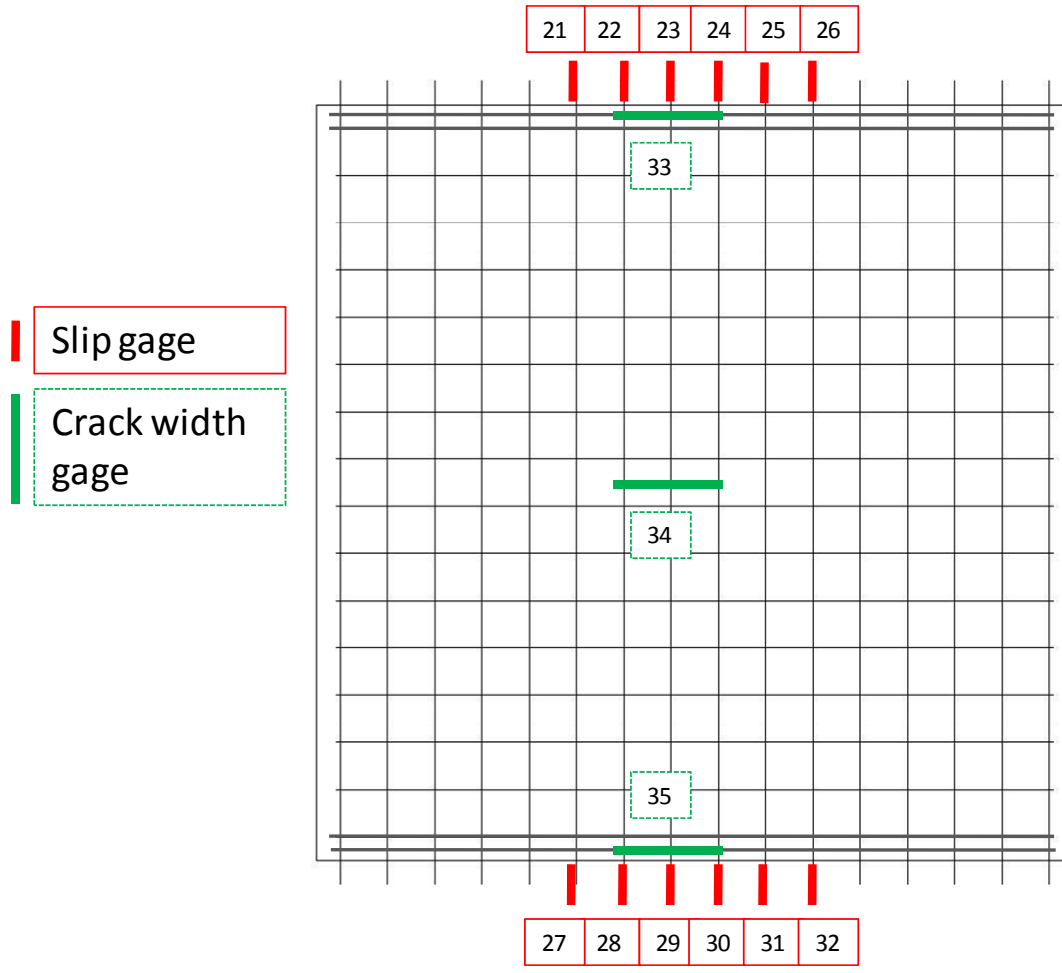


Figure 5.12 Gage layout for Specimen M1

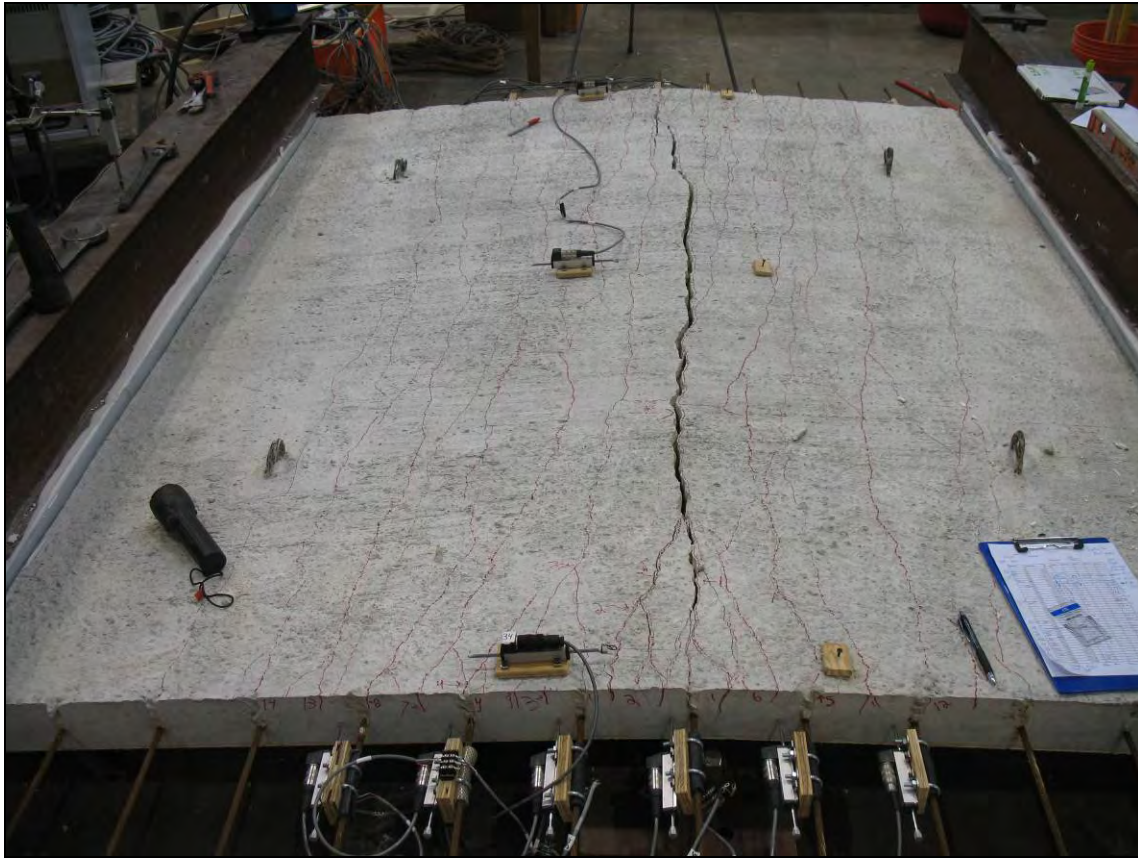


Figure 5.13 Specimen M1 after testing (the near edge is the double-bar edge)

5.5 TESTING OF SPECIMEN C3

Specimen C3 was provided by Plant A, with no internal gages. It was tested on November 6, 2009, but its casting date is unknown. After testing two other specimens, it was clear that slip gages provided the most useful data. Therefore, a total of 20 slip gages were attached to Specimen C3. Three crack-width gages were also used, to maintain consistency with Specimen M1. Gage locations are shown in Figure 5.14.

Specimen C3 was tested to failure, which was again marked by a popping noise as the transverse reinforcement ruptured, similar to Specimen M1. Because Specimen C3 had no additional reinforcement, however, the center crack (over the knife edge) opened very wide over the full length of the panel. Specimen C3 after testing is shown in Figure 5.15. Because the center crack opens the widest, the center strand experiences the most

slip. Unfortunately, on one edge of the panel, the main crack occurred precisely where the slip gage was in contact with the panel (Figure 5.16). The crack was so wide that the plunger slipped into the crack, and therefore could no longer record slip. In future tests, this can be prevented by connected a small disk to the tip of the plunger, so that it would not fit in a crack.

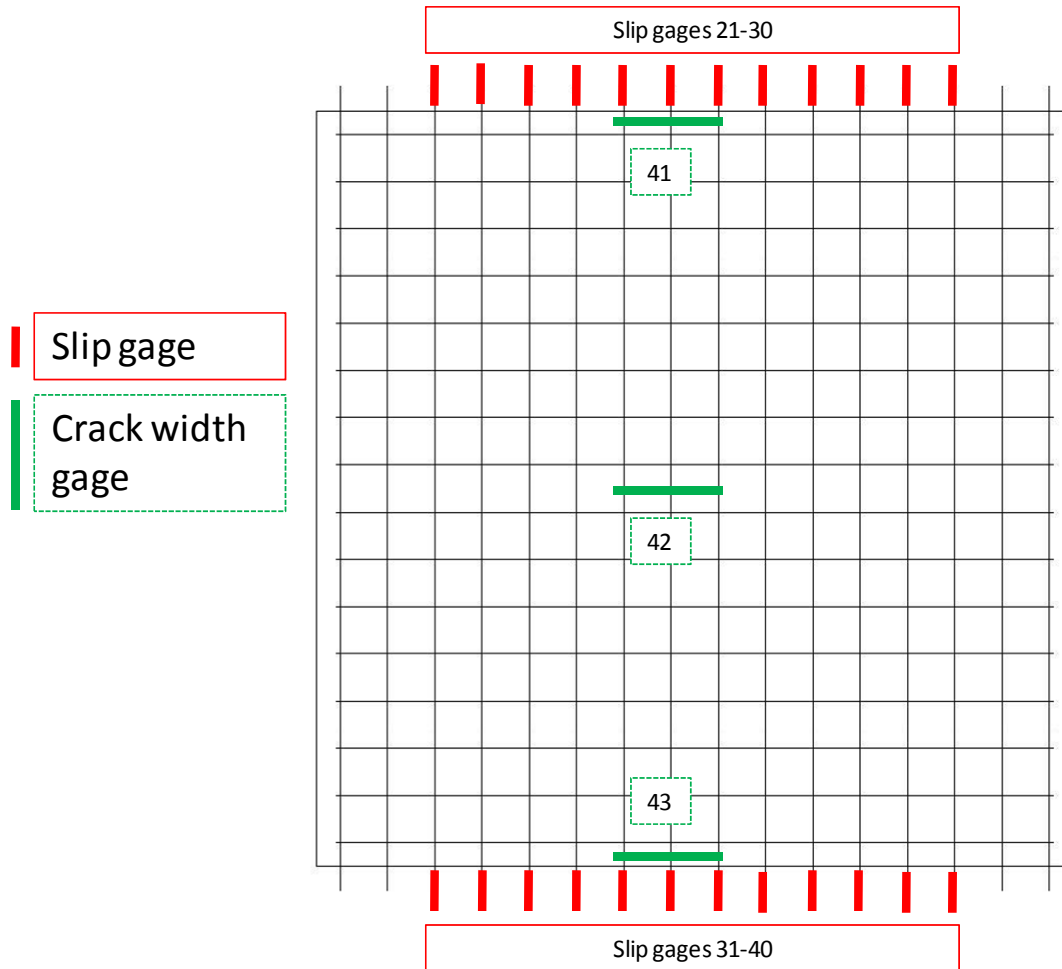


Figure 5.14 Gage locations for Specimen C3

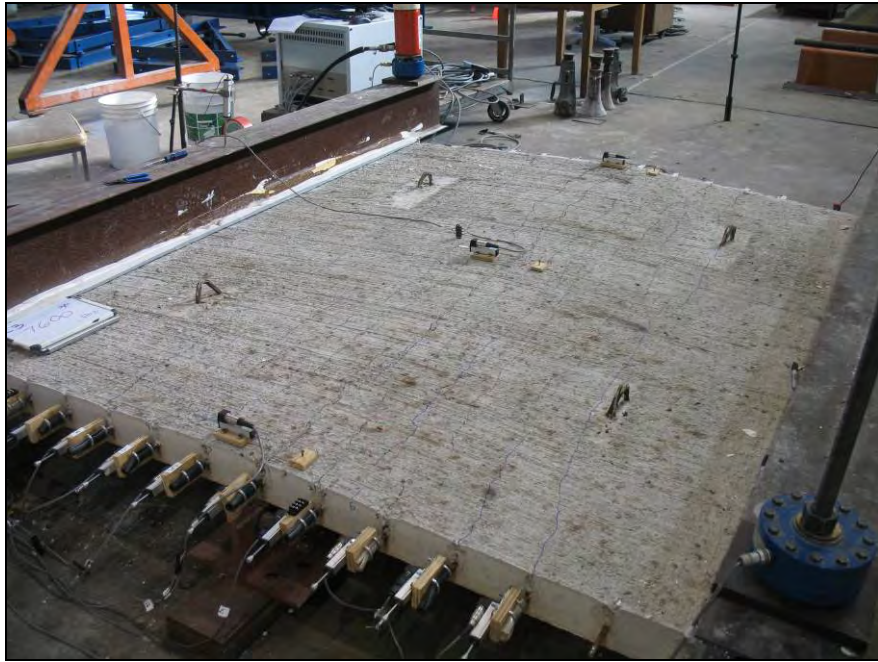


Figure 5.15 Photograph of Specimen C3



Figure 5.16 Gage 26 shown with the plunger stuck in the major crack of Specimen C3

CHAPTER 6

Fabrication and Panel Monitoring at Plant B

6.1 FIELD FABRICATION

Six panels were cast at Plant B on February 18, 2010. Of the six panels, four were instrumented and two were not. Of the four instrumented panels, two were modified with additional edge reinforcement. Those two panels are referred to as Specimens M3 and M4. The two unmodified and instrumented panels are referred to as Specimens C4 and C5. Specimens M3, M4, C4 and C5 are intended for long-term monitoring. The two panels without instrumentation are considered short-term and are intended for laboratory testing. One short-term panel is modified with additional edge reinforcement and one is unmodified. They are referred to as M5 and C6, respectively.

6.1.1 Panel Design

TxDOT's specifications for panel design and fabrication are summarized in Section 2.1.3 of this thesis. The relevant details of Plant B's panel design are described in the following two sections.

6.1.1.1 Reinforcement

Plant B uses D7.5 wires at 4 in. in the transverse direction and D3.5 wires at 18 in. in the longitudinal direction. A photograph of the reinforcement in place at Plant B is shown in Figure 6.1. The only difference between the practices of Plant A and Plant B is that at Plant B, the meshes are placed below the strands. Once the strands are stressed, the mesh is lifted with a hook and tied to the strands.

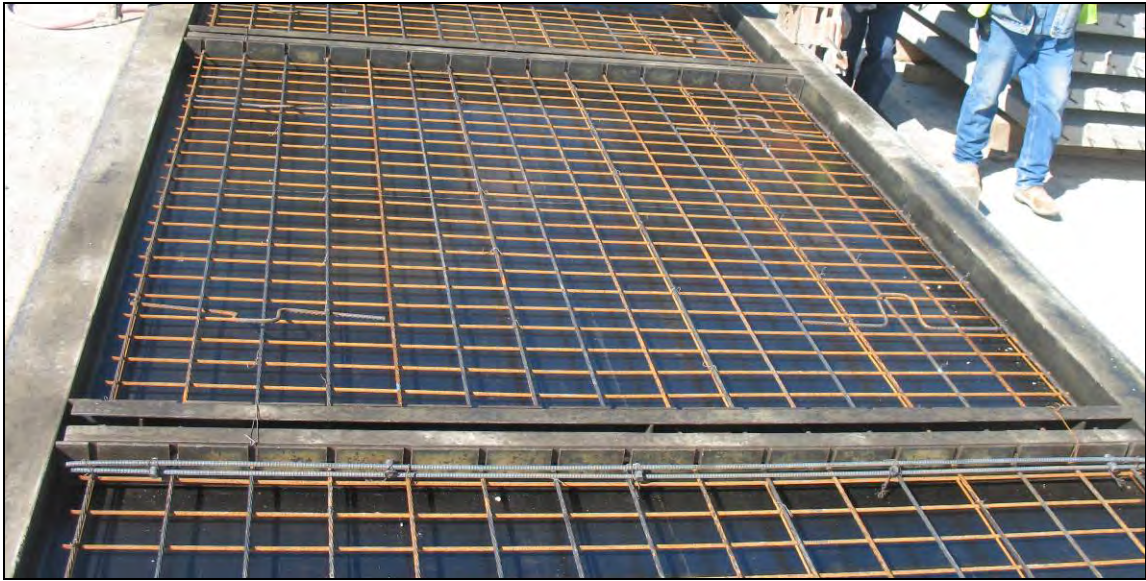
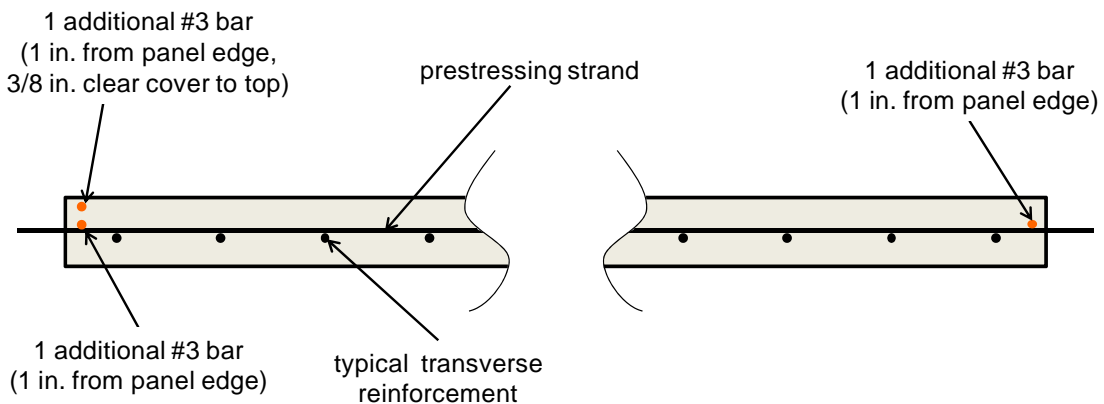


Figure 6.1 Transverse reinforcement in place at Plant B

In addition to Plant B's standard mesh reinforcement, extra reinforcing bars were tied at the edges of Specimens M3, M4, and M5. The layout of the additional reinforcement (detailed in Section 4.1.1.1) is the same used for Specimens M1 and M2, which were cast at Plant A. The section and plan views of the reinforcement layout are shown in Figure 6.2 and Figure 6.3, respectively.



**Figure 6.2 Section view of reinforcement layout in panels M3, M4, and M5
(modifications shown in orange)**

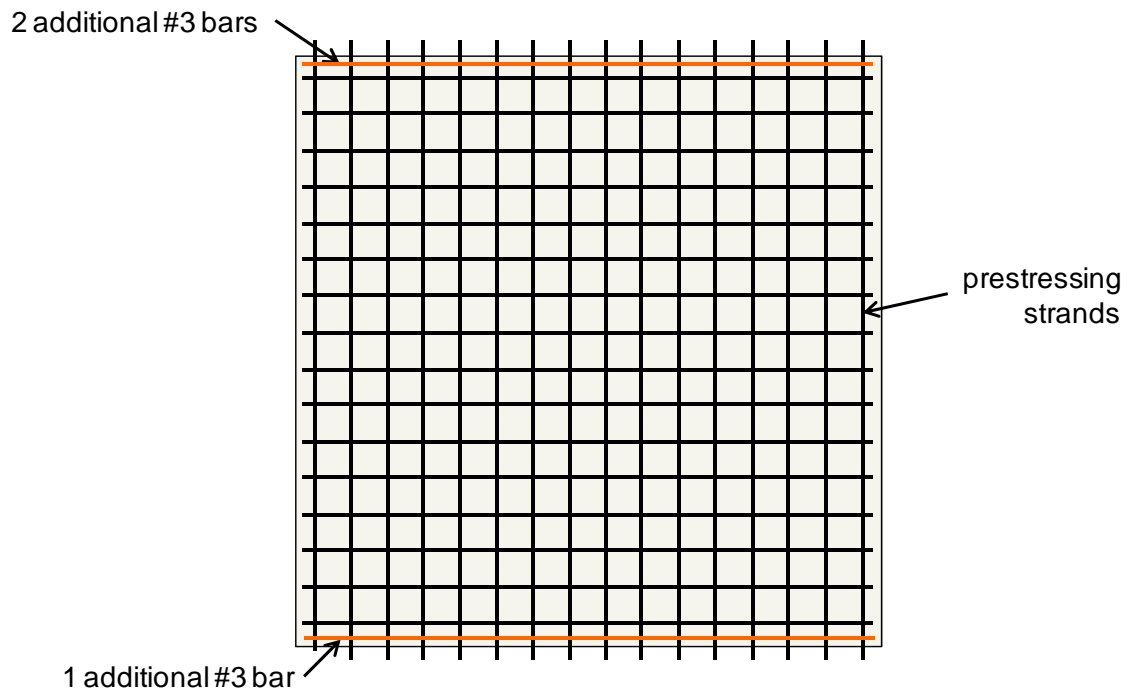


Figure 6.3 Plan view of reinforcement layout in panels M3, M4, and M5
(modifications shown in orange)

6.1.1.2 Concrete Mixture Design

Plant B uses a panel mixture with river-gravel aggregate. TxDOT specifies a concrete compressive strength of 4000 psi for release and 5000 psi for design. Concrete cylinders taken from the same batch as the specimens had an average 28-day compressive strength of 10,640 psi. Details of Plant B's mixture design and material testing are given in the Appendix.

6.1.2 Instrumentation

6.1.2.1 Data Acquisition

The data acquisition systems used at Plant B were the same as those used at Plant A (described in Section 4.1.2.1).

6.1.2.2 Strain Gages

The gage layout used for the specimens cast at Plant B was slightly altered from the layout used for the specimens cast at Plant A. The biggest difference is that no foil reinforcing-bar gages were used for the Plant B specimens. Although it was originally thought that those reinforcing-bar gages might help permit comparisons between the different edge reinforcement options, crack widths proved to be the most useful criterion for that comparison. Additionally, the transverse embedment gages in the edge regions provide essentially the same data as the foil reinforcing-bar gages.

Since no foil reinforcing-bar gages were installed, 10 channels were available for each CR5000, 9 of which were used for additional embedment gages, distributed over the panels to provide a more complete picture of how losses vary within a panel. The last open channel was used for a thermocouple. Although the CR5000 unit records the ambient temperature, knowing the temperature inside of the panel would be helpful for determining how thermal expansion affects prestress losses.

The final modification to the instrumentation plan for the specimens cast at Plant B was the addition of a vibrating wire gage (VWG). One VWG was placed at the center of each panel. Each specimen has the same gage layout, shown below in Figure 6.4. The thermocouples, not shown in Figure 6.4, were tied to the center of the panel.

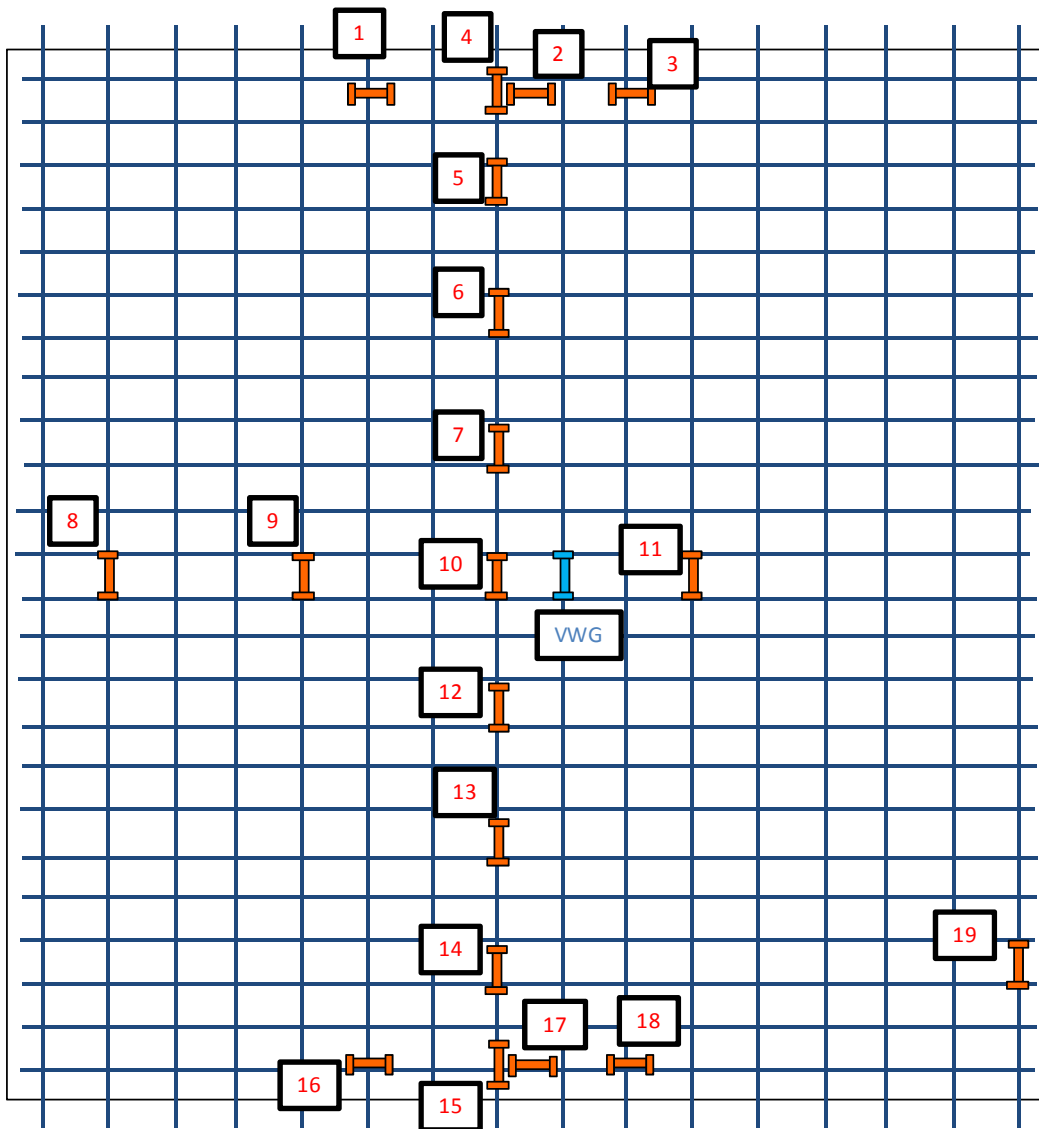


Figure 6.4 Gage layout and numbering scheme for Panels M3, M4, C4, and C5

The embedment gages, shown in Figure 4.7, are the same type used at Plant A (PMFL-60-8LT). The embedment gages were tied beneath the prestressing strands with the same zip tie method explained in Section 4.1.2.2. An embedment gage installed at Plant B is shown in Figure 6.5.



Figure 6.5 Concrete embedment gage installed parallel to a prestressing strand

The VWGs, labeled Number 21 in Figure 6.4, are Geocon's Model 4200. The VWGs were installed like the embedment gages, in the center of the panels, and parallel to the strands. Figure 6.6 shows a VWG installed alongside an embedment gage in panel formwork at Plant B. The VWGs were included primarily to confirm the long-term quality of the other gages, such as the PMFL-60-8LT foil embedment gages. An additional benefit of adding the VWGs is that they are independent of the CR5000 system. If something were to go wrong with the CR5000 unit and some data were lost or corrupted, the VWG data could be used to replace the lost data.

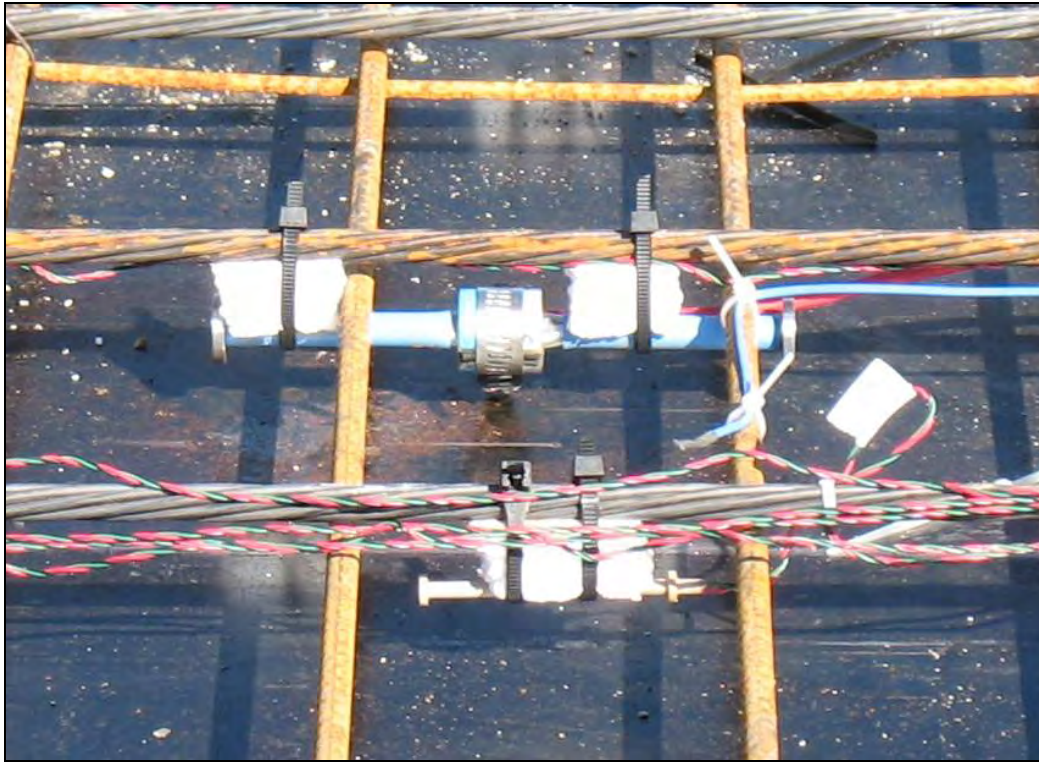


Figure 6.6 VWG installed next to an embedment gage

6.1.3 Fabrication

Installing the gages and routing the wires out of all four panels took approximately three hours (Figure 6.7). The vibrating screed used at Plant B, shown in Figure 6.8, was much larger than the screed used at Plant A. The maximum clearance under the screed was much less than the height of the wooden boxes housing the data-loggers. Therefore, the gages couldn't be wired into the CR5000's until after the concrete had been placed. This required additional time, since at Plant A the gages had been already wired to the data-loggers before they were installed.



Figure 6.7 Installing gages at Plant B



Figure 6.8 Vibrating screed used at Plant B

When the research team finished installing gages, the panel crew at Plant B began casting the panels. Concrete was poured into the forms from a sidewinder concrete truck, as shown in Figure 6.9.



Figure 6.9 Sidewinder pouring concrete into forms and over gages

Once the concrete was in place, the vibrating screed was driven over the top of the formwork, as shown in Figure 6.10. Because the embedment gages were hung below the strands and the wires were zip-tied to reinforcing bars, the screed shouldn't have damaged any of the electronics. The wires were routed out of the sides of the panels alongside strands. The external lengths of the wires were wrapped into a plastic bag and the screed was raised over the bag as it moved from one panel to the next.



Figure 6.10 Vibrating screed being maneuvered over a panel at Plant B

A member of Plant B's panel crew followed behind the screed with a broom, giving the panels a rough finish. After the panels were finished, they were covered in wet burlap to cure. At this point, research team was able to connect the wires to the data-loggers and begin to measure the strains in the panels.

The research team returned to Plant B the following day to observe strand release and confirm that the electronics were functioning properly. The strands are slowly released by gradual torch cutting, as shown in Figure 6.11. Strain readings from the VWGs were recorded immediately before and after the strands were released, so that elastic shortening could be calculated accurately.



Figure 6.11 Strands being torch released at Plant B

After the strands were released, the panels were lifted by cranes and stacked alongside the prestressing beds, as shown in Figure 6.12. The four panels with gages were stacked together, and the two panels without gages were stacked together. All six remained in storage at that location for a week.



Figure 6.12 Stacked panels being placed in the storage area at Plant B

6.2 TRANSPORTATION AND STORAGE

The six panels from Plant B were delivered to Ferguson Lab on March 1, 2010. The panels had been tightly secured to the truck bed by straps, as shown in Figure 6.13. The straps were not necessarily aligned with the dunnage, however, so securely strapping them to the truck bed introduces bending stresses.



Figure 6.13 Plant B panels arrive at Ferguson Lab

The panels were stacked outside Ferguson Lab, alongside the panels from Plant A. The 4 instrumented panels are intended for long-term monitoring of prestress force. They were stacked together with the data-loggers strapped to the top panel, as shown in Figure 6.14. The 2 short-term panels were temporarily stacked next to the long-term panels. At some point, they will be moved into the lab for testing.



Figure 6.14 Panels from Plant B stacked outside of Ferguson Lab

6.3 PANEL MONITORING

Once stacked at Ferguson Lab, monitoring the panels was very simple. The CR5000 data-logger was programmed to record a strain reading from each gage in each panel every thirty minutes. Periodically, a researcher would download the data and compile it in a master file. Unfortunately, one data-logger malfunctioned and the early strain readings from Panel C4 were lost. However, since VWGs were installed in each of the long-term panels, elastic shortening data are still available.

CHAPTER 7

Test Results

7.1 PRESTRESS LOSSES

7.1.1 Short-Term Prestress Losses (Elastic Shortening)

7.1.1.1 Estimated Values using AASHTO Equation

The 2008 AASHTO *LRFD Design Manual* (AASHTO LRFD, 2008) presents the following equation to predict the short-term prestress losses (due to elastic shortening) of a prestressed bridge member:

$$\Delta f_{pES} = \frac{A_{ps} f_{pbt} (I_g + e_m^2 A_g) - e_m M_g A_g}{A_{ps} (I_g + e_m^2 A_g) + \frac{A_g I_g E_{ci}}{E_p}} \quad (C5.9.5.2.3a-1)$$

When this equation is applied to the TxDOT PCP, the predicted loss in prestress due to elastic shortening is 5.1 ksi. This calculation is based on a minimum specified release strength for the concrete of 4,000 psi, a corresponding elastic modulus of 3,740 ksi, and an assumed unit weight of 147.5 lb/ft³.

7.1.1.2 Measured Values

Strains in the test panels were measured during release at each plant, and those measured strain values were used to monitor the change of stress in prestressing strands during release. It was assumed that the force in each strand immediately prior to release was 16.1 kips. It was also assumed that the strain in each strand was equal to the strain in nearby concrete. Gage #6 (from Figure 4.5 and Figure 4.6) is located in the center of the panels cast at Plant A. The changes of stress in the prestressing strand at the center of

Specimens C2, M1, and M2 are shown in Figure 7.1, Figure 7.2, and Figure 7.3, respectively. Release data for Specimen C1 are not available.

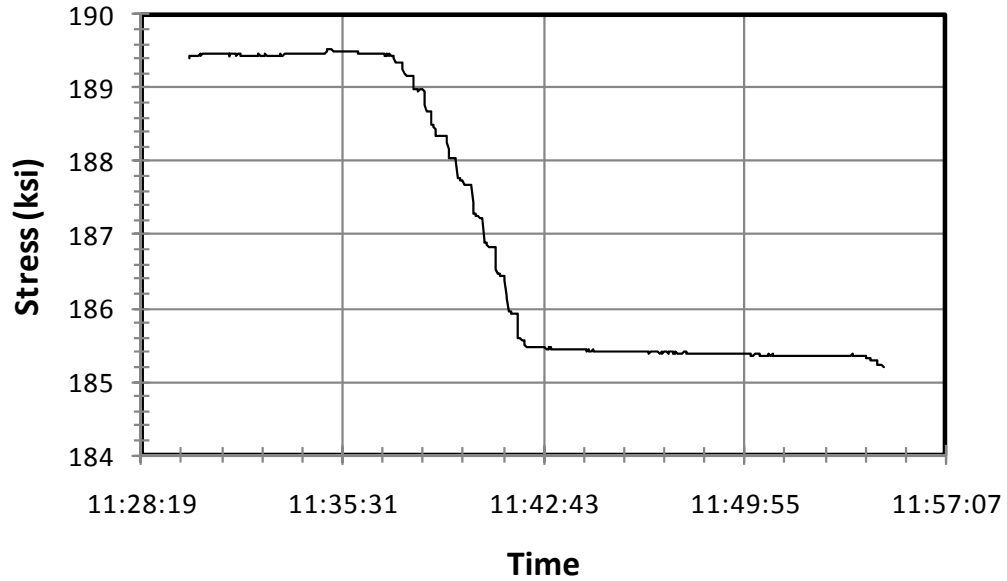


Figure 7.1 Stress in prestressing strands at the center of Specimen C2 during release

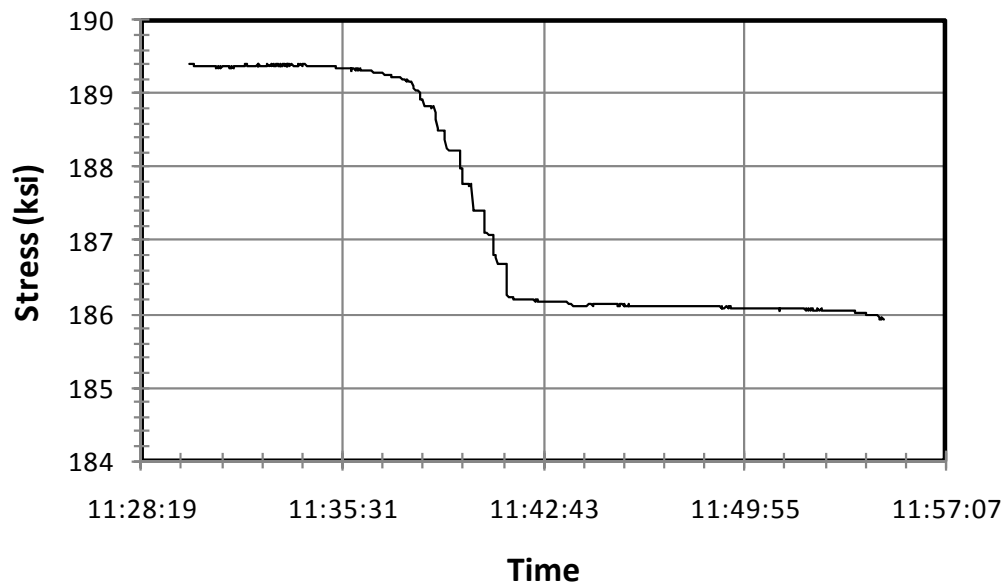


Figure 7.2 Stress in prestressing strands at the center of Specimen M1 during release

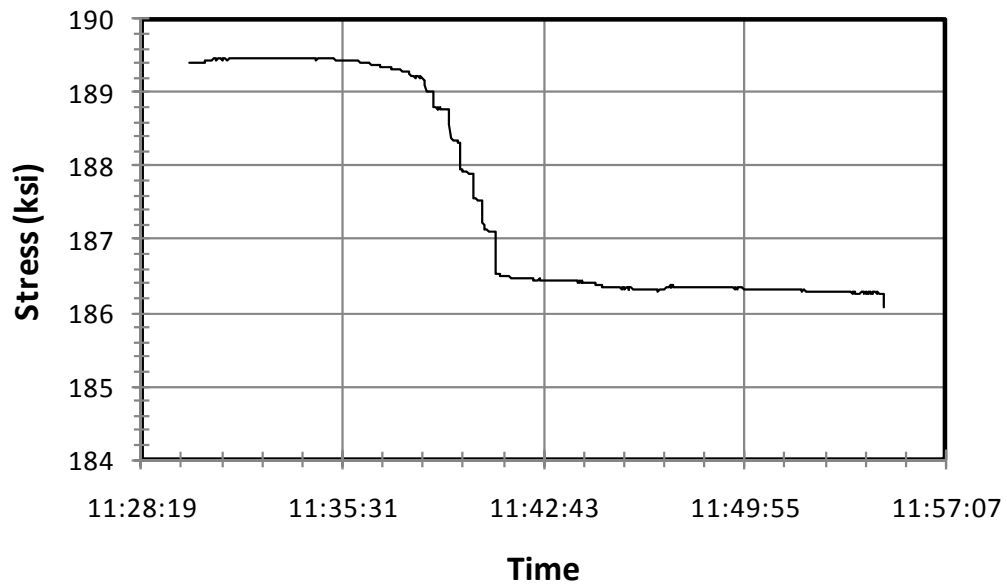


Figure 7.3 Stress in prestressing strands at the center of Specimen M2 during release

Elastic shortening in the panels from Plant A resulted in an average prestress loss of 3.5 ksi. The strand stress was calculated in the same way for the specimens from Plant B. Data from Gages #10 (Figure 6.4) were used to plot the stress variation in the center of Specimens C4, C5, M3, and M4 during release.

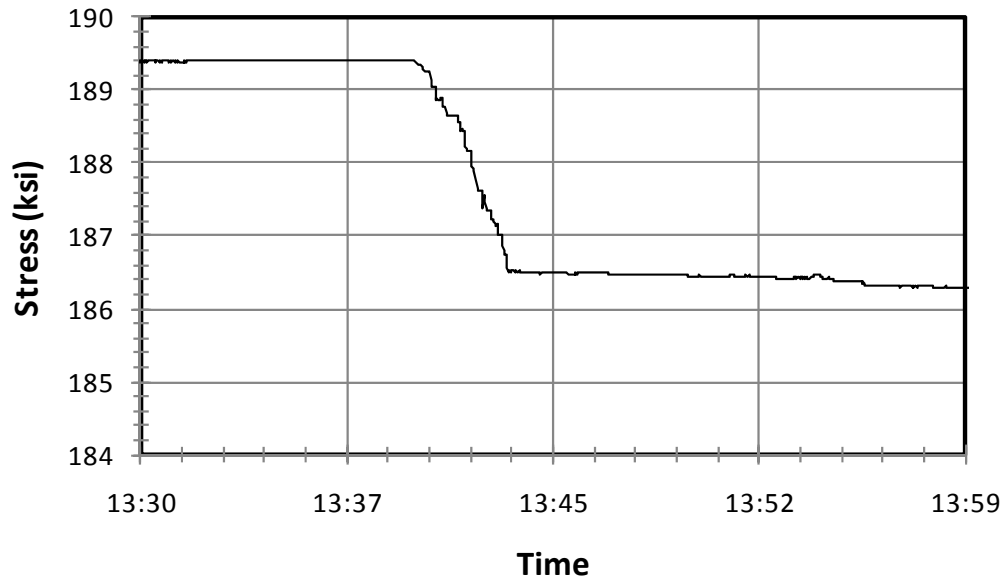


Figure 7.4 Stress in prestressing strands at the center of Specimen C4 during release

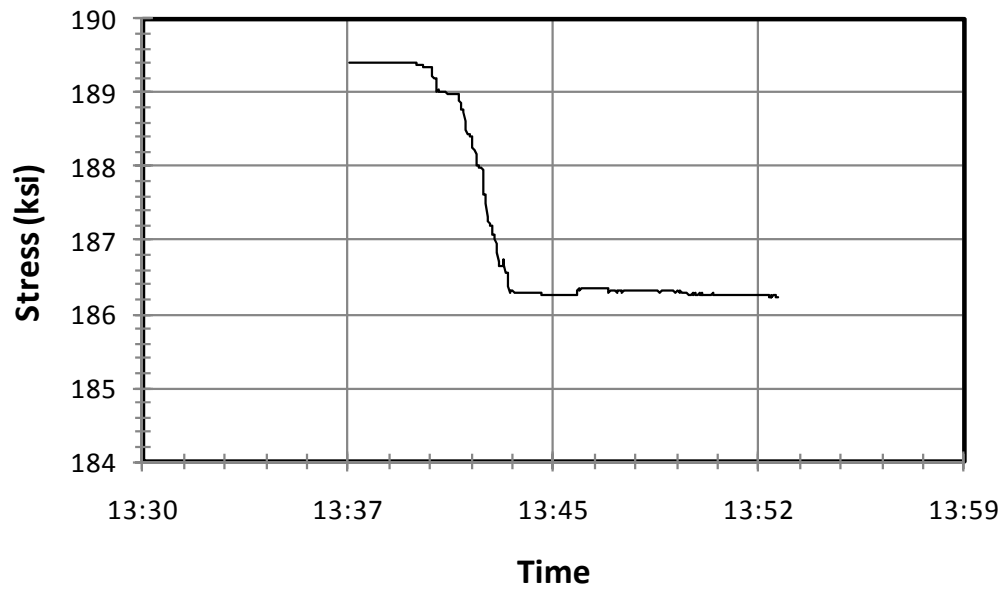


Figure 7.5 Stress in prestressing strands at the center of Specimen C5 during release

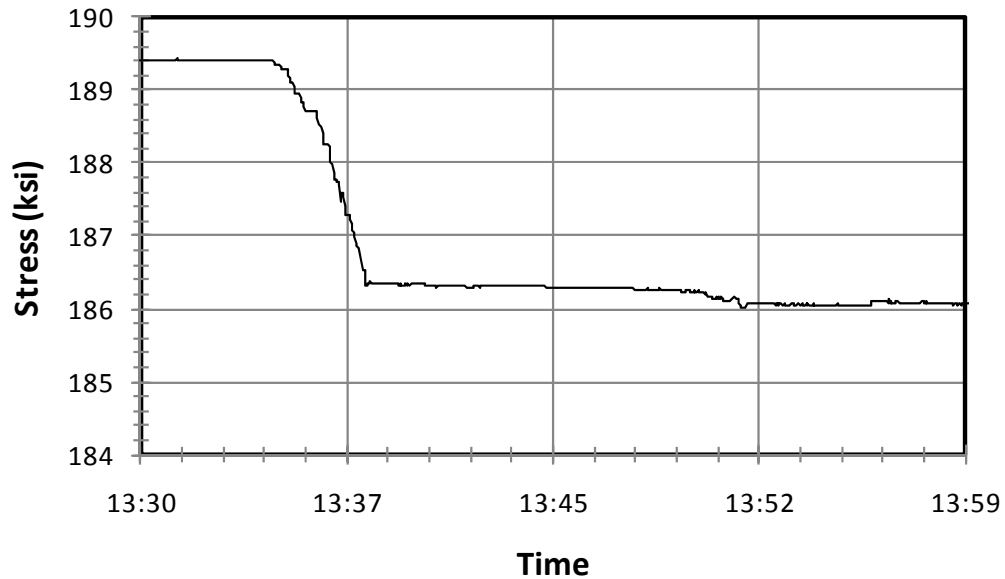


Figure 7.6 Stress in prestressing strands at the center of Specimen M3 during release

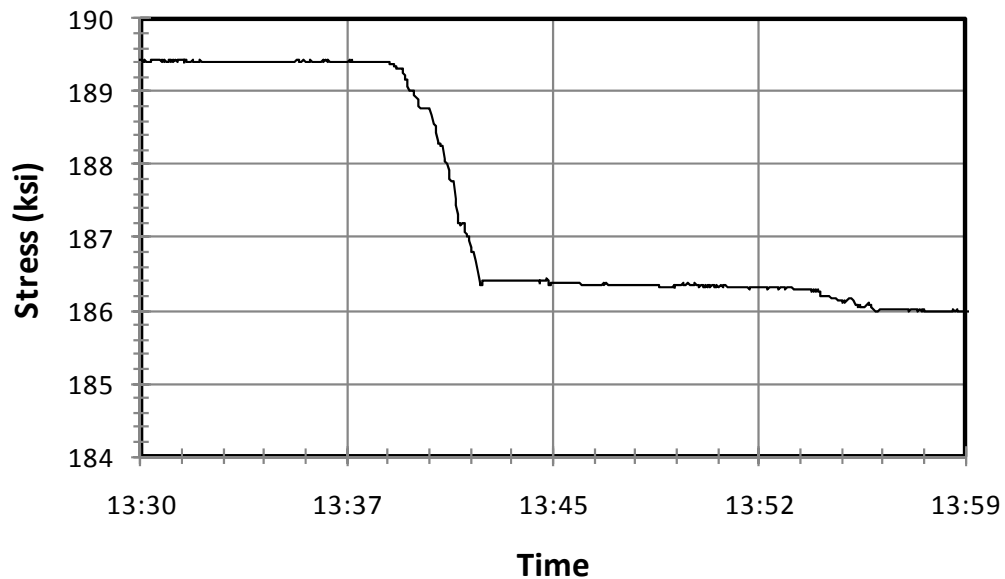


Figure 7.7 Stress in prestressing strands at the center of Specimen M4 during release

Elastic shortening in panels from Plant B resulted in an average prestress loss of 3.2 ksi. Vibrating wire gages (VWGs) were installed next to Gages #10 in the panels from Plant B. The average prestress loss measured by the VWGs was 3.1 ksi. In Table

7.1 are compared the predicted and measured values of elastic shortening for all panels monitored.

Table 7.1 Calculated versus measured values of elastic shortening (ksi)

AASHTO 2008		
Eq. (5.9.5.2.3a-1)	5.0	
Plant A Panels		Gage #6
C2	4.0	
M1	3.3	
M2	3.1	
<i>Average</i>	3.5	
Plant B Panels		Gages #10
		VWG
C4	3.0	3.2
C5	3.1	3.1
M3	3.1	3.1
M4	3.4	2.9
<i>Average</i>	3.2	3.1

7.1.2 Long-Term Prestress Losses (Creep, Shrinkage, and Relaxation)

7.1.3 Estimated Losses

7.1.3.1 AASHTO 2004

TxDOT currently designs bridges to meet the 2004 AASHTO Specifications. When applied to TxDOT's panel design, the 2004 AASHTO equations predict an ultimate prestress loss of 24.2 ksi (calculations provided in the Appendix). These values are time-independent.

7.1.3.2 AASHTO 2008

The AASHTO prestress loss equations were significantly changed in 2008, to give time-dependent values. Since the specimens of this study are monitored over time and tested at various ages, a time-dependent prediction method provides a more reasonable comparison. When evaluated at 10,000 days, the 2008 equations predict an ultimate prestress loss of 32.6 ksi. Predicted time-dependent prestress losses for individual specimens (based on age) are summarized in Table 7.2, and calculations are provided in the Appendix.

7.1.4 Observed Losses

Data acquisition systems were set to record a strain value every thirty minutes. Barring maintenance or malfunction, the panels were monitored continuously once fabricated. These long-term strain data were used to calculate long-term prestress losses.

To better understand the effects of creep, shrinkage, and relaxation, it was necessary to correct the data for the effects of temperature. For this purpose, thermal expansion was assumed to be linear and the coefficient of thermal expansion (CTE) was assumed constant. The limestone-aggregate panels from Plant A were assumed to have a CTE of $6 \times 10^{-6}/^{\circ}\text{C}$. Temperature data for the Plant A specimens were recorded directly by the data-logger, whose temperature records provide an accurate estimate of the temperature of the air at the location of the panels.

The temperature of the air at the location of the panels was not necessarily a perfect indicator of the temperature in each individual panel, however. Because the panels were stacked in piles of four, three, or two (depending on the date), and because the order in which the panels were stacked was not consistent, whichever panel was on the top of the stack would receive direct sunlight while the other three would be shaded. Nevertheless, air temperature was the only datum available for the Plant A specimens, and a CTE of $6 \times 10^{-6}/^{\circ}\text{C}$ was used with the air temperature data to provide an average temperature correction for all the panels.

Each panel from Plant A had 4 PMFL embedment gages installed parallel to the strands (Figure 4.5 and Figure 4.6). Gage #6 is located in the center of the panel, where prestress losses are expected to be the highest. Data from Gages #6 in the four Plant A panels were used to calculate the prestress losses. Figure 7.8, Figure 7.9, Figure 7.10, and Figure 7.11 show the stress in the strand in the center of each Plant A panel. Because Specimens C1 and M1 were tested and destroyed in the lab, there is not as much data for them. Because the time axes on the plots are all scaled the same, however, the data can be directly compared.

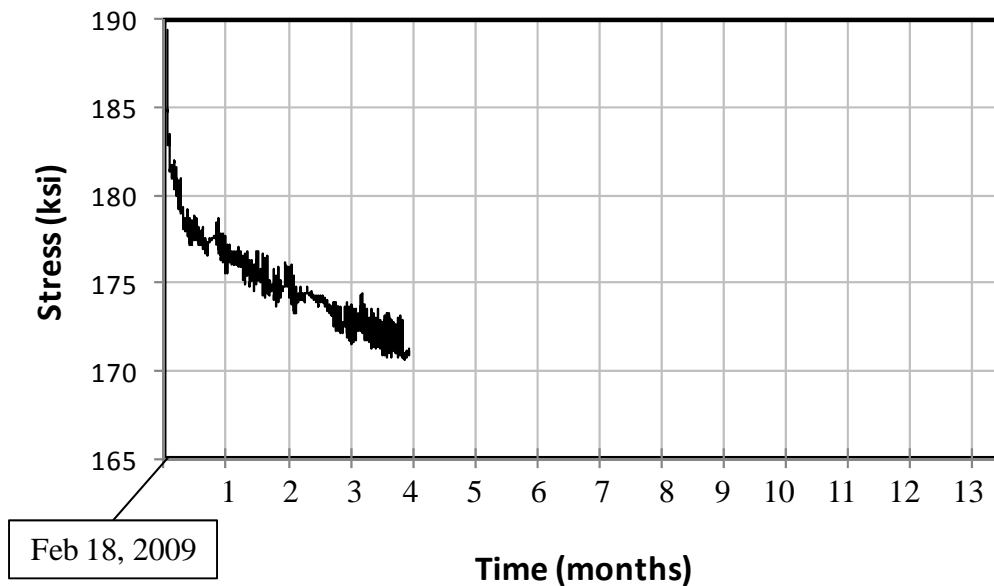


Figure 7.8 Stress in the strand at the center of Specimen C1

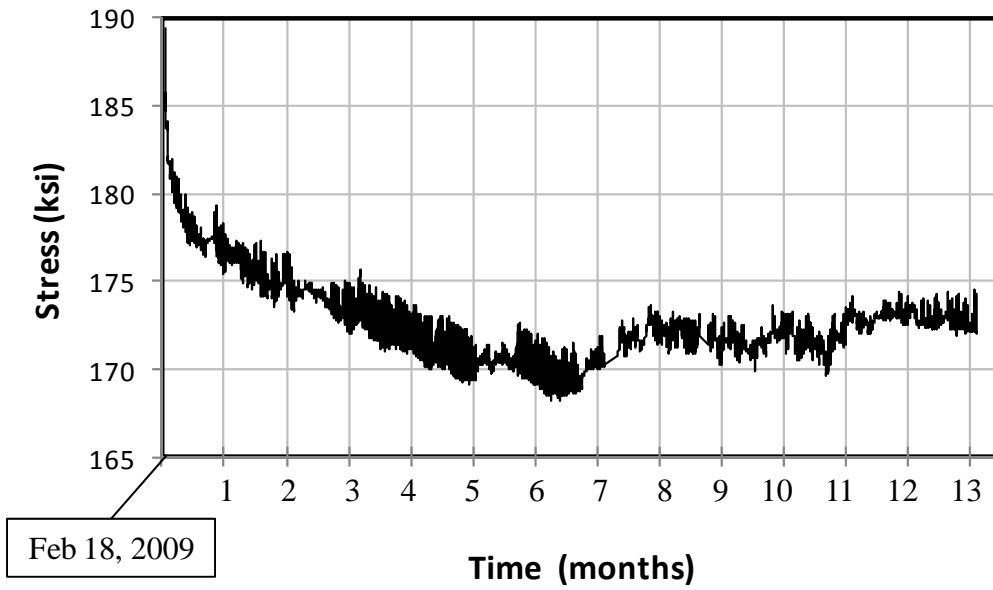


Figure 7.9 Stress in the strand at the center of Specimen C2

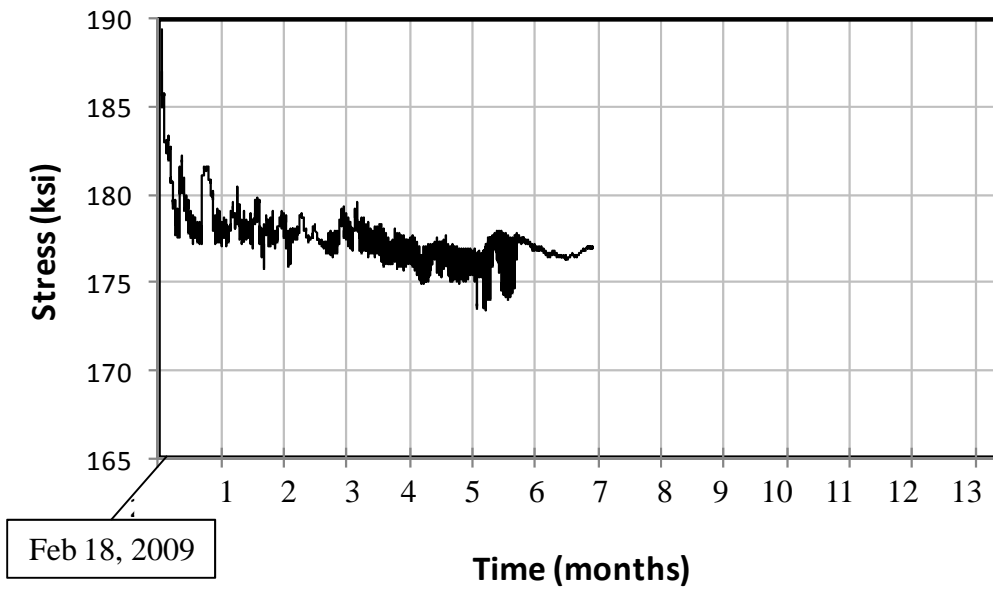


Figure 7.10 Stress in the strand at the center of Specimen M1

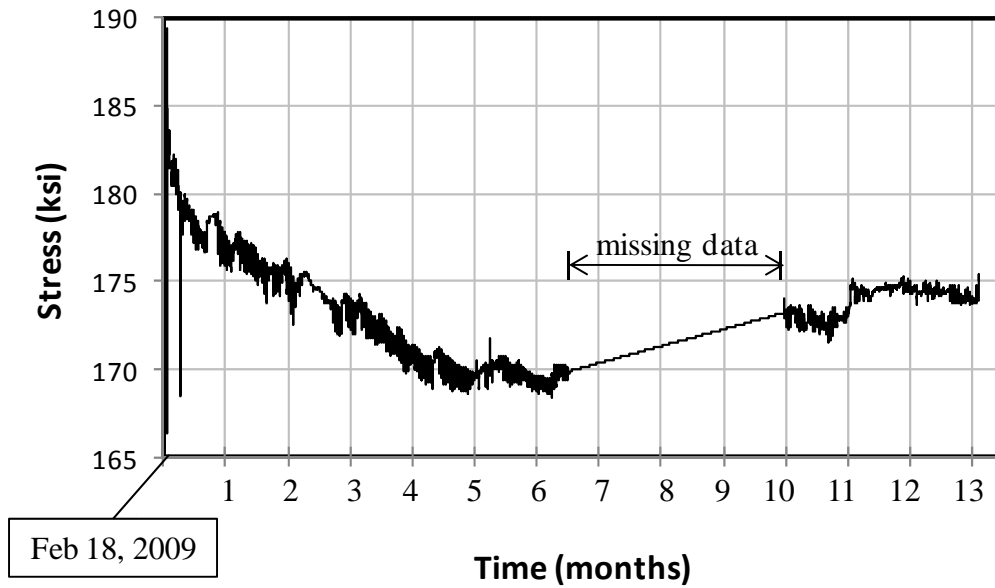


Figure 7.11 Stress in the strand at the center of Specimen M2

Specimens C2 and M2 have been monitored for over a year. After about seven months, the stress in the panels stabilized. Due to atmospheric changes such as increased humidity, some losses were even shown to recover, slightly. Of the four Plant A panels monitored, the greatest prestress loss recorded was 23.1 ksi in Specimen M2. Figure 7.12 shows the stresses in the center of each panel, plotted on a single set of axes. Also included in the plot are the lump-sum 45-ksi prestress loss currently used by TxDOT, the total loss predicted by the 2004 AASHTO method, and the total loss predicted by the 2008 AASHTO method.

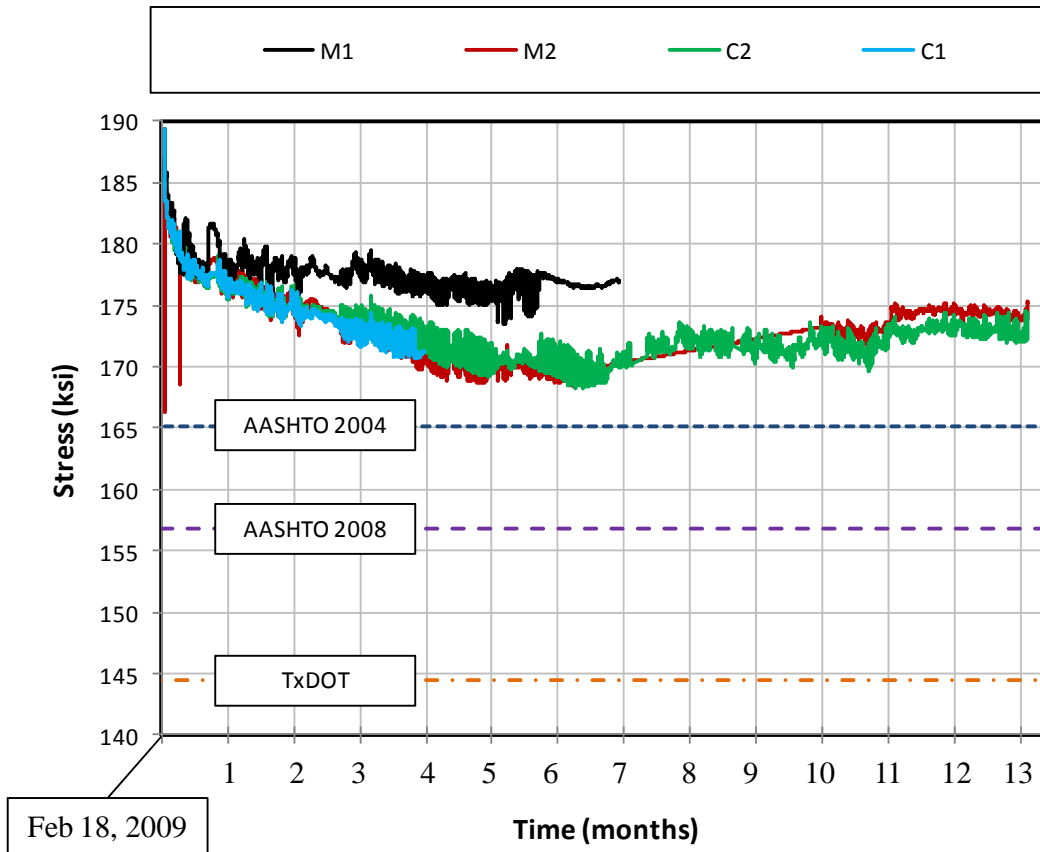


Figure 7.12 Long-term stresses in the center strand of Plant A panels as well as lump-sum code values

For the river-gravel panels from Plant B, a CTE of $7.5 \times 10^{-6} / ^\circ\text{C}$ was used. The four panels fabricated at Plant B each had a thermocouple installed in the center of the panel, permitting a more accurate correction for temperature. Additionally, VWGs were installed in the center of the Plant B panels, next to Gage #10 (Figure 6.4). The VWG data provides a good way to check the performance of the PMFL embedment gages. Gage #10 is the center gage for the Plant B specimens. The data from Gages #10 were used to calculate the stress in the strand in the center of each panel. Those data are presented in Figure 7.8, Figure 7.9, Figure 7.10, and Figure 7.11. A portion of the data from Specimen C5 was corrupted and unusable.

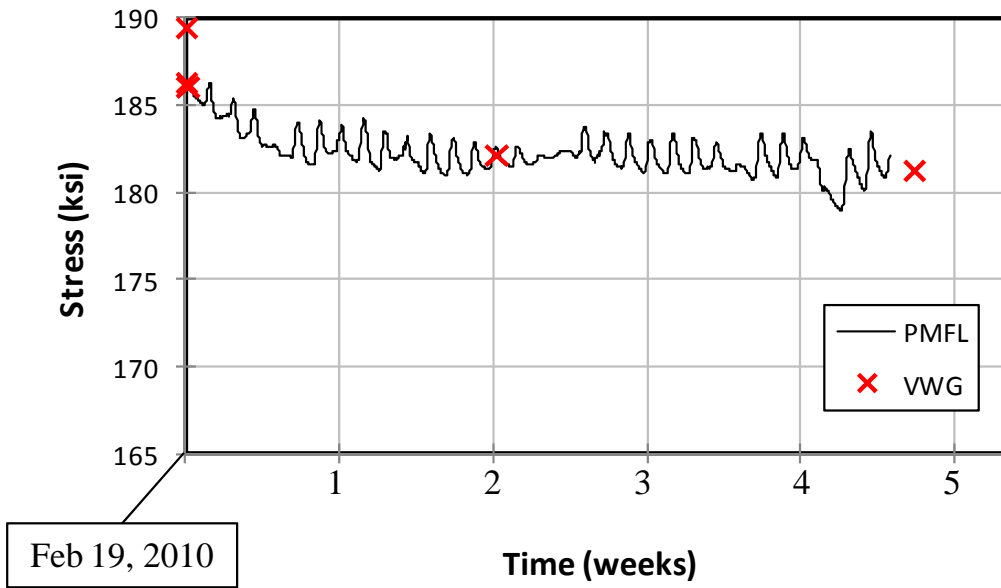


Figure 7.13 Stress in the strand at the center of Specimen C4

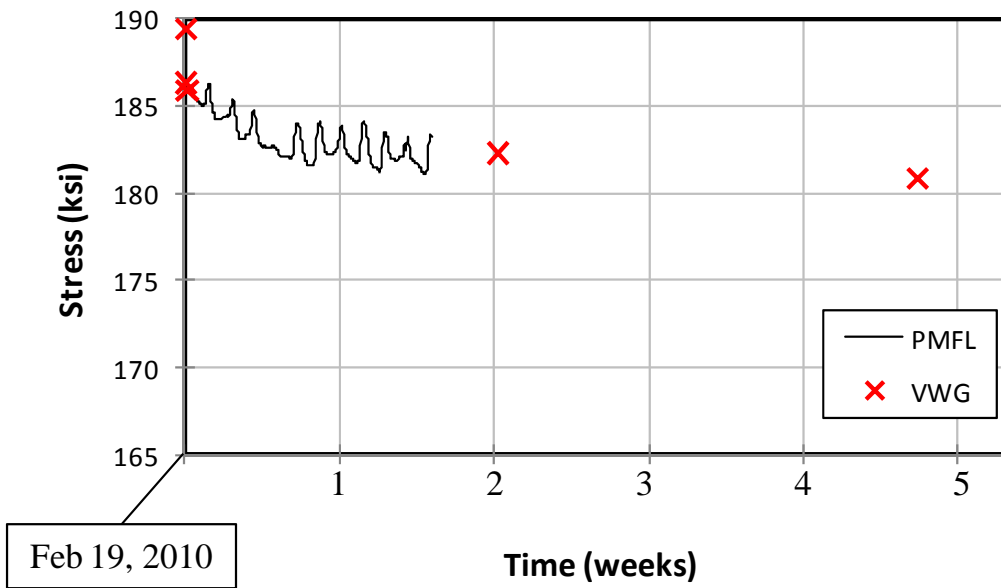


Figure 7.14 Stress in the strand at the center of Specimen C5

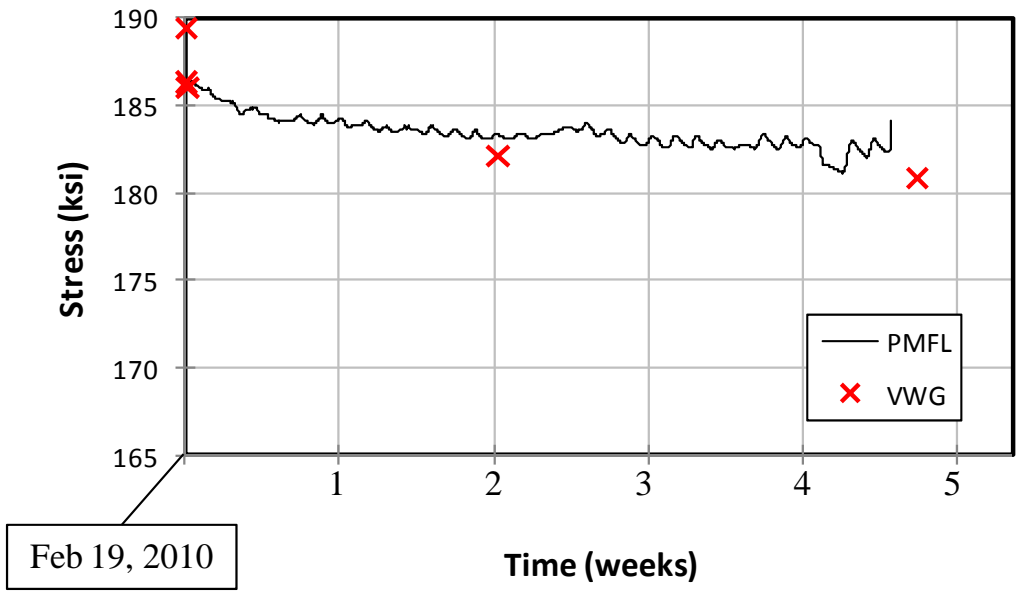


Figure 7.15 Stress in the strand at the center of Specimen M3

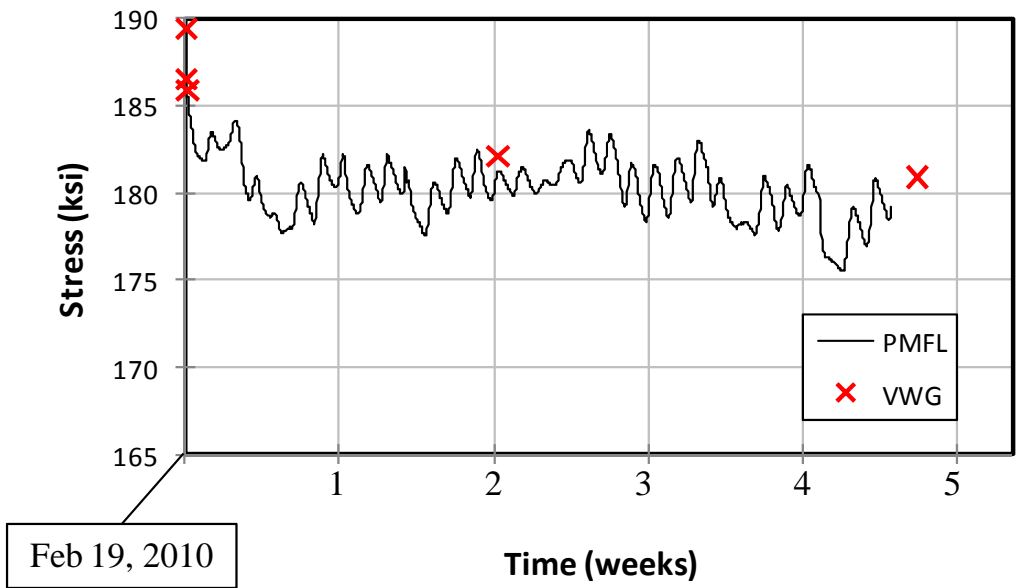


Figure 7.16 Stress in the strand at the center of Specimen M4

Comparing the PMFL data to the VWG data shows a good agreement between the two. One month of data, however, is not enough to confirm this agreement, so the VWGs must continue to be monitored.

Insufficient data exist from the Plant B panels to estimate final losses. As shown in Figure 7.17, visual comparison of the first month of data from the limestone-aggregate panels (Plant A) to the first month of data from the river-gravel aggregate panels (Plant B) indicates that the two sets of panels are behaving similarly. On average, during the first month, prestress losses were about 10% lower for the river-gravel panels than for the limestone-aggregate panels.

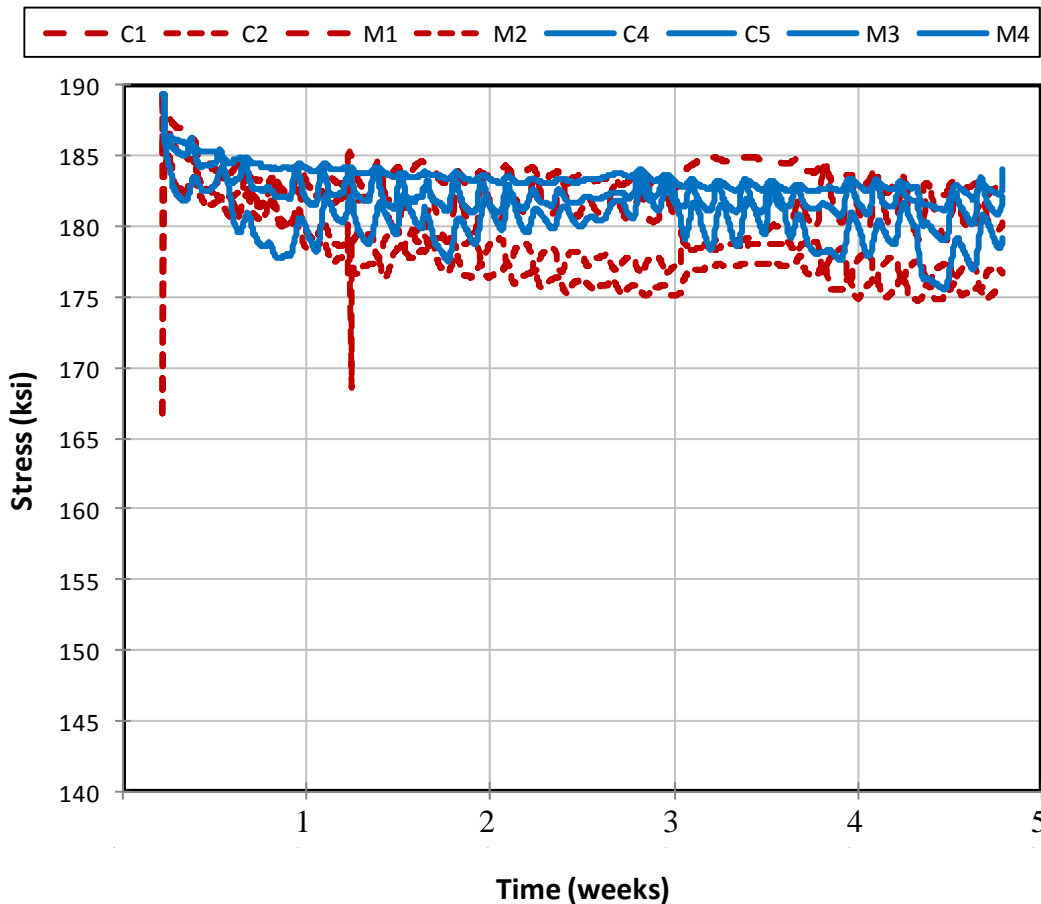


Figure 7.17 Stress in the strand at the center of limestone and river-gravel panels (limestone is dashed and river-gravel is solid)

Table 2 provides a summary of total prestress loss measurements and predictions. For the Plant A panels, the 2008 AASHTO equations over-predicted prestress losses by an average of 40%. However, the 2004 AASHTO equation predicted an ultimate prestress loss of 24 ksi. The largest losses measured so far have been 23 ksi. If prestress losses have stabilized in Specimen M2, then the 2004 AASHTO equations are quite accurate.

Table 7.2 Summary of long-term prestress losses and predictions

Plant A Panels	Age (days)	PMFL #(ksi)	VWG (ksi)	AASHTO 2008 (ksi)
C1	138	19.1	-	26.4
C2	397	21.2	-	30.1
M1	202	16.0	-	28.1
M2	397	23.1	-	30.1
Average		19.8		28.7
Plant B Panels				
C4	33	10.4	8.2	17.5
C5	33	-	8.4	17.5
M3	33	8.3	8.6	17.5
M4	33	13.9	8.5	17.5
Average		10.9	8.4	17.5
	AASHTO 2004	AASHTO 2008		
At 10,000 days	24.2	34.0		

7.2 TRANSVERSE TENSILE STRESSES DURING RELEASE

Transverse strains in the test panels were measured during release at each plant, and those measured strain values were used to estimate tensile stresses in the edges of the panels during release. TxDOT requires a compressive strength of 5,000 psi for release but material tests reported by Plants A and B indicate an average release strength of 6,500 psi. Assuming a compressive strength of 6,500 psi, Equation 7.1 was used to calculate an average modulus of elasticity of concrete at release.

$$E_c = 57000\sqrt{f'_c} \quad \text{Equation 7.1}$$

Based on the measured strains and the assumed modulus of elasticity, the tensile stresses in the edges of the panels were calculated. The maximum tensile stresses calculated in each panel are summarized in Table 7.3.

Table 7.3 Summary of maximum calculated tensile stresses at panel edges during release

Plant	Panel	Strain (in/in)	Tensile Stress (psi)
A	C2	0.00004	184
A	M1	0.000023	106
A	M2	0.000028	129
B	C4	0.00005	230
B	C5	0.000036	165
B	M3	0.000019	87
B	M4	0.00003	138

Several different methods exist for experimentally determining the tensile strength of concrete. Three common ways of measuring tensile strength are shown below in Figure 7.18. The most common of the three is the modulus of rupture (MOR) test.

The tensile strength determined by an MOR test is generally taken to be $7.5\sqrt{f'_c}$.

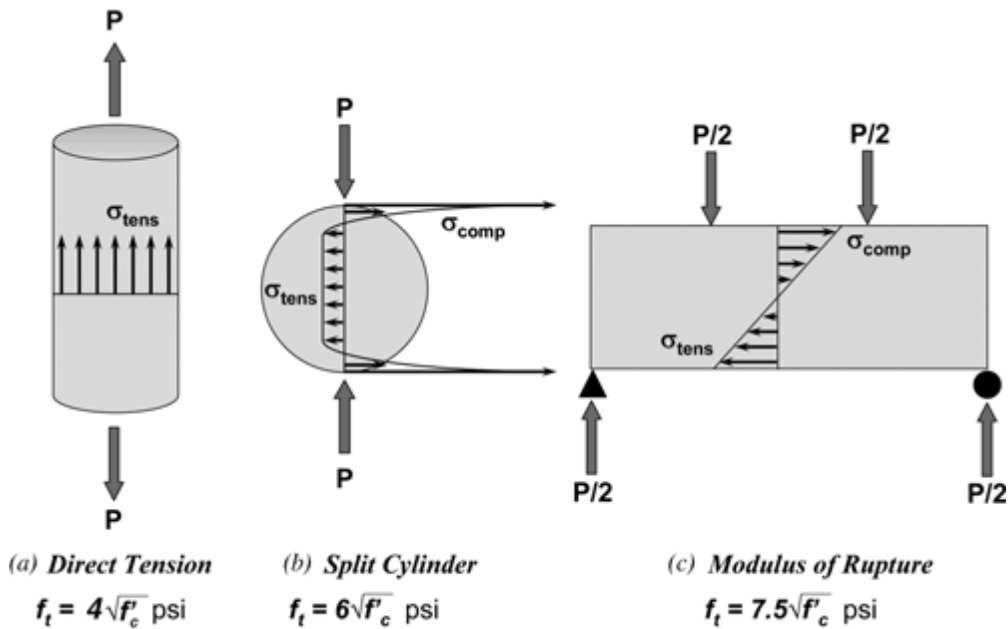


Figure 7.18 Testing methods used to determine tensile strength of concrete
(Tuchscherer, 2009)

A compilation of 1330 data points taken from MOR tests over the last 80 years is shown in Figure 7.19. Various models relating the tensile strength of concrete to $\sqrt{f'_c}$ are also plotted in Figure 7.19. The figure shows that the tensile strength of concrete is highly variable, and that $7.5\sqrt{f'_c}$ is an approximation which tends to be conservative at high compressive strengths. According to Figure 7.19, the lowest MOR values reported for tests of concrete with a compressive strength of 5,000-6,500 psi are around 400-500 psi. A direct tensile strength would be expected to be 4/7.5 (53%) of 400-500 psi, which is 210-265 psi. The greatest tensile stress calculated in the panels during release was 230 psi. While the stresses measured in the panel test specimens do not exceed most of the reported tensile strengths plotted in Figure 7.19, they may exceed a few. In short, it is clear that the maximum tensile stresses inferred from strains measured at panel edges during release were in the neighborhood of the cracking strength of concrete. On average, concrete stresses should be below the cracking strength, but in some instances

panels may crack, based on the information presented in Table 7.3, Figure 7.18, and Figure 7.19. This observation is consistent with the frequency of panel cracking and rejection seen in precast plants.

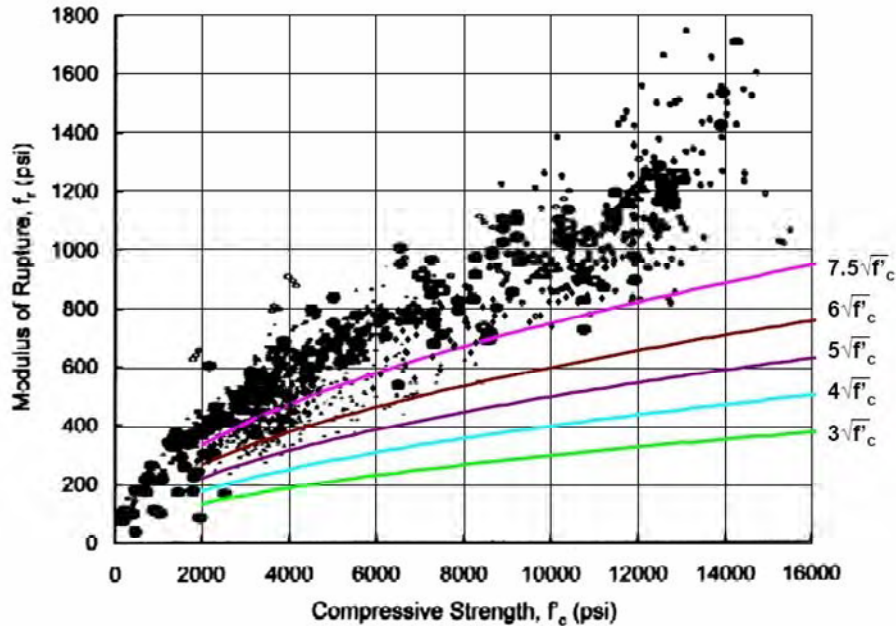


Figure 7.19 Relationship between modulus of rupture and compressive strength of concrete (Tuchscherer, 2009)

7.3 EFFECTIVENESS OF BURSTING REINFORCEMENT

A secondary goal of this thesis is to determine the feasibility of controlling cracking with additional transverse reinforcement in panel edges. The M-series test specimens have a modified design which includes additional reinforcing bars at the edges. One edge of each panel has one additional #3 reinforcing bar. The other edge has two additional bars, one spaced 5/8 in. above the other. All additional bars were placed in the top half of the panel.

To compare how well the additional bars controlled crack growth, panel Specimens C1, C3, and M1 were tested in the lab as described in Chapter 5. Because of unexpected issues encountered while testing Specimen C1 (also described in Chapter 5),

results from Specimen C3 were used instead of Specimen C1. While the panels were bent over the knife edge, cracks were counted, crack widths were measured, and the panel edges were photographed. Specimens C3 and M1 were both tested to failure, indicated by the rupture of the reinforcement.

An edge of Specimen C3 after testing is shown in Figure 7.20. With no additional reinforcing bars, the crack distribution is fairly uniform. A small number of cracks formed, most coinciding with the location of a strand.



Figure 7.20 Edge of Specimen C3 after testing

The single-bar edge of Specimen M1 after testing is shown in Figure 7.21. Compared to Specimen C3, the additional bar resulted in a 20% decrease in crack spacing and a 27% increase in number of cracks. A decrease in crack spacing also means a decrease in crack widths. Although the main crack is very wide at the center of each panel, that crack width is kept small at the single-bar edge of the modified specimen.

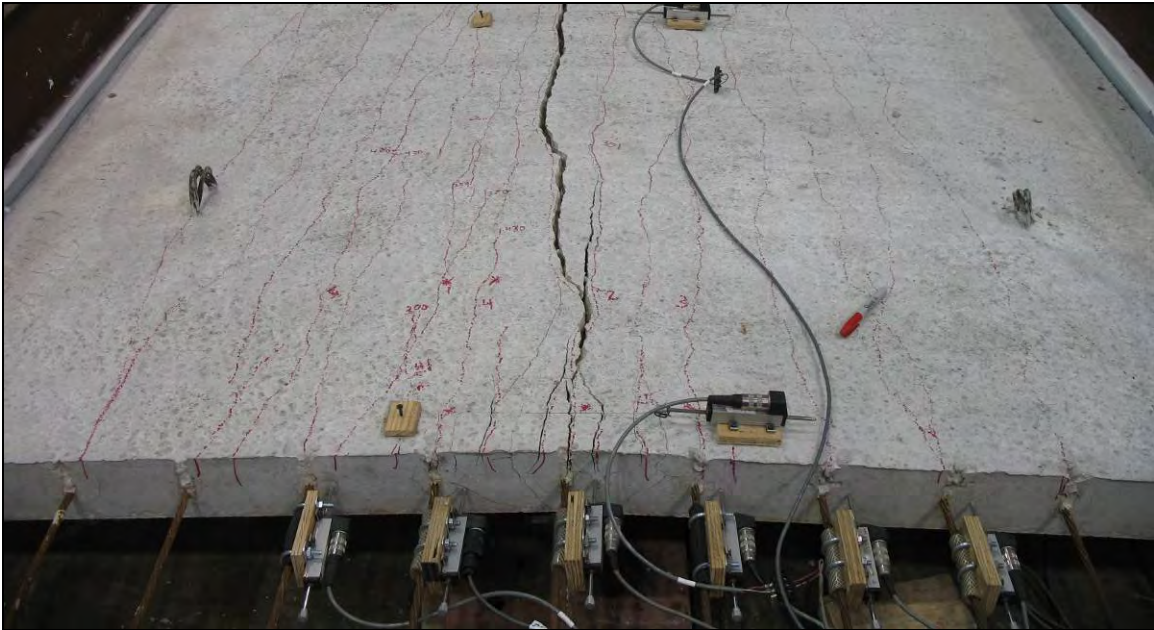


Figure 7.21 Single-bar edge of Specimen M2 after testing

The double-bar edge of Specimen M1 after testing is shown in Figure 7.22. Compared to the single-bar, the double-bar creates even smaller crack spacings and an additional 17% more cracks. Some of the cracks are still aligned with the prestressing strands, but because the number of cracks is so high, the width of any single crack is smaller than it would be with fewer total cracks. Considering all three edges, it is clear that more transverse reinforcement results in more cracks with smaller spacing and smaller widths. Prestress loss occurs only if a crack is collinear with a strand. For each edge condition, some collinear cracks formed. The collinear cracks are smaller in width, however, with an additional bar than without. Collinear crack widths are even smaller when two additional bars are added rather than one.

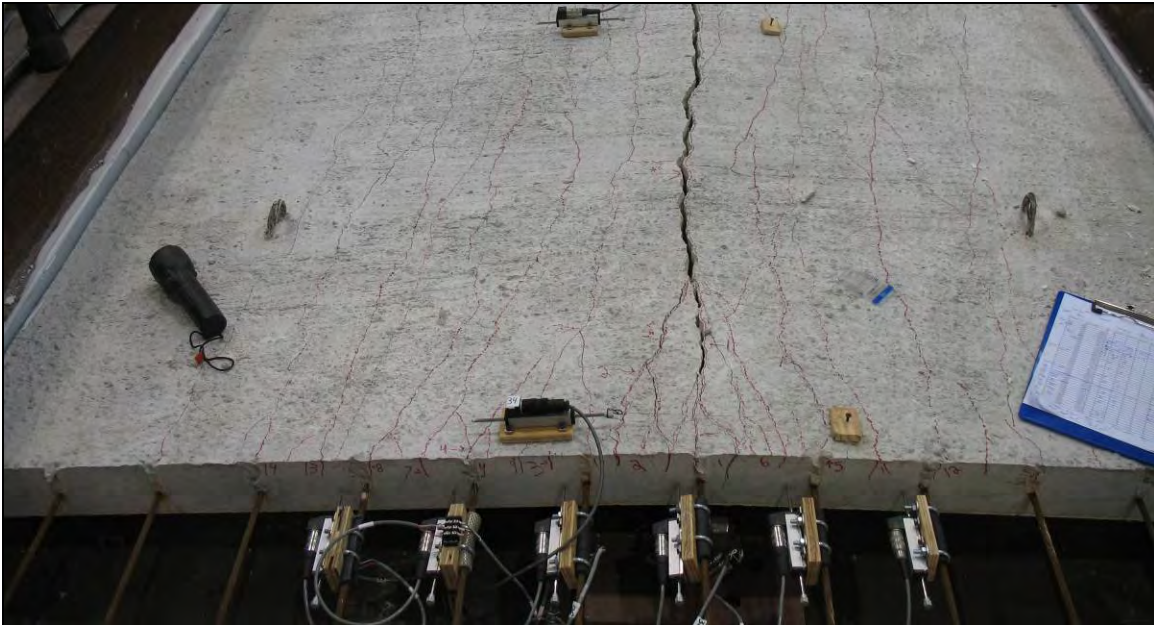


Figure 7.22 Double-bar edge of Specimen M2 after testing

7.4 EFFECTS OF CRACKING ON PRESTRESS LOSSES

In this research, the main question regarding cracks in PCPs is how panel cracking affects the loss of prestress in the strands. Based on the knife-edge tests described in Chapter 5, which included the use of slip gages to monitor strand slip as cracking occurred, it was observed that strands do not slip unless a crack coincides directly with the strand.

As the panels were tested in transverse flexure, crack widths over strands were measured with crack comparators. The smallest measureable crack width was 0.002 in. Common crack widths observed in rejected panels by TxDOT inspectors are estimated by TxDOT to be 0.01 in. Assuming that measured strand slip is distributed evenly along the length of a strand, it is possible to estimate the total amount of prestress remaining in one prestressing strand for which slip is measured (example calculation shown in the Appendix). In reality, any measured slip was likely to be concentrated in the development length of the strand, near the edge of the panel. However, it is conservative to assume the slip is distributed along the entire strand. Figure 7.23 shows the

relationship between crack width and percentage prestress force remaining in particular strands. The strands represented are those that had a collinear crack wide enough to be measured by with a crack comparator. This included one crack on the double-bar edge of Specimen M1, three cracks on the single-bar edge of Specimen M1, and four cracks from Specimen C3 (no additional reinforcement). The cracks from Specimen C3 are shown with solid lines, and the cracks from Specimen M1 are shown with dashed lines.

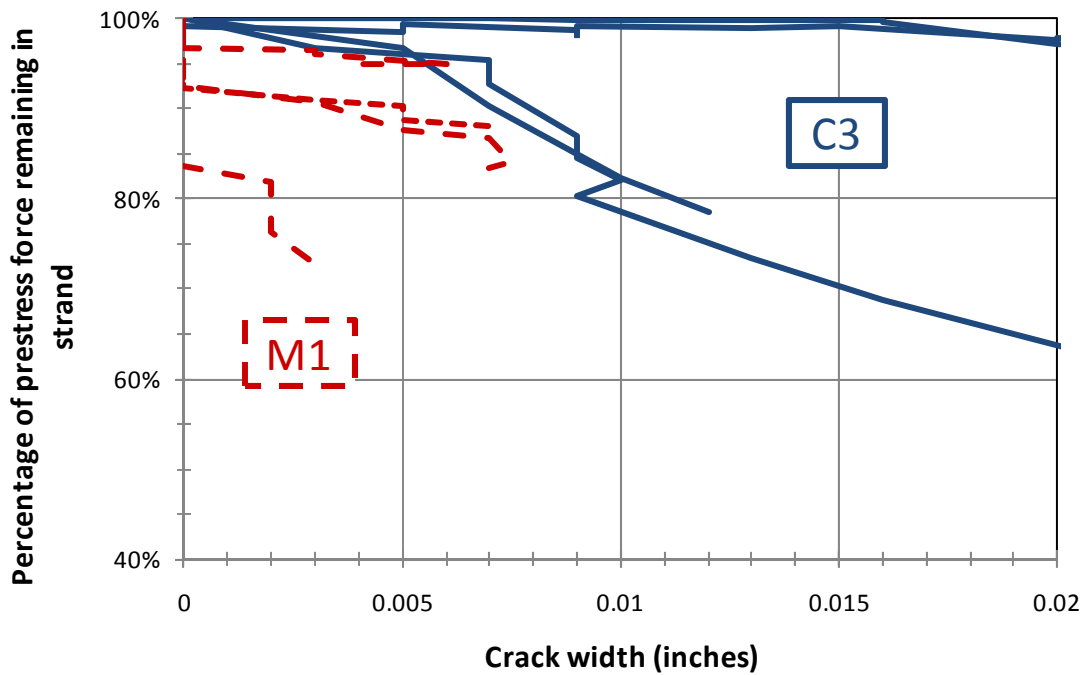


Figure 7.23 Percentage of prestress force remaining in a strand vs. width of collinear crack (typical crack widths)

As shown in Figure 7.23, the collinear cracks in Specimen M1 never exceeded 0.008 in. in width. The cracks in Specimen C3 reached much larger widths, up to 0.06 in. However, such wide cracks are not relevant in this study. The main observation to be made from Figure 7.23 is that in panels with the minimum required transverse reinforcement, collinear cracks up to 0.01-in. wide cause a loss of prestress in the affected strand of no more than a 20%, and sometimes of less than 3%. Considering that

there are 16 strands in one PCP, a loss of 20% of the prestress force in two different strands would result in a 2.5% reduction of prestress force in the PCP.

To evaluate the probable consequences of collinear cracks with widths corresponding to those commonly observed by TxDOT inspectors in the field, Figure 7.23 is scaled for crack widths up to 0.02 in. To evaluate the effect of cracks wide enough to cause a significant loss of prestress, however, it is necessary to plot much larger crack widths. As shown in Figure 7.24, when crack widths reach 0.05 in., losses begin to reach 50%. A prestress loss of 50% in two strands of a panel would result in a 6.3% reduction of the prestress force in that PCP.

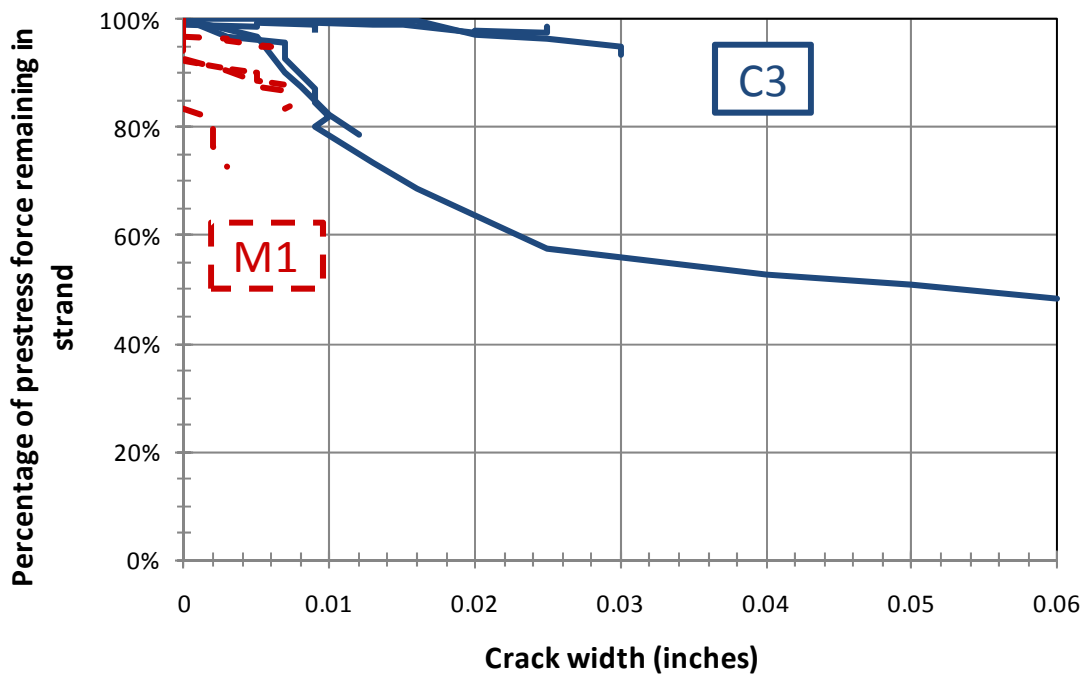


Figure 7.24 Percentage of prestress force remaining in a strand vs. the width of a collinear crack (wide cracks)

CHAPTER 8

Summary, Conclusions, and Recommendations

8.1 SUMMARY OF THESIS

Within the context of Study 6348, the goal of the specific research described here is to reduce cracking of precast, prestressed panels (PCPs). One way to accomplish this would be to reduce the initial prestress force. The initial prestress force could be reduced if it could be shown that the actual prestress losses were significantly lower than assumed. To be able to calculate actual prestress losses, ten precast panels were fabricated at two different precasting facilities. Eight of those panels were instrumented with embedded concrete strain gages, and panel strains were monitored over the life of the panels. Based on the observed strains and on assumed relationships between stress and strain, actual prestress losses were calculated, and were found to be no larger than 24 ksi.

Experiments were conducted to determine the effects of panel cracking on prestress losses, and to evaluate the effectiveness of additional transverse reinforcement as a means of controlling cracks. Three panels fabricated at Plant A were tested at Ferguson Lab. Two panels were standard design TxDOT panels, and one panel had additional transverse reinforcement at both edges. Cracks parallel to the strands were induced into all three panels by bending them over a knife edge centered on the panel. During each test, prestress losses were estimated as a function of crack width using data from slip gages installed on critical strands of all three panels. The total number of cracks was also counted and the crack widths were measured by hand, to help assess the effect of the additional transverse reinforcing bars.

8.2 CONCLUSIONS

- 1) Longitudinal cracks form in precast, prestressed panels for many reasons. The most important is the initial prestress force in the concrete from the strands. Due to the nature of the bond between the strand and the concrete, the initial prestress produces circumferential tensile stresses in the concrete perpendicular to the axis of the strand. When these circumferential tensile stresses exceed the tensile strength of the concrete surrounding the strand, they produce radial cracks that propagate along the strand. The panel edges, where the highest prestress forces are transferred, are the critical regions for this cracking.
- 2) Other factors contributing to panel cracking are improper handling, storage, or transport. Panels are typically lifted from the prestressing beds using cranes and embedded lifting loops; then stacked 4 to 6 panels high with wood blocking (dunnage); and finally strapped or chained to truck beds and transported to the job site. Any uneven or sudden stresses caused in the critical edge regions of the panels could cause a crack. Sudden spikes in stress are common during transportation.
- 3) If a radial panel crack touches a strand, it decreases the circumferential stiffness of the concrete surrounding the strand, and thereby weakens the bond between the concrete and the strand. The wider the crack is, the greater the decrease in bond strength, and the greater the possible loss in prestress force.
- 4) In panels tested in the laboratory to induce flexural cracks parallel to the strands, minimal strand slip (less than 20%) was observed until the cracks were as wide as 0.01 in. This width is in the range of widths observed in the field. It is logical to

conclude that such crack widths do not significantly reduce the level of effective prestress in the panels.

8.3 RECOMMENDATIONS FOR DESIGN

- 1) Based on the panel testing completed to date, the present value of lump-sum prestress losses assumed in design (45 ksi) could be reduced to 25 ksi. This value is consistent with the 2004 AASHTO refined method for prestress loss prediction, and has been shown in this thesis to be a conservative (high) estimate of prestress losses in PCPs. However, such a change should not be implemented until all testing is complete and the change is supported by a more comprehensive set of data.
- 2) If the initial prestress force for PCPs could be reduced from 16.1 kips per strand to 14.4 kips per strand, the reduction of 1.7 kips per strand would be consistent with a change in estimated prestress loss from 45 to 25 ksi. This would reduce the initial prestress force by about 10.5%, which should reduce the frequency of crack occurrence.

8.4 RECOMMENDATIONS FOR IMPLEMENTATION

- 1) Additional reinforcing bars, oriented perpendicular to the prestressing strands, should be placed at each panel edge 1 inch below and 1 inch above the prestressing strands. This additional transverse reinforcement will help control crack widths and crack propagation parallel to the strands in the critical region of the panel. Although this transverse reinforcement will not prevent the formation of cracks, it will control the width of any cracks that form, and thereby reduce strand slip and associated loss of prestress.

- 2) Cracking in panels can be reduced by controlling flexural tensile stresses perpendicular to the strands. Panels should be stacked with dunnage in a straight vertical line. For transport, stacks of panels should be secured to trucks using straps placed in line with the dunnage. If dunnage is not placed in continuous vertical lines, the weight of the upper panels in a stack can produce flexural tensile stresses in the lower panels. If straps are not aligned with the dunnage, they can produce flexural tensile stresses in the strapped panels. Flexural tensile stresses can be increased by the dynamic response of the vehicle during transport.
- 3) TxDOT specifications require that a panel be rejected if a crack is found within 1 in. of a strand running parallel with the strand for at least 1/3 of the length of the strand. This rejection criterion reflects recommendations in the literature published by major prestressed concrete groups. The research described in this thesis, however, shows that strand slip does not begin until crack widths become very large. Based on research described in this thesis, TxDOT may choose to amend their rejection criterion to include a maximum allowable crack width of 0.05 in.

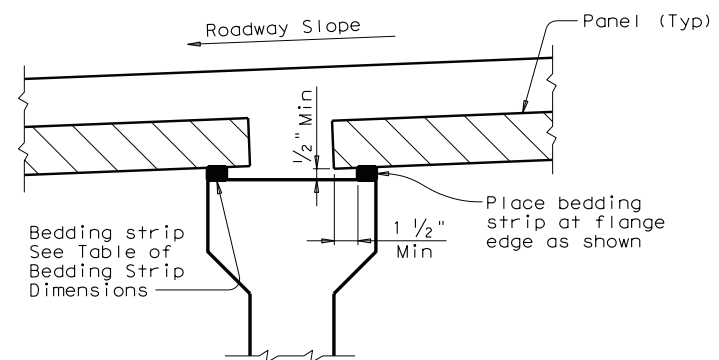
8.5 RECOMMENDATIONS FOR FUTURE INVESTIGATION

- 1) At least 12 more panels should be subjected to long-term monitoring. This increased sample size will provide a better knowledge of the statistical distribution of prestress losses, and will increase the credibility of our recommendations. The sample should include winter and summer panels, as well as limestone and river-gravel panels.
- 2) If a lower initial prestress force is accepted, trial bridge decks should be constructed using that lower prestress force.

APPENDIX

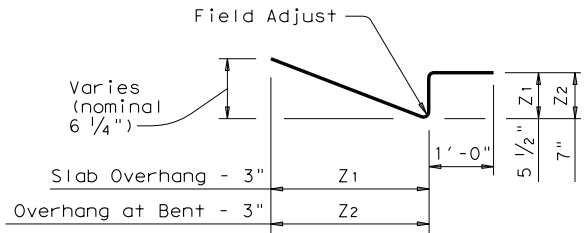
A.1 TXDOT PLANS

DISCLAIMER: The use of this standard is governed by the "Texas Engineering Practice Act". No warranty of any kind is made by TxDOT for any purpose whatsoever. TxDOT assumes no responsibility for the conversion of this standard to other formats or for incorrect results or damages resulting from its use.

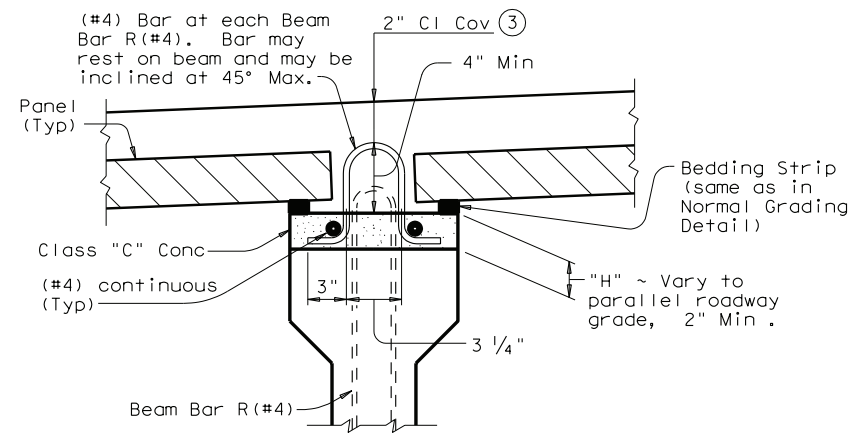


NORMAL GRADING DETAIL^①
 Showing Prestressed Concrete I-Beams.
 (Other Beam Types Similar)

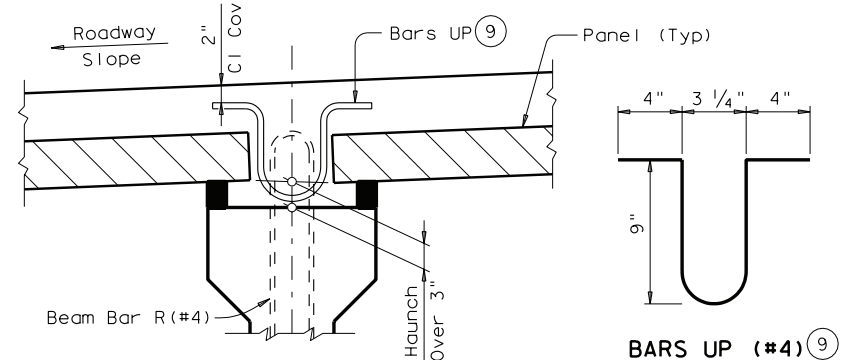
TABLE OF BEDDING STRIP DIMENSIONS		
WIDTH	HEIGHT ^②	
	Min	Max
1" (Min)	1/2"	2"
1 1/4"	1/2"	2 1/2"
1 1/2"	1/2"	3"
1 3/4"	1/2"	3 1/2"
2" (Max)	1/2"	4"



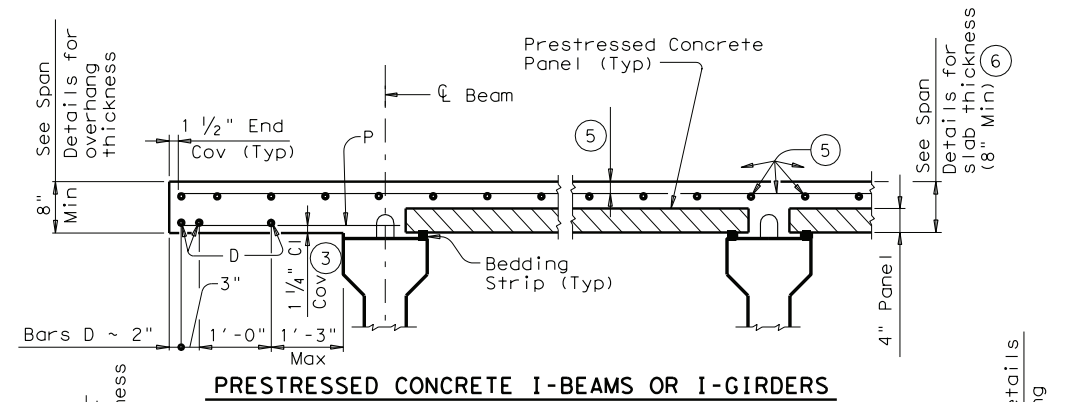
BARS Z (#4)^⑦



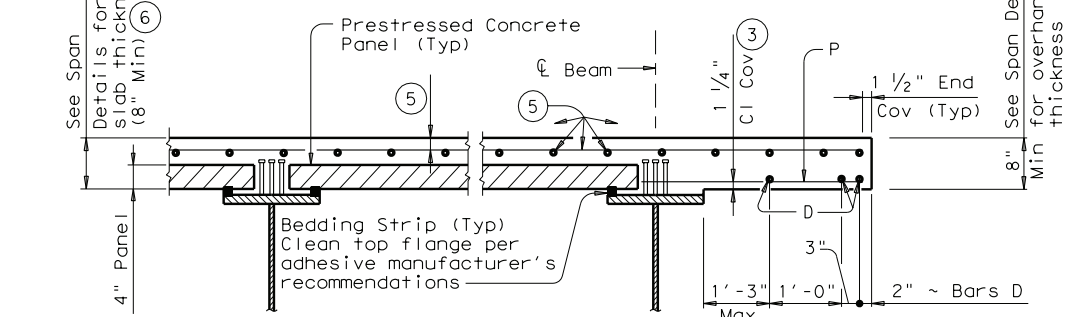
SPECIAL GRADING DETAILS FOR CONCRETE BEAMS^④
 Showing Prestressed Concrete I-Beams.
 (U-Beams and I-Girders Similar)



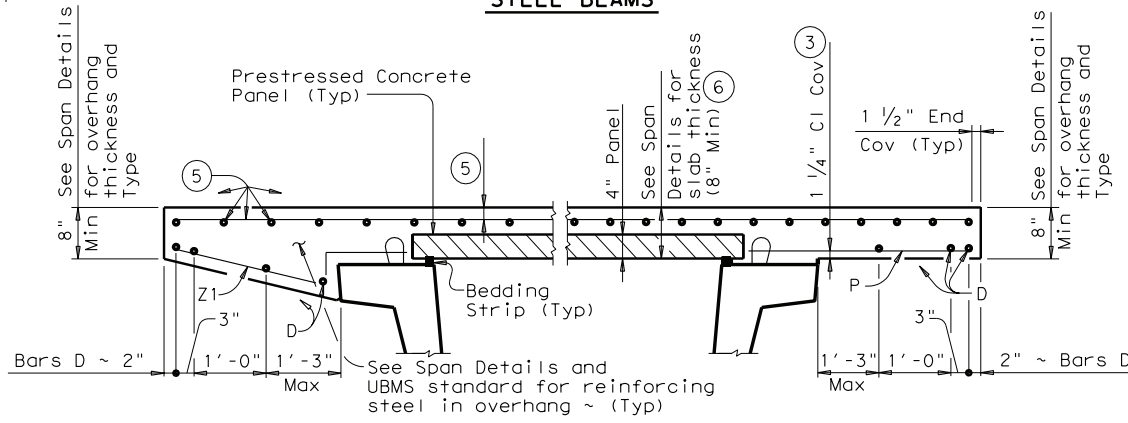
HAUNCH REINFORCING DETAIL
 Showing Prestressed Concrete I-Beams.
 (U-Beams and I-Girders Similar)



PRESTRESSED CONCRETE I-BEAMS OR I-GIRDERS



STEEL BEAMS



SLOPED OVERHANG WITH PRESTR CONC U-BEAMS **NORMAL OVERHANG WITH PRESTR CONC U-BEAMS**

TYPICAL PART TRANSVERSE SECTIONS

- ① To reduce the quantity of cast-in-place concrete, bedding strip thickness may be increased in 1/4" increments. Bedding strips must be comprised of one layer. Bond bedding strips to the beams with an adhesive compatible with bedding strips. Bedding strips over 2.5" high may need to be bonded to panels. The same thickness strip must be used under any one panel edge and the maximum change in thickness between adjacent panels must be 1/4". Alternatively, bedding strips may be cut to grade. Panels may be supported by an alternate method, using a commercial product, if approved by the Engineer of Bridge Design, Bridge Division.
- ② Height must not exceed twice the width.
- ③ Clear cover shall be as indicated unless otherwise shown on Span Details.
- ④ For use where the distance between top of beam and finished grade can not be achieved within tolerances on cast-in-place slab thickness and thickness of bedding strips. Control dimensions shown in Normal Grading Detail still apply.
- ⑤ See Span Details for top slab reinforcement and clear cover. Longitudinal top slab reinforcement may rest on top of prestressed concrete panels if necessary to maintain clear cover.
- ⑥ The actual thickness constructed may exceed the slab thickness shown on the Span Details but, the extra thickness shall be no more than 2" for Prestressed Concrete I-Beams and 1" for Prestressed Concrete U-Beams and Steel Beams. Bearing Seat Elevations or finished grade may be adjusted.
- ⑦ Bars Z1(#4) shall be field adjusted to match actual slope of slab overhangs. Width of slab overhang will vary along span with curved slab edges. Adjust Bar Z1(#4) dimensions to maintain proper cover. Bars Z2(#4) are located at Inv-T stems only.
- ⑧ Max Spacing as listed unless otherwise shown.
- ⑨ Space Bars UP(#4) with Beam Bars R(#4) in all areas where measured haunch exceeds 3".

CONSTRUCTION NOTES:

Erected panels must bear uniformly on bedding strips of extruded polystyrene placed along top flange edges.

If additional blocking is needed, special grading details for supporting the panels and extra reinforcing between beam and slab will be considered subsidiary to deck construction.

Care must be taken to ensure proper cleaning of construction debris and consolidation of concrete mortar under the edges of the panels. Bedding strips must be placed at beam flange edges so that adequate space is provided for the mortar to flow a minimum of 1 1/2" under the panels as the slab concrete is placed. To allow the proper amount of mortar to flow between beam and panel, the minimum vertical opening must be at least 1/2". Roadway cross-slope reduces the opening available for entry of the mortar. Bedding strips varying in thickness across the beam are therefore required.

All reinforcing steel in the cast-in-place slab must be Grade 60. See Table of Reinforcing Steel for size and spacing of reinforcement. Orientation of reinforcement (normal or skewed) must match that shown on the Span Details.

If the top and bottom layer of reinforcing steel is shown on the Span Details to be epoxy coated, then the A, D, E, P, & Z bars must be epoxy coated.

For clear span between U-beams less than or equal to 18", see Permissible Slab Forming Detail on Miscellaneous Slab Detail sheets, UBMS.

Bar Laps, where required, must be as follows:

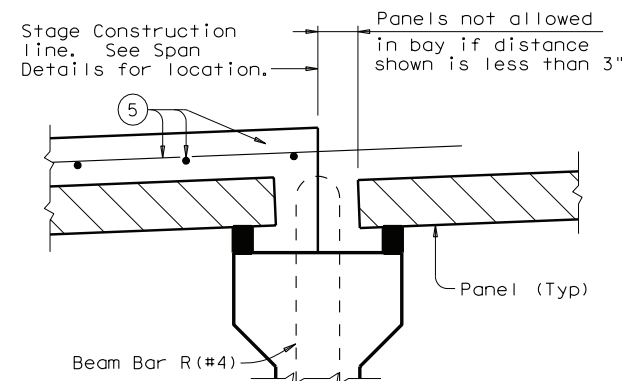
- Uncoated ~ #4 = 1'-5"
- ~ #5 = 1'-9"
- Epoxy Coated ~ #4 = 2'-1"
- ~ #5 = 2'-7"

GENERAL NOTES:

Designed according to AASHTO LRFD Specifications. Use of Prestressed Concrete Panels is not permitted for horizontally curved steel plate or tub girders. See Span Details for other possible restrictions on their use.

These details are to be used in conjunction with the Span Details and applicable Standard sheets.

Any additional reinforcement or concrete required on this standard is to be considered subsidiary to the bid item "Reinforced Concrete Slab".



STAGE CONSTRUCTION LIMITATIONS ON PANELS

Showing Prestressed Concrete I-Beams.
 (Other Beam Types Similar)

TABLE OF REINFORCING STEEL ^⑧		
BAR	SIZE	Max Spa (in.)
A	#5	~
D	#5	9
E	#5	6
P	#4	18
UP	#4	~
Z	#4	18



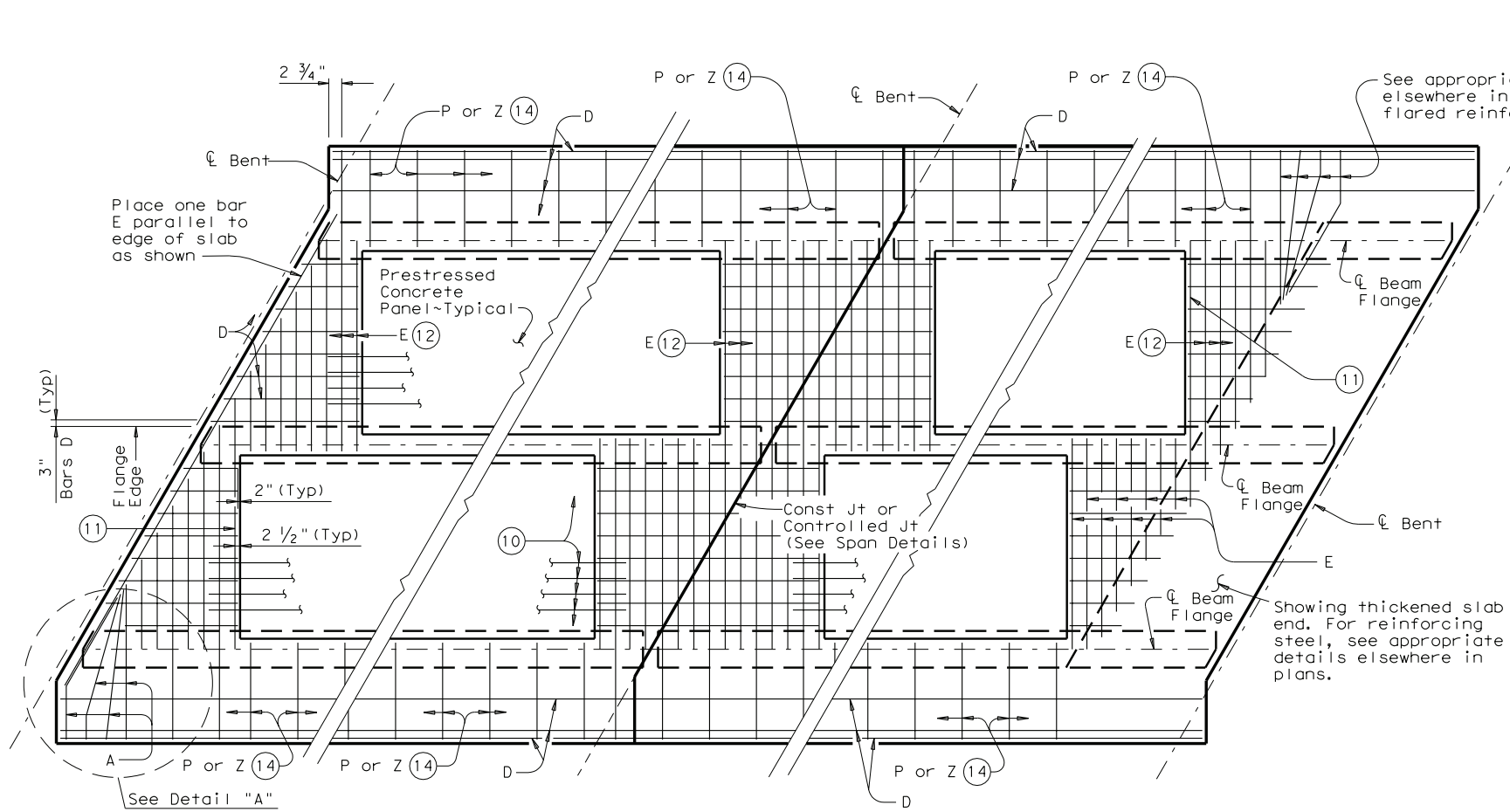
PRESTRESSED CONCRETE PANELS
OPTIONAL DECK DETAILS FOR BEAM SPANS

PCP

FILE: pcpsfde1.dgn	DN: TxDOT	CK: TxDOT	DW: TxDOT	CR: TxDOT
© TxDOT April 2006	DISTRICT	FEDERAL AID PROJECT		SHEET
REVISIONS				
08-07: Added I-Girders and added note to WWR splice detail.				
COUNTY	CONTROL	SECT	JOB	HIGHWAY

ACC:	
LEVELS DISPLAYED	
1	

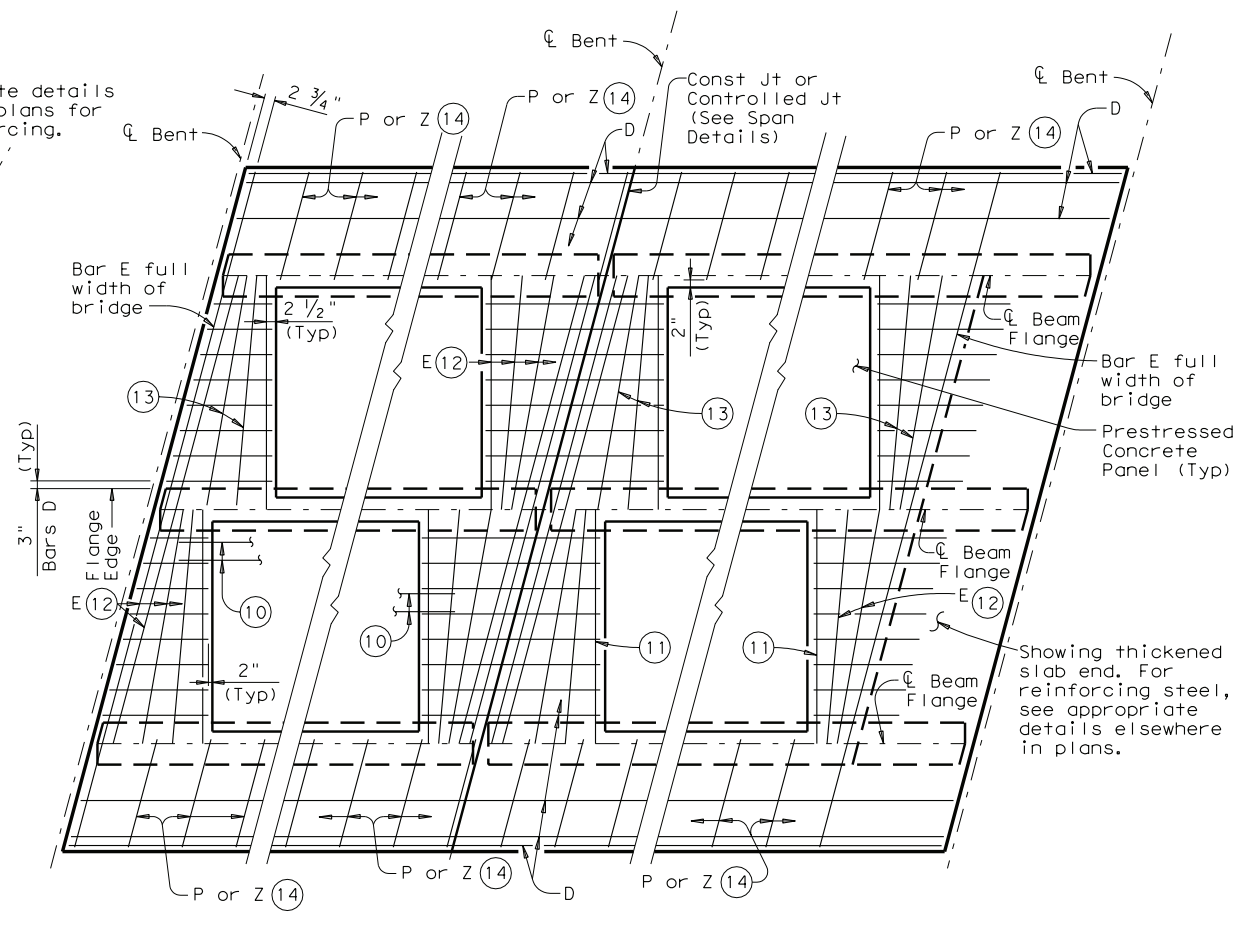
DISCLAIMER: The use of this standard is governed by the "Texas Engineering Practice Act". No warranty of any kind is made by TxDOT for any purpose whatsoever. TxDOT assumes no responsibility for the conversion of this standard to other formats or for incorrect results or damages resulting from its use.



AT ALL SPAN ENDS UNLESS NOTED OTHERWISE
 AT INTERIOR BENTS
 AT THICKENED END SLABS ON STEEL, CONC I-BEAMS, I-GIRDERS OR U-BEAMS

PLAN OF SLABS WITH NORMAL REINFORCEMENT

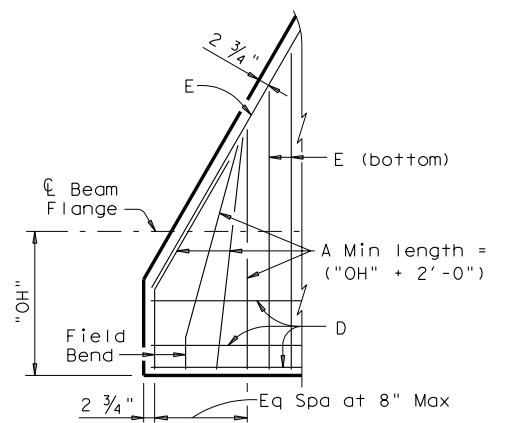
(Showing bottom reinforcing steel. See Span Details for top reinforcement steel.)



AT ALL SPAN ENDS UNLESS NOTED OTHERWISE
 AT INTERIOR BENTS
 AT THICKENED END SLABS ON STEEL, CONC I-BEAMS, I-GIRDERS OR U-BEAMS

PLAN OF SLABS WITH SKEWED REINFORCEMENT

(Showing bottom reinforcing steel. See Span Details for top reinforcement steel.)



DETAIL "A"

APPROXIMATE QUANTITIES FOR ONE SQUARE FOOT OF SLAB (15)	
Slab Thickness (In.)	Class S Concrete CY
8	0.0123
8 1/4	0.0131
8 1/2	0.0139

(For Contractor's information only)

- (8) Max Spacing as listed unless otherwise shown.
- (10) At connection with cast-in-place slab, extend longitudinal panel reinforcement 1'-0" (+2", -0") past panel end. Alternatively, provide (#3) x 2'-0" dowels at 6" Max spacing and extend dowels 1'-0" past panel end.
- (11) Maintain one Bar E(#5) parallel to panel ends (Typ).
- (12) Bars E(#5) not continuous over beam flanges must overlap beam flange 6" Min.
- (13) Add flared Bars E(#5) (Min Spa = 2", Max Spa = 10") as required at panel ends.
- (14) Where possible, Bars E(#5) may be extended into overhangs to replace Bars P(#4). Bars Z(#4) are required for sloped overhangs with U-Beams.
- (15) These approximate quantities are for a typical square foot of cast-in-place slab over the PCP. They do not include an allowance for slab overhangs, thickened ends at diaphragms, or the portion between panels over the beams.

TABLE OF REINFORCING STEEL (8)		
BAR	SIZE	Max Spa (in.)
A	#5	~
D	#5	9
E	#5	6
P	#4	18
UP	#4	~
Z	#4	18

LEVELS DISPLAYED	ACC:
1	



**PRESTRESSED CONCRETE PANELS
 OPTIONAL DECK DETAILS
 FOR BEAM SPANS**

PCP

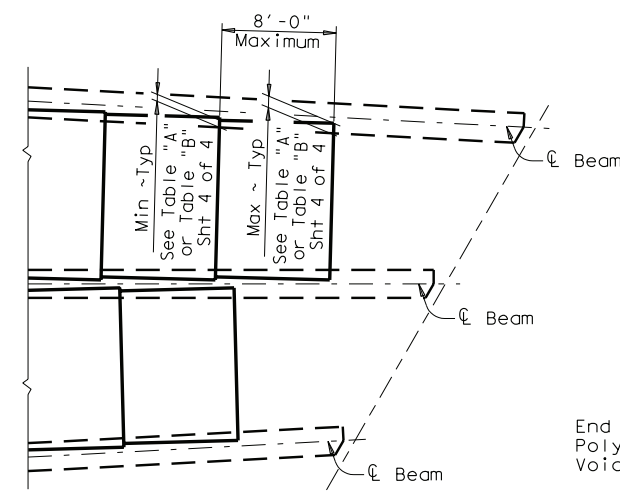
FILE: pcpstd1.dgn	DN: TxDOT	CK: TxDOT	DW: TxDOT	CR: TxDOT
© TxDOT April 2006	DISTRICT	FEDERAL AID PROJECT		SHEET
REVISIONS				
08-07: Added I-Girders and added note to WWR splice detail.	COUNTY	CONTROL	SECT	JOB HIGHWAY

DISCLAIMER: The use of this standard is governed by the "Texas Engineering Practice Act". No warranty of any kind is made by TxDOT for any purpose whatsoever. TxDOT assumes no responsibility for the conversion of this standard to other formats or for incorrect results or damages resulting from its use.

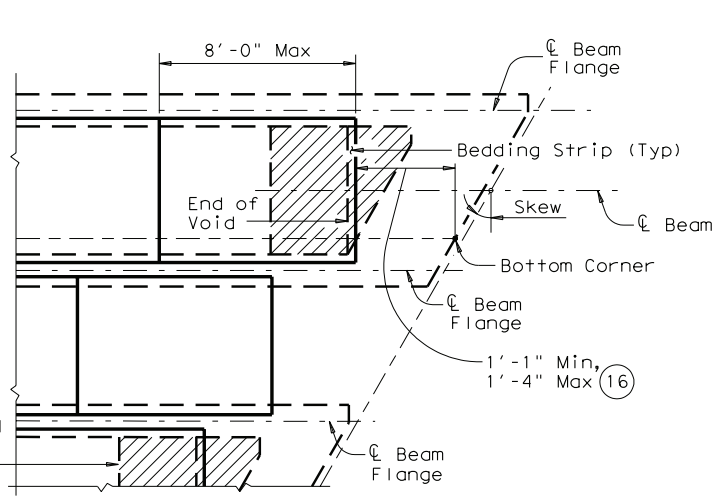
ACC:

1	
2	
3	
4	
5	
6	
7	
8	
9	
10	
11	
12	
13	
14	
15	
16	
17	
18	
19	
20	

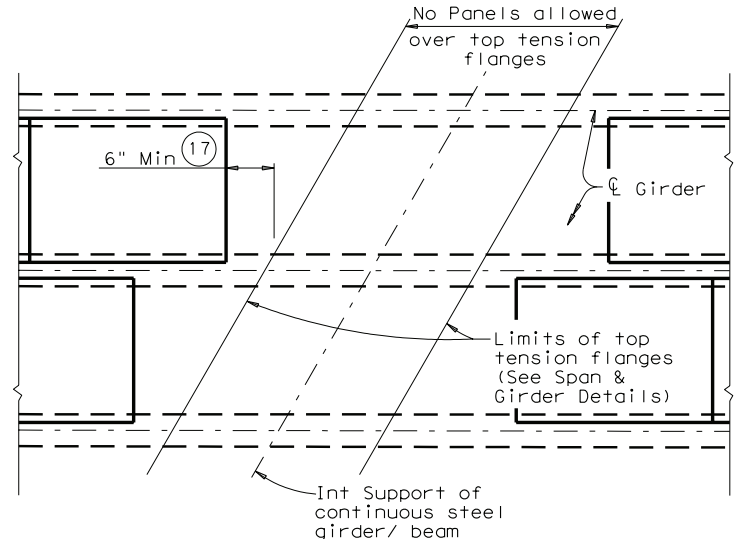
LEVELS DISPLAYED



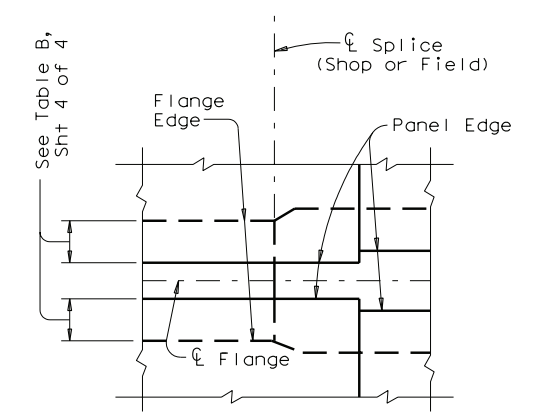
AT ENDS OF FLARED I-BEAMS OR I-GIRDERS
(Showing thickened slab end condition)



AT ENDS OF CONC U-BEAMS

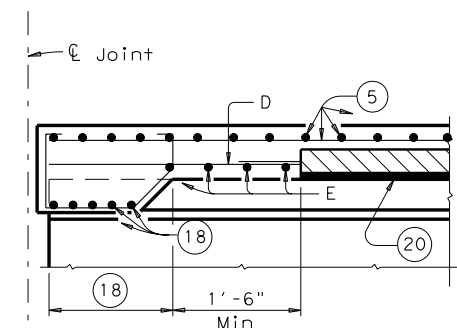


AT INT SUPPORTS OF CONTINUOUS STEEL GIRDERS

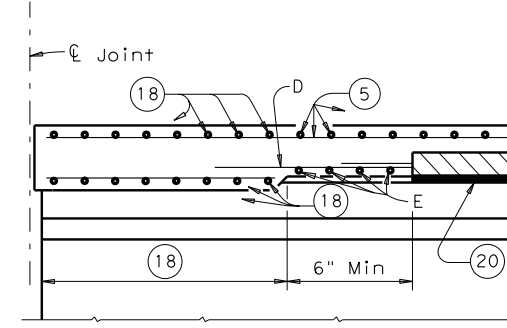


PLAN AT SPLICE
(Showing Steel Bms with flange width transition)

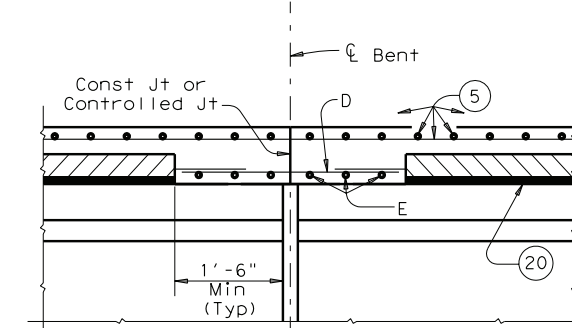
PART PLANS OF PANEL PLACEMENT



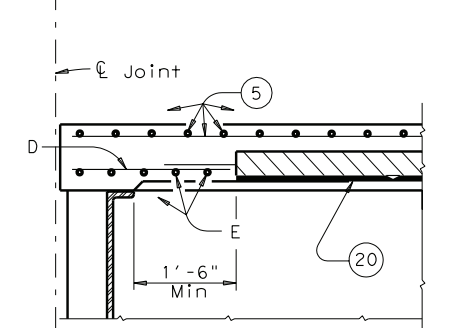
AT THICKENED SLAB ENDS FOR PRESTR CONC U-BMS



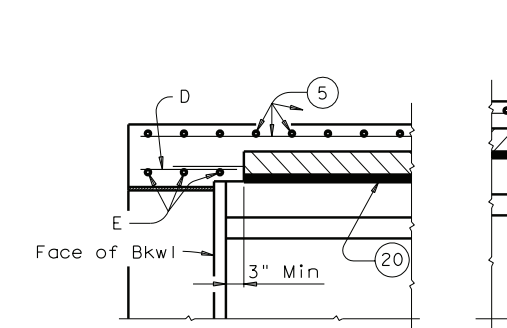
AT THICKENED SLAB ENDS FOR PRESTR CONC I-BMS AND STEEL BMS



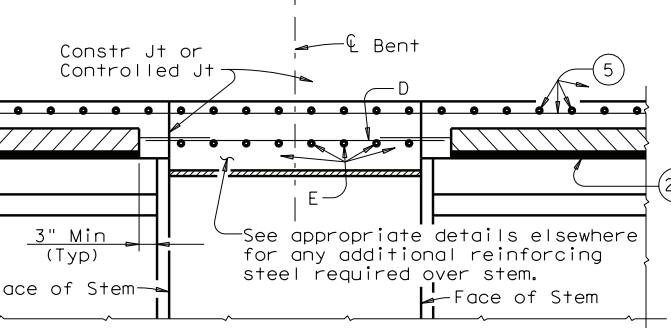
AT SLAB CONTINUOUS OVER CONVENTIONAL INTERIOR BENTS FOR ALL SIMPLE SPAN BMS



AT CONVENTIONAL END DIAPHRAGMS FOR STEEL BMS



AT SLAB OVER ABUTMENT BACKWALL FOR ALL BMS

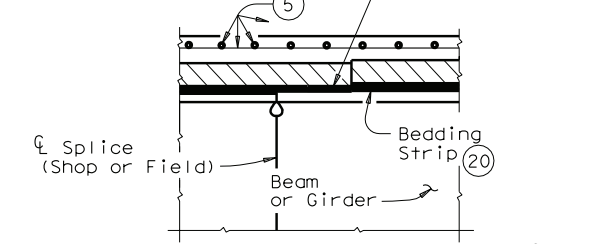


AT SLAB CONTINUOUS OVER INVERTED-T BENTS FOR ALL BMS

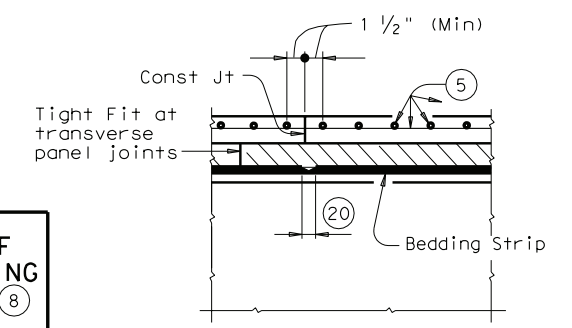
ELEVATIONS AT BEAM ENDS

- 5 See Span Details for top slab reinforcement and clear cover. Longitudinal top slab reinforcement may rest on top of prestressed concrete panels if necessary to maintain clear cover.
- 8 Max Spacing as listed unless otherwise shown.
- 16 For panel placement at ends of dapped end U-Beams, with Skews under 30°, use 2'-9" ± 1" or with Skews 30° thru 45°, use 3'-3" ± 1".
- 17 Location of concrete placement sequence boundaries and bolted field splices should be considered by the contractor in determining panel limits.
- 18 See appropriate thickened slab end details for reinforcing and limits of thickened slab end.
- 19 When flange thickness differs or flange cover plates are used the Contractor must compensate by using different thickness bedding strips to assure that the tops of Precast Panels are within 1/4" of alignment. See Normal Grading Detail for additional notes.
- 20 Butt adjacent bedding strips together with adhesive. Cut v-notches, approx 1/4" deep, in the top of the bedding strips at 8' o.c..

Contractor to field cut bedding strip to adjust for difference in flange thickness.



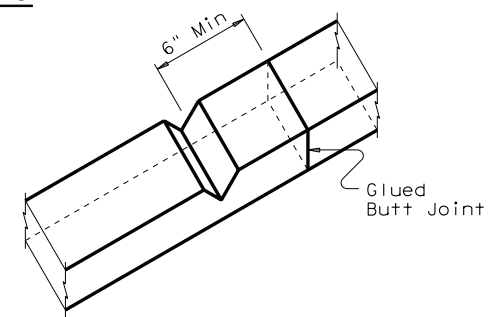
ELEVATION AT SPLICE
(Showing Steel Bms with different flange thickness)



TRANSVERSE PANEL JOINTS AND SLAB CONST JOINTS

TABLE OF REINFORCING STEEL

BAR	SIZE	Max Spa (in.)
A	#5	~
D	#5	9
E	#5	6
P	#4	18
UP	#4	~
Z	#4	18



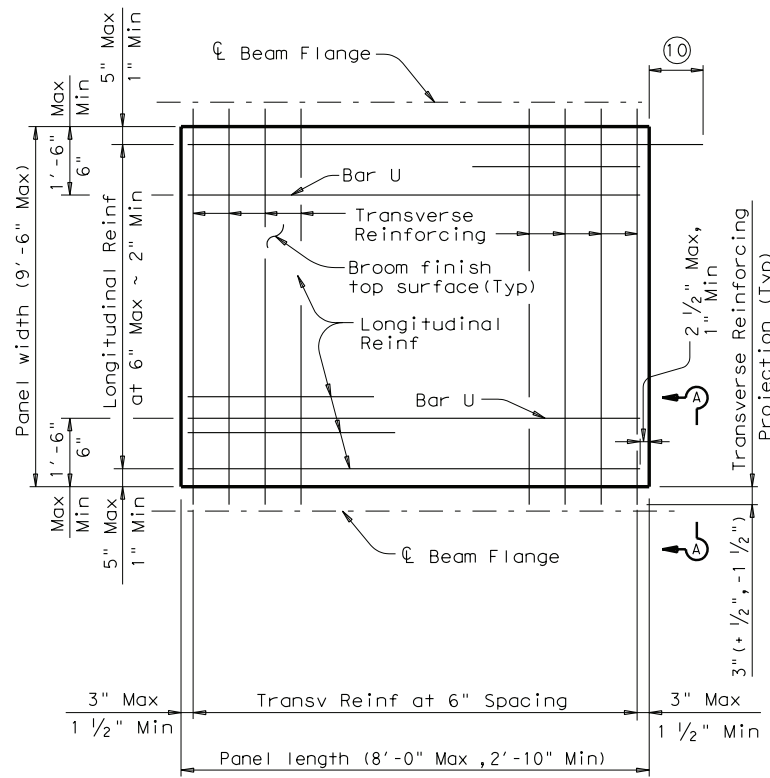
EXAMPLE OF BEDDING STRIPS BUTTED TOGETHER WITH V-NOTCH

PRESTRESSED CONCRETE PANELS
OPTIONAL DECK DETAILS FOR BEAM SPANS

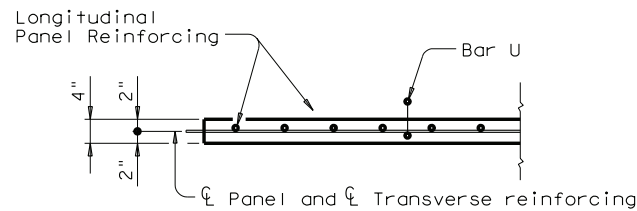
PCP

FILE: pcpstd1.dgn	DN: TxDOT	CK: TxDOT	DW: TxDOT	CR: TxDOT
© TxDOT April 2006	DISTRICT	FEDERAL AID PROJECT	SHEET	
REVISIONS				
08-07: Added I-Girders and added note to WWR splice detail.	COUNTY	CONTROL	SECT	JOB
				HIGHWAY

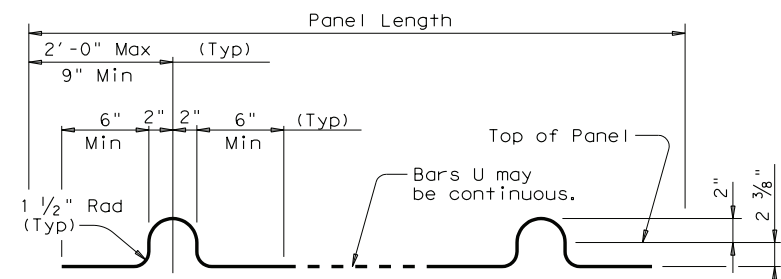
DISCLAIMER: The use of this standard is governed by the "Texas Engineering Practice Act". No warranty of any kind is made by TxDOT for any purpose whatsoever. TxDOT assumes no responsibility for the conversion of this standard to other formats or for incorrect results or damages resulting from its use.



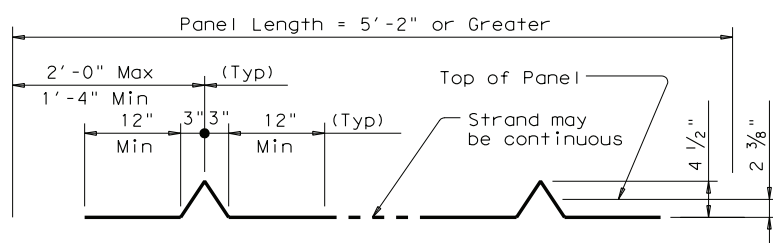
TYPICAL PANEL PLAN



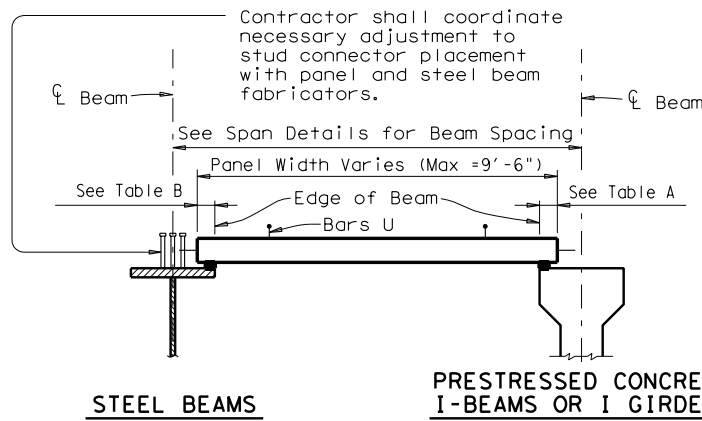
SECTION A-A



BARS U (#3)

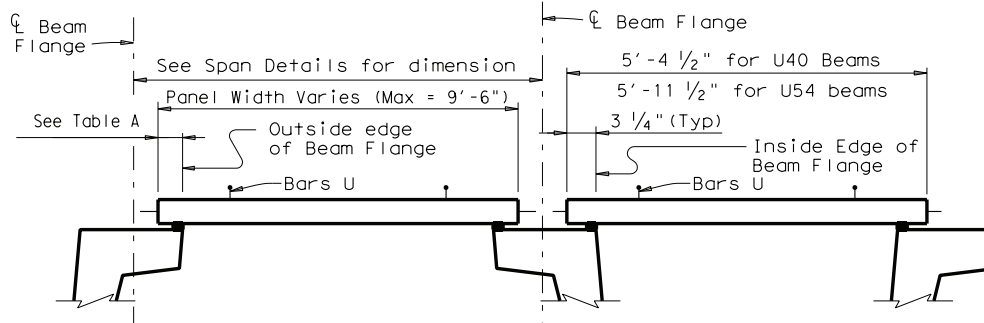


OPTIONAL STRAND FOR BARS U



STEEL BEAMS

PRESTRESSED CONCRETE I-BEAMS OR I GIRDERS



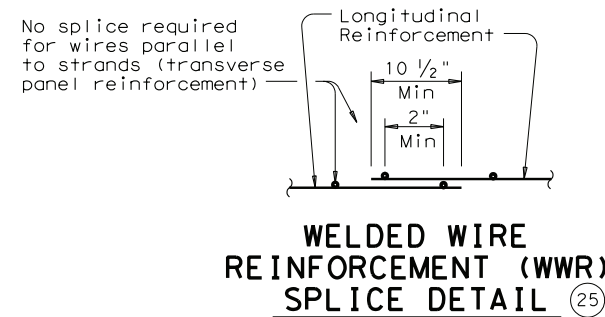
PRESTRESSED CONCRETE U-BEAMS

TYPICAL SECTIONS FOR DETERMINING PANEL WIDTH

- ⑩ At connection with cast-in-place slab, extend longitudinal panel reinforcement 1'-0" (+2", -0") past panel end. Alternatively, provide (#3) x 2'-0" dowels at 6" Max Spacing and extend dowels 1'-0" past panel end.
- ⑪ Four loops required per panel.
- ⑫ Four loops required per panel. 3/8" or 1/2" strands may be used.
- ⑬ Normal dimensions must be used on spans with parallel beams. Maximum and Minimum dimensions apply only to spans with flared beams.
- ⑭ See Normal Grading Detail on Sht 1 of 4 for lap requirements and bedding strip dimensions. Some laps shown in tables cannot utilize all bedding strip widths.
- ⑮ One Splice allowed per panel.

Beam Type	Normal (In.)	Min (In.)	Max (In.)
A	3	2 1/2	3 1/2
B	3	2 1/2	3 1/2
C	4	3	4 1/2
IV	6	4	7 1/2
VI	6 1/2	4 1/2	8 1/2
U40	5 1/2	5 1/2	7
U54	5 1/2	5 1/2	7
Tx28-70	6	4	7 1/2

Top Flange Width	Normal (In.)	Min (In.)	Max (In.)
11" to 12"	2 3/4	2 1/2	2 3/4
Over 12" to 15"	3 1/4	3	3 1/4
Over 15" to 18"	4	3	4 3/4
Over 18"	5	3 1/2	6 1/4



WELDED WIRE REINFORCEMENT (WWR) SPLICE DETAIL

FABRICATION NOTES:

All concrete for panels is to be Class H. Use Class H (HPC) concrete for panels if required elsewhere in plans. Release strength f'_{ci} = 4000 psi. Minimum 28 day strength f'_{c} = 5000 psi. Remove laitance from top panel surface. A minimum of 90 percent of the top surface area must have the required broom finish. Shop drawings for the fabrication of panels will not require the Engineer's approval if fabrication is in accordance with the details shown on this standard. A panel layout which identifies location of each panel must be developed by the fabricator. Permanently mark each panel in accordance with the panel layout. A copy of the layout is to be provided to the Engineer.

TRANSVERSE PANEL REINFORCEMENT:

For panel widths over 5', use 3/8" or 1/2" Dia (270k) prestressing strands with an initial tension of 16.1 kips per strand. For panel widths over 3'-6" up to and including 5', use 3/8" or 1/2" Dia (270k) prestressing strands with an initial tension of 16.1 kip per strand. Optionally, #4 Grade 60 reinforcing bars may be used in lieu of prestressed strands. For panel widths up to 3'-6", use #4 Grade 60 reinforcing bars (prestressed strands are not allowed). Place transverse panel reinforcement at panel centroid and space at 6" Max.

LONGITUDINAL PANEL REINFORCEMENT:

Any of the following options may be used for longitudinal panel reinforcement:

- (#3) Grade 60 reinforcing steel at 6" Max Spacing. No splices allowed.
- 3/8" Dia prestressing strands at 4 1/2" Max Spacing (unstressed). No splices allowed.
- 1/2" Dia prestressing strands at 6" Max Spacing (unstressed). No splices allowed.
- Deformed Welded Wire Reinforcement (WWR) (ASTM A497) providing 0.22 sq in per foot of panel width. Wires larger than D11 not permitted. Provide transverse wires to ensure proper handling of reinforcing. One splice per panel is allowed. See WWR Splice Detail. No combination of longitudinal reinforcement options in a panel is allowed. Place longitudinal panel reinforcement above transverse panel reinforcement.



PRESTRESSED CONCRETE PANELS
OPTIONAL DECK DETAILS
FOR BEAM SPANS

PCP

FILE: pcpsfde1.dgn	DN: TxDOT	CK: TxDOT	DW: TxDOT	CR: TxDOT
© TxDOT April 2006	DISTRICT	FEDERAL AID PROJECT		SHEET
REVISIONS				
08-07: Added I-Girders and added note to WWR splice detail.	COUNTY	CONTROL	SECT	JOB HIGHWAY

LEVELS DISPLAYED	ACC:
1	

A.2 CONCRETE MIXTURE DESIGNS

A.2.1 Concrete mixture for Plant A

Mix Design Number:	80FHME60	Date:	Nov 18, 08
Total Sacks of Cementious:	8.00	Air:	1.5%
Percent Fly Ash:	25.00%	Release / Design Strength	5000 / 9000
W/Cm Ratio / Gallons / yd:	0.31	Slump:	6" - 8.5"
Sacks of Cement:	6.00	Water Factor:	3.5 gal./sack
Total lbs. Cementious:	752	Yield cu.ft./cu.yd.	27.0

Aggregate Moisture		Aggregate Absorption		June 2, 2008 lbs. Cement / yd. 564 Na2O Equivalent Alkalies% 0.48 SO3 4.2 Alkali Content per cubic yard
Coarse Aggregate 1 - Moisture Reading	0.00%	0.00%		
Coarse Aggregate 2 - Moisture Reading	0.00%	0.00%		
Fine Aggregate 1 - Moisture Reading	0.00%	0.00%		
Fine Aggregate 2 - Moisture Reading	0.00%	0.00%		

Materials	1 CY (Basic @ SSD)	Specific Gravity	Cubic Feet	Moisture Adjustments	4.00 CY (Adjusted)
Capital Cement Type III	Cement 1	3.15	2.87 cu.ft.	Lbs	2,256 Lbs
Headwaters F Ash Plant # 1.2	Pozzolan	2.42	1.24 cu.ft.	Lbs	752 Lbs
BCW Well	Water	1.00	3.73 cu.ft.	0.0 Lbs	932.0 Lbs
3/4" Grade 5 Vulcan (1604 Pit)	Coarse Agg. 1	1.825	11.38 cu.ft.	0 Lbs	7,300 Lbs
	Coarse Agg. 2			0 Lbs	0 Lbs
Vulcan Mfg. Sand (1604)	Fine Agg. 1	1.172	7.37 cu.ft.	0 Lbs	4,689 Lbs
	Fine Agg. 2			0 Lbs	0 Lbs
Air Entraining		1.50%	0.41 cu.ft.		Total Agg. 11,989 Lbs
Yield cu.ft. / cu.yd.			27.00 cu.ft.		
Total Weight / cu.yd.			3982 Lbs/cu.yd.		15929 lbs / batch
Density lbs. / cu.ft.			147.5 lbs./cu.ft.		

SUPER			
Euclid SPC	Admix 1	6.00 fl.oz./cwt	Percent Solids 40
RETARDER			
Euclid TR	Admix 2	3.00 fl.oz./cwt	Percent Solids 49

OTHER ADMIXTURES			
	Admix 3	fl.oz./cwt	Percent Solids
	Admix 4	fl.oz./cwt	Percent Solids
			Dosage
			Dosage

TEST RESULTS			
Test Date:	11/18/2008	Actual Unit Weight:	147.80
Test Start Time:	8:20	Air Content:	2.7%
Ambient Air Temp:	56	Concrete Temp.:	67
		Theoretical Unit Weight:	147.5 lbs./cu.ft.
		Unit Weight + % Air added:	
		Actual Yield @ yds.	4.0
			26.94 cu.ft. / cu.yd.

A.2.2 Concrete mixture for Plant B

CONCRETE DESIGN / PILOT TEST WORKSHEET

Producer: XXXXXXXXXX

Date 05/26/09
 Design No. 437-9.09
 Concrete Class H
 Mix Design Option No. #1
 Revised Date 10/09

AGGREGATE CHARACTERISTICS

Aggregate	SP Gravity	SSD Unit Wt LBS / Cu. Ft.	% Solids	Source	F.M./Grade
Fine [FA]	2.63	101.83	62.05%	Hanson Arena	2.7
Coarse [CA]	2.58	101.29	62.92%	Hanson Eagle Lake	Grade 4

DESIGN FACTORS		w/cm Ratio	0.260	CA% of Total Agg. by Vol.	58.76%
CA Factor [CAF]	0.650	Air Factor [AF]		2.0%	Theor. Unit Wt of Conc.
Cement Factor [CF]	8.51	sks/cy	Cement Source / Type	Alamo Type III LA	
Water Factor [WF]	2.90	gal/sk	Water Source	Well Water (Approved)	
SCM 1 Percent	25.0%	SCM 1 Source/Type		Fly ash Type F Headwaters - Jewitt, Tx.	SP.GR. 2.51
SCM 2 Percent		SCM 2 Source/Type			SP.GR.

Batch Design [One Sack]	Volume: 1-Sk Batch [Cu Ft]	Vol to Wt [Lb] Vol x 62.4 x Sp Gr	1-Sack Batch Wt	Full Size Batch Factor	Full Size Batch Wts
1. Concrete Yield = $\frac{\text{CuFt per CuYd}}{\text{CF}}$	$\frac{27}{8.5} = 3.173$				
2. Volume CA = Yield x CAF x Solids	$3.173 \times 0.65 \times 0.629 = 1.298$	$\times 62.4 \times 2.58 = 208.89$		8.51	* 1,778
3. Volume Mortar = Yield - Vol CA	$3.173 - 1.298 = 1.875$				
4. Volume Water = $\frac{\text{WF}}{\text{Gals Wat per CuFt}}$	$\frac{2.9}{7.5} = 0.387$	$\times 62.4 \times 1.00 = 24.13$		8.51	* 205
5. Volume SCM 1	$\frac{94 \times 25\%}{62.4 \times 2.51} = 0.150$	$\times 62.4 \times 2.51 = 23.50$		8.51	200
6. Volume SCM 2	$\frac{94 \times 0}{62.4 \times 0} = 0$	$\times 62.4 \times 0 = 0$		8.51	-
7. Volume One Sk Cement	$\frac{94 \times 75\%}{62.4 \times 3.10} = 0.364$	$\times 62.4 \times 3.10 = 70.50$		8.51	600
8. Volume Entrained Air = Yield x AF	$3.173 \times 0.020 = 0.063$				
9. Volume Paste = Vol Cem+Water+Air	$0.514 + 0.387 + 0.063 = 0.965$				
10. Volume FA = Vol Mortar - Paste	$1.875 - 0.965 = 0.911$	$\times 62.4 \times 2.63 = 149.44$		8.51	* 1,272
11. Yield [Summation of 2, 4, 5, 6, 7, 8, & 10 to Check Number 1 above]	$= 3.173$			TOTAL Batch Wts	* 4,055
12. FA Factor = $\frac{\text{Vol FA}}{\text{FA Solids} \times \text{Vol Mortar}}$	$\frac{0.911}{0.620 \times 1.875} = 0.78$	$\frac{0.911}{1.164} = 0.78$		* Correct for Free Moisture & Absorption	

Cyl No	Age	Area	Load	Stress	Cyl No	Age	Area	Load	Stress
1	16 hrs.	12.50	75,950	6,080	3	3 day	12.50	102,510	8,200
2	16 hrs.	12.50	79,765	6,380	4	3 day	12.50	100,345	8,030
16 hrs. Hr Avg				6,230	3 Day Avg				8,120
Cyl No	Age	Area	Load	Stress	Cyl No	Age	Area	Load	Stress
5	7 day	12.50	114,595	9,170	7	14 day	12.50	127,495	10,200
6	7 day	12.50	111,690	8,940	8	14 day	12.50	129,570	10,370
7 Day Avg				9,060	14 Day Avg				10,290

Cyl No	Age	Area	Load	Stress	Remarks
9	28 day	12.50	132,480	10,600	Cyl made @ 2:45 pm
10	28 day	12.50	133,315	10,670	
28 Day Avg				10,640	

Slump	7.75	Admixture / Type	Sika Viscocrete 2110	Dosage (oz/100 lbs)	7.0	% solids	40
Air Temperature	85	Admixture / Type	Sika Plastiment	Dosage (oz/100 lbs)	1.5	% solids	33
Concrete Temperature	78	Admixture / Type		Dosage (oz/100 lbs)		% solids	
Actual Unit Weight	149.76	Admixture / Type		Dosage (oz/100 lbs)		% solids	

A.3 GAGE INFORMATION

A.2.1 PMFL-60-8LT

TML STRAIN GAUGE TEST DATA

GAUGE TYPE : PMFL-60 TESTTED ON : SS400

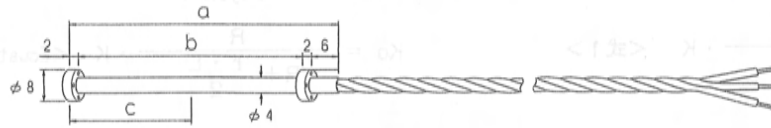
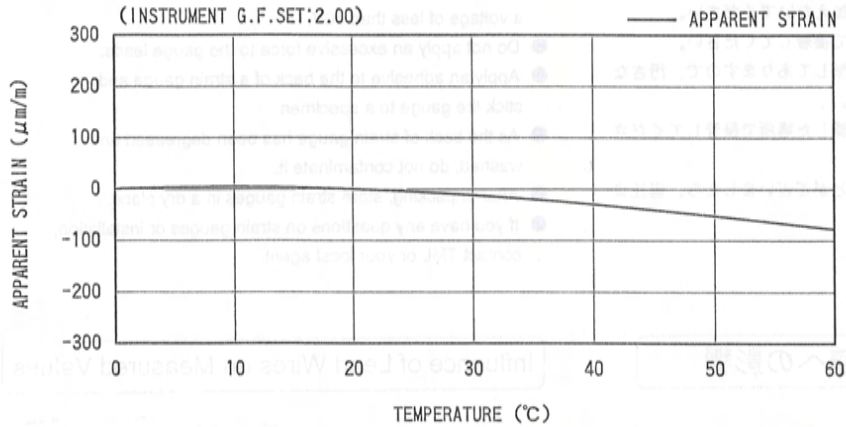
LOT NO. : P515615 COEFFICIENT OF THERMAL EXPANSION : 11.8 $\times 10^{-6}/^{\circ}\text{C}$

GAUGE FACTOR : 2.11 $\pm 1\%$ DATA NO. : V0011

THERMAL OUTPUT (ϵ_{app} : APPARENT STRAIN)

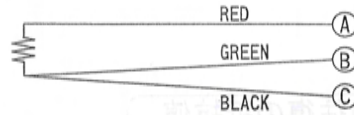
$$\epsilon_{app} = 2.35 \times 10^{-1} + 9.16 \times 10^{-1} \times T^1 - 5.11 \times 10^{-2} \times T^2 + 2.36 \times 10^{-4} \times T^3 \quad (\mu\text{m/m})$$

TOLERANCE : $\pm 1.8 [(\mu\text{m/m})/^{\circ}\text{C}]$, T : TEMPERATURE



GAUGE TYPE	a	b	c
PMFL-50	60	50	27
PMFL-60	70	60	32

(Unit:mm)



(120Ω 1gauge 3wire-system)

Tokyo Sokki Kenkyujo Co., Ltd.

8-2, Minami-ohi 6-chome
 Sinagawa-ku, Tokyo 140-8560, Japan
 E-mail sales@tml.jp

A.2.2 VWG (Geocon's Model 4200)

APPENDIX A - SPECIFICATIONS**A.1 Strain Gage**

Model:	4200	4202	4204	4210	4212	4214
Range (nominal):	3000 $\mu\epsilon$					
Resolution:	1.0 $\mu\epsilon^1$	0.4 $\mu\epsilon^1$	1.0 $\mu\epsilon^1$	0.4 $\mu\epsilon^1$	0.4 $\mu\epsilon^1$	0.4 $\mu\epsilon^1$
Calibration Accuracy	0.1%FSR					
Batch Factor Accuracy	0.5%FSR					
System Accuracy:	2.0% FSR ²					
Stability:	0.1%FS/yr					
Linearity:	2.0% FSR					
Thermal Coefficient:	12.2 $\mu\epsilon/^\circ\text{C}$					
Frequency Range Hz:	450-1200	1400-3500	800-1600	1400-3500	1400-3500	1400-3500
Dimensions (gage): (Length \times Diameter)	6.125 \times 0.750" 155 \times 19 mm	2.250 \times 0.625" 57 \times 16 mm	4.125 \times 0.750" 105 \times 19 mm	10.250 \times 2" 260 \times 50 mm	12.250 \times 2" 311 \times 50 mm	14.250 \times 2" 362 \times 50 mm
Dimensions (coil):	0.875 \times 0.875" 22 \times 22 mm	NA				
Coil Resistance:	180 Ω	50 Ω	50 Ω	180 Ω	180 Ω	180 Ω
Temperature Range:	-20 to +80° C					

Table A-1 Strain Gage Specifications**Notes:**

¹ Depends on the readout; figures in Table A-1 pertain to the GK-401 Readout.

² System Accuracy takes into account hysteresis, non-linearity, misalignment, batch factor variations, and other aspects of the actual measurement program. System Accuracy to 1.0% FS may be achieved through individual calibration of each strain gage.

A.2 Thermistor (see Appendix C also)

Range: -80 to +150° C

Accuracy: $\pm 0.5^\circ\text{C}$

APPENDIX B - THEORY OF OPERATION

A vibrating wire attached to the surface of a deforming body will deform in a like manner. The deformations alter the tension of the wire and hence also its natural frequency of vibration (resonance). The relationship between frequency (period) and deformation (strain) is described as follows:

Model:	4200	4202	4204
Gage Length (L_g):	6.000 inches	2 inches	4.000 inches
Wire Length (L_w):	5.875 inches	2 inches	3.875 inches
Gage Factor:	3.304	0.391	1.422

Table B-1 - Embedment Strain Gage Theoretical Parameters

Note: The examples below are calculated using the VCE-4200 gage parameters. Substitute the values from Table B-1 for the VCE-4202/4204 strain gages. **These equations do not apply to the VCE-4202X/4210/4212/4214 strain gages.**

1. The fundamental frequency (resonant frequency) of vibration of a wire is related to its tension, length and mass by the equation:

$$f = \frac{1}{2L_w} \sqrt{\frac{F}{m}}$$

Where;

L_w is the length of the wire in inches.

F is the wire tension in pounds.

m is the mass of the wire per unit length (pounds, sec.²/in.²).

2. Note that:

$$m = \frac{W}{L_w g}$$

Where;

W is the weight of L_w inches of wire (pounds).

g is the acceleration of gravity (386 in./sec.²).

3. and:

$$W = \rho a L_w$$

Where;

ρ is the wire material density (0.283 lb./in.³).

a is the cross sectional area of the wire (in.²).

4. Combining equations 1, 2 and 3 gives:

$$f = \frac{1}{2L_w} \sqrt{\frac{Fg}{\rho a}}$$

5. Note that the tension (F) can be expressed in terms of strain, e.g.:

$$F = \epsilon_w E a$$

Where;

ϵ_w is the wire strain (in./in.).

E is the Young's Modulus of the wire (30 x 10⁶ Psi).

6. Combining equations 4 and 5 gives:

$$f = \frac{1}{2L_w} \sqrt{\frac{\epsilon_w E g}{\rho}}$$

7. Substituting the given values for E, g and ρ yields:

$$f = \frac{101142}{L_w} \sqrt{\epsilon_w}$$

8. On channel 'A', which displays the period of vibration, T, multiplied by a factor of 10^6 :

$$T = \frac{10^6}{f}$$

9. Combining equations 7 and 8 gives:

$$\epsilon_w = \frac{97.75 L_w^2}{T^2}$$

10. Equation 9 must now be expressed in terms of the strain in the surface of the body to which the gage is attached. Since the deformation of the body must equal the deformation of the wire:

$$\epsilon_w L_w = \epsilon L_g$$

Where;

ϵ is the strain in the body.

L_g is the gage length (in inches).

11. Combining equations 9 and 10 gives:

$$\epsilon = \frac{97.75}{T^2} \cdot \frac{L_w^3}{L_g}$$

Where; (for the VCE-4200 Strain Gage)

L_w is 5.875 inches.

L_g is 6.000 inches.

12. Therefore:

$$\epsilon = 3.304 \times 10^3 \left[\frac{1}{T^2} \right]$$

(Note that T is in seconds x 10^6 and ϵ is in inches per inch)

13. The display on position "D" of the GK-401/403 Readout is based on the equation:

$$\epsilon = 3.304 \times 10^9 \left[\frac{1}{T^2} \right]$$

Note that in this formula ϵ is in micro inches per inch and T is in seconds x 10^6

Alternatively $\epsilon = 3.304 \times 10^{-3} f^2$ microstrain. Where f is the frequency in Hz

The squaring, inverting and multiplication by the factor, 3.304×10^9 , is all done internally by the microprocessor so that the displayed reading on Channel D is given in terms of microinches per inch (ϵ).

APPENDIX C - THERMISTOR TEMPERATURE DERIVATION

Thermistor Type: YSI 44005, Dale #1C3001-B3, Alpha #13A3001-B3

Resistance to Temperature Equation:

$$T = \frac{1}{A + B(\ln R) + C(\ln R)^3} - 273.2$$

Equation C-1 Convert Thermistor Resistance to Temperature

Where: T = Temperature in °C.

LnR = Natural Log of Thermistor Resistance

A = 1.4051×10^{-3} (coefficients calculated over the -50 to +150° C. span)

B = 2.369×10^{-4}

C = 1.019×10^{-7}

Ohms	Temp	Ohms	Temp	Ohms	Temp	Ohms	Temp	Ohms	Temp
201.1K	-50	16.60K	-10	2417	+30	525.4	+70	153.2	+110
187.3K	-49	15.72K	-9	2317	31	507.8	71	149.0	111
174.5K	-48	14.90K	-8	2221	32	490.9	72	145.0	112
162.7K	-47	14.12K	-7	2130	33	474.7	73	141.1	113
151.7K	-46	13.39K	-6	2042	34	459.0	74	137.2	114
141.6K	-45	12.70K	-5	1959	35	444.0	75	133.6	115
132.2K	-44	12.05K	-4	1880	36	429.5	76	130.0	116
123.5K	-43	11.44K	-3	1805	37	415.6	77	126.5	117
115.4K	-42	10.86K	-2	1733	38	402.2	78	123.2	118
107.9K	-41	10.31K	-1	1664	39	389.3	79	119.9	119
101.0K	-40	9796	0	1598	40	376.9	80	116.8	120
94.48K	-39	9310	+1	1535	41	364.9	81	113.8	121
88.46K	-38	8851	2	1475	42	353.4	82	110.8	122
82.87K	-37	8417	3	1418	43	342.2	83	107.9	123
77.66K	-36	8006	4	1363	44	331.5	84	105.2	124
72.81K	-35	7618	5	1310	45	321.2	85	102.5	125
68.30K	-34	7252	6	1260	46	311.3	86	99.9	126
64.09K	-33	6905	7	1212	47	301.7	87	97.3	127
60.17K	-32	6576	8	1167	48	292.4	88	94.9	128
56.51K	-31	6265	9	1123	49	283.5	89	92.5	129
53.10K	-30	5971	10	1081	50	274.9	90	90.2	130
49.91K	-29	5692	11	1040	51	266.6	91	87.9	131
46.94K	-28	5427	12	1002	52	258.6	92	85.7	132
44.16K	-27	5177	13	965.0	53	250.9	93	83.6	133
41.56K	-26	4939	14	929.6	54	243.4	94	81.6	134
39.13K	-25	4714	15	895.8	55	236.2	95	79.6	135
36.86K	-24	4500	16	863.3	56	229.3	96	77.6	136
34.73K	-23	4297	17	832.2	57	222.6	97	75.8	137
32.74K	-22	4105	18	802.3	58	216.1	98	73.9	138
30.87K	-21	3922	19	773.7	59	209.8	99	72.2	139
29.13K	-20	3748	20	746.3	60	203.8	100	70.4	140
27.49K	-19	3583	21	719.9	61	197.9	101	68.8	141
25.95K	-18	3426	22	694.7	62	192.2	102	67.1	142
24.51K	-17	3277	23	670.4	63	186.8	103	65.5	143
23.16K	-16	3135	24	647.1	64	181.5	104	64.0	144
21.89K	-15	3000	25	624.7	65	176.4	105	62.5	145
20.70K	-14	2872	26	603.3	66	171.4	106	61.1	146
19.58K	-13	2750	27	582.6	67	166.7	107	59.6	147
18.52K	-12	2633	28	562.8	68	162.0	108	58.3	148
17.53K	-11	2523	29	543.7	69	157.6	109	56.8	149
								55.6	150

Table C-1 Thermistor Resistance versus Temperature

APPENDIX D - HIGH-TEMPERATURE THERMISTOR LINEARIZATION
High Temperature Thermistor Linearization using SteinHart-Hart Log Equation

Thermistor Type: Thermometrics BR55KA822J

Basic Equation:
$$T = \frac{1}{A + B(\ln R) + C(\ln R)^3} - 273.2$$

Where: T = Temperature in °C
 $\ln R$ = Natural Log of Thermistor Resistance
 $A = 1.02569 \times 10^{-3}$
 $B = 2.478265 \times 10^{-4}$
 $C = 1.289498 \times 10^{-7}$

Note: Coefficients calculated over -30° to +260° C. span.

Temperature Calculation and Error Table

Temp	R (ohms)	LnR	LnR ³	Calculated Temp	Diff	FS Error	Temp	R (ohms)	LnR	LnR ³	Calculated Temp	Diff	FS Error
-30	113898	11.643	1578.342	-30.17	0.17	0.06	120	407.62	6.010	217.118	120.00	0.00	0.00
-25	86182	11.364	1467.637	-25.14	0.14	0.05	125	360.8	5.888	204.162	125.00	0.00	0.00
-20	65805	11.094	1365.581	-20.12	0.12	0.04	130	320.21	5.769	191.998	130.00	0.00	0.00
-15	50684.2	10.833	1271.425	-15.10	0.10	0.03	135	284.95	5.652	180.584	135.00	0.00	0.00
-10	39360	10.581	1184.457	-10.08	0.08	0.03	140	254.2	5.538	169.859	140.01	-0.01	0.00
-5	30807.4	10.336	1104.068	-5.07	0.07	0.02	145	227.3	5.426	159.773	145.02	-0.02	-0.01
0	24288.4	10.098	1029.614	-0.05	0.05	0.02	150	203.77	5.317	150.314	150.03	-0.03	-0.01
5	19294.6	9.868	960.798	4.96	0.04	0.01	155	183.11	5.210	141.428	155.04	-0.04	-0.01
10	15424.2	9.644	896.871	9.98	0.02	0.01	160	164.9	5.105	133.068	160.06	-0.06	-0.02
15	12423	9.427	837.843	14.98	0.02	0.01	165	148.83	5.003	125.210	165.08	-0.08	-0.03
20	10061.4	9.216	782.875	19.99	0.01	0.00	170	134.64	4.903	117.837	170.09	-0.09	-0.03
25	8200	9.012	731.893	25.00	0.00	0.00	175	122.1	4.805	110.927	175.08	-0.08	-0.03
30	6721.54	8.813	684.514	30.01	-0.01	0.00	180	110.95	4.709	104.426	180.07	-0.07	-0.02
35	5540.74	8.620	640.478	35.01	-0.01	0.00	185	100.94	4.615	98.261	185.10	-0.10	-0.04
40	4592	8.432	599.519	40.02	-0.02	-0.01	190	92.086	4.523	92.512	190.09	-0.09	-0.03
45	3825.3	8.249	561.392	45.02	-0.02	-0.01	195	84.214	4.433	87.136	195.05	-0.05	-0.02
50	3202.92	8.072	525.913	50.01	-0.01	-0.01	200	77.088	4.345	82.026	200.05	-0.05	-0.02
55	2693.7	7.899	492.790	55.02	-0.02	-0.01	205	70.717	4.259	77.237	205.02	-0.02	-0.01
60	2276.32	7.730	461.946	60.02	-0.02	-0.01	210	64.985	4.174	72.729	210.00	0.00	0.00
65	1931.92	7.566	433.157	65.02	-0.02	-0.01	215	59.819	4.091	68.484	214.97	0.03	0.01
70	1646.56	7.406	406.283	70.02	-0.02	-0.01	220	55.161	4.010	64.494	219.93	0.07	0.02
75	1409.58	7.251	381.243	75.01	-0.01	0.00	225	50.955	3.931	60.742	224.88	0.12	0.04
80	1211.14	7.099	357.808	80.00	0.00	0.00	230	47.142	3.853	57.207	229.82	0.18	0.06
85	1044.68	6.951	335.915	85.00	0.00	0.00	235	43.673	3.777	53.870	234.77	0.23	0.08
90	903.64	6.806	315.325	90.02	-0.02	-0.01	240	40.533	3.702	50.740	239.69	0.31	0.11
95	785.15	6.666	296.191	95.01	-0.01	0.00	245	37.671	3.629	47.788	244.62	0.38	0.13
100	684.37	6.528	278.253	100.00	0.00	0.00	250	35.055	3.557	45.001	249.54	0.46	0.16
105	598.44	6.394	261.447	105.00	0.00	0.00	255	32.677	3.487	42.387	254.44	0.56	0.19
110	524.96	6.263	245.705	110.00	0.00	0.00	260	30.496	3.418	39.917	259.34	0.66	0.23
115	461.91	6.135	230.952	115.00	0.00	0.00							

Table B-2: High Temperature Thermistor Resistance versus Temperature.

A.4 PRESTRESS LOSS PREDICTIONS (AASHTO)

A.4.1 2004 AASHTO

Prestress loss calculations according to AASHTO (2004) are summarized below.

AASHTO 2004 Prestress Loss Calculations

Gross Section Properties	
h [in]	4
y_t [in]	2
y_b [in]	2
A_g [in ²]	384
I_g [in ⁴]	512
ρ_s [in]	200
w_{sw} [klf]	400
e_{cl} [in]	0.00
e_{end} [in]	0.00
A_{ps} [in ²]	1.36
y_s [in]	2.06
A_s [in ²]	0.62

Strand Stresses	
f_{pj} [ksi]	189.4
P_j [kips]	257.6
f_{po} [ksi]	184.3
P_o [kips]	250.7

Concrete Age	
t_i [days]	1
t_f [days]	100000

Span Properties	
L_{span} [ft]	6
L_{beam} [ft]	8
$M_{g, span}$ [kin]	21600.0
$M_{g, beam}$ [kin]	38400

Material Properties	
n	7.6
n_{LT}	6.8
Concrete	
f'_{ci} [ksi]	4
E_{ci} [ksi]	3739
f'_c [ksi]	5
E_c [ksi]	4180
w_c [kcf]	0.1475
Strand	
f_{pu} [ksi]	270
f_{py} [ksi]	243
E_p [ksi]	28500

Total Loss		
$\Delta f_{pT} = \Delta f_{pES} + \Delta f_{pSR} + \Delta f_{pCR} + \Delta f_{pR2}$	Δf_{pT} [ksi]	24.2
	Δf_{pES} [ksi]	5.1
	Δf_{pSR} [ksi]	6.5
	Δf_{pCR} [ksi]	8.0
	Δf_{pR2} [ksi]	4.5

Elastic Shortening		
$\Delta f_{pES} = \frac{E_p}{E_{ci}} f_{cgp}$	Δf_{pES} [ksi]	5.1
	f_{cgp} [ksi]	0.7
$f_{cgp} = 0.7 f_{pu} A_{ps} \left(\frac{1}{A_g} + \frac{e^2 c^2}{I_g} \right) - \frac{M_{g,beam} e c}{I_g}$		

Shrinkage		
$\Delta f_{pSR} = 17.0 - 0.150H$	Δf_{pSR} [ksi]	6.5
	H [%]	70

Creep		
$\Delta f_{pCR} = 12.0 f_{cgp} - 7.0 \Delta f_{cpd} \geq 0$	Δf_{pCR} [ksi]	8.0
	f_{cgp} [ksi]	0.7
	Δf_{cpd} [ksi]	0.0

Relaxation		
$\Delta f_{pR2} = \frac{3}{10} [20 - 0.4 \Delta f_{pES} - 0.2 (\Delta f_{pSR} + \Delta f_{pCR})]$	Δf_{pR2} [ksi]	4.5

A.4.2 2008 ASHTO

Prestress loss calculations according to AASHTO (2008) are summarized below.

AASHTO 2008 Prestress Loss Calculations

Gross Section Properties	
h [in]	4
y_t [in]	2
y_b [in]	2
A_g [in ²]	384
I_g [in ⁴]	512
p_s [in]	200
w_{sw} [klf]	400
e_{cl} [in]	0.00
e_{end} [in]	0.00
A_{ps} [in ²]	1.36
y_s [in]	2.06
A_s [in ²]	0.62

Strand Stresses	
f_{pj} [ksi]	189.4
P_j [kips]	257.6
f_{po} [ksi]	184.4
P_o [kips]	250.8

Concrete Age	
t_i [days]	1
t_f [days]	100000

Span Properties	
L_{span} [ft]	8
L_{beam} [ft]	8
$M_g, span$ [kin]	38400.0
$M_g, beam$ [kin]	38400

Material Properties	
n	7.6
n_{LT}	6.8
Concrete	
f'_{ci} [ksi]	4
E_{ci} [ksi]	3739
f'_c [ksi]	5
E_c [ksi]	4180
w_c [kcf]	0.1475
K1	1.0
Strand	
f_{pu} [ksi]	270
f_{py} [ksi]	243
E_p [ksi]	28500

Total Loss		
$\Delta f_{pT} = \Delta f_{pES} + \Delta f_{pLT}$	Δf_{pT} [ksi]	34.0
	Δf_{pES} [ksi]	5.0
$\Delta f_{pLT} = (\Delta f_{pSR} + \Delta f_{pCR} + \Delta f_{pR1})_{id}$	Δf_{pSR} [ksi]	15.8
	Δf_{pCR} [ksi]	10.7
	Δf_{pR} [ksi]	2.6

Elastic Shortening		
$\Delta f_{pES} = \frac{A_{ps} f_{pstr} (I_g + e_{ci}^2 A_g) - e_{ci} M_p A_g}{A_{ps} (I_g + e_{ci}^2 A_g) + \frac{A_g I_g E_{ci}}{E_p}}$	Δf_{pES} [ksi]	5.0
	f_{pbt} [ksi]	189.4

Shrinkage		
$\Delta f_{pSR} = \varepsilon_{bid} E_p K_{id}$ $\varepsilon_{bid} = k_s k_{hs} k_f k_{td} (0.48 \cdot 10^{-3})$ $K_{id} = \frac{1}{1 + \frac{E_p A_{ps}}{E_{ci} A_g} \left(1 + \frac{A_g e_{ci}^2}{I_g} \right) [1 + 0.7 \psi_B(t_f, t_i)]}$ $\psi_B(t_f, t_i) = 1.9 k_s k_{hc} k_{td} t_i^{-0.118} \quad k_{hc} = 1.56 - 0.008H$ $k_s = 1.45 - 0.13 \frac{V}{S} \quad k_{td} = \frac{(t_f - t_i)}{61 - 4f'_{ci} + (t_f - t_i)}$ $k_{hs} = 2.00 - 0.014H \quad k_f = \frac{5}{1 + f'_{ci}}$	Δf_{pSR} [ksi]	15.8
	ε_{bid} [in/in]	0.0006
	k_s	1.21
	k_{hs}	1.02
	k_f	1.00
	k_{td}	1.00
	V/S	1.8
	H [%]	70
	K_{id}	0.9
	$\Psi_b(t_f, t_i)$	2.3
	k_{hc}	1.00

Creep		
$\Delta f_{pCR} = \frac{E_p}{E_{ci}} f_{cgp} \psi_b(t_f, t_i) K_{id}$	Δf_{pCR} [ksi]	10.7
	f_{cgp} [ksi]	0.7

Relaxation		
$\Delta f_{pR1} = \frac{f_{pt}}{K_L} \left(\frac{f_{pt}}{f_{py}} - 0.55 \right)$ $\Delta f_{pR2} = \Delta f_{pR1}$	Δf_{pR1} [ksi]	1.3
	f_{pt} [ksi]	184
	K_L	30
	Δf_{pR2} [ksi]	1.3

A.5 EXAMPLE CALCULATIONS

A.5.1 Percentage prestress force remaining based on measured slip.

Calculations for percentage prestress force remaining in Specimen C3 based on the data from Gage #4 are summarized below.

$$\% \text{ Prestress Force Remaining} = 1 - \frac{\text{Slip}}{\text{Max Slip}}$$

$$\text{Max Slip} = \frac{\sigma L}{E_s 2}$$

Specimen C3

Gage #4

σ	175	ksi
E_s	29000	ksi
L	96	inches

Max Slip	0.290	inches
----------	-------	--------

Crack Width (inches)	Slip (inches)	Prestress Remaining
0	0.0000	100.00%
0	0.0000	100.00%
0.007	0.0000	100.00%
0.009	0.0007	99.77%
0.013	0.0004	99.87%
0.016	0.0005	99.83%
0.016	0.0003	99.91%
0.016	0.0008	99.72%
0.02	0.0083	97.13%
0.025	0.0105	96.39%
0.03	0.0152	94.75%
0.03	0.0168	94.18%
0.03	0.0182	93.71%
0.03	0.0192	93.37%

REFERENCES

- AASHTO (2004): *LRFD Bridge Design Specifications*, 3rd Edition, American Association of State Highway and Transportation Officials, Washington, D.C.
- AASHTO (2005): *LRFD Bridge Design Specifications*, Interim 2005 Edition, American Association of State Highway and Transportation Officials, Washington, D.C.
- AASHTO (1975): *Standard Specifications for Highway Bridges*, 11th Edition, American Association of State Highway and Transportation Officials, Washington, D.C.
- AASHTO (1961): *Standard Specifications for Highway Bridges*, 8th Edition, American Association of State Highway and Transportation Officials, Washington, D.C.
- Abrams (1913): Abrams, D. A., "Tests of Bond Between Concrete and Steel," *University of Illinois Bulletin*, University of Illinois, Urbana, No. 71, Dec.
- ACI Committee 209 (1971): "Effects of Concrete Constituents, Environment, and Stress on Creep and Shrinkage of Concrete," *ACI Special Publication SP 27-1*, American Concrete Institute, Farmington Hills, MI.
- ACI Committee 209 (1992): *Prediction of Creep, Shrinkage, and Temperature Effects in Concrete Structures*, American Concrete Institute, Farmington Hills, MI.
- ACI Committee 318 (2008): *Building Code Requirements for Structural Concrete and Commentary*, American Concrete Institute, Farmington Hills, MI.
- ACI-ASCE Committee 323 (1958): "Tentative Recommendations for Prestressed Concrete - Committee Closure," *ACI Journal, Proceedings*, American Concrete Institute, Farmington Hills, MI, No. 54, pp. 1291-1299.
- Barker (1975): Barker, J. M., "Research, Application, and Experience with Precast Prestressed Bridge Deck Panels." *PCI Journal*, Precast/Prestressed Concrete Institute, Chicago, IL, pp. 66-85.
- Barnoff *et al.* (1977): Barnoff, R., Orndorff, J., Harbaugh, R., and Rainey, D., "Full Scale Test of a Prestressed Bridge with Precast Deck Panels," *PCI Journal*, Precast/Prestressed Concrete Institute, Chicago, IL, V. 22, No. 5, Sep.-Oct., pp. 66-82.

- Bazant *et al.* (1980): Bazant, Z. P., and Panula, L., "Creep and Shrinkage Characterization for Analyzing Prestressed Concrete Structures." *PCI Journal*, Precast/Prestressed Concrete Institute, Chicago, IL, May-June, pp. 86-122.
- Berwanger *et al.* (1976): Berwanger, C., and Sarkar, A. F., "Thermal Expansion of Concrete and Reinforced Concrete." *ACI Journal*, American Concrete Institute, Farmington Hills, MI, Nov., pp. 618-621.
- Cousins *et al.* (1990): Cousins, T. E., Johnson, D. W., and Zia, P., "Transfer and Development Length of Epoxy Coated and Uncoated Prestressing Strands." *PCI Journal*, Precast/Prestressed Concrete Institute, Chicago, IL, July-Aug., pp. 92-103.
- Deshmukh (2004): Deshmukh, G., "Replacement Prioritization of Precast Deck Panel Bridges in Florida," MS Thesis, University of South Florida, Tampa, FL.
- Emanuel *et al.* (1977): Emanuel, J. H., and Hulsey, J. L., "Prediction of the thermal coefficient of expansion of concrete." *ACI Journal*, American Concrete Institute, Farmington Hills, MI, Apr., pp. 149-155.
- Erickson (1957): Erickson, E.L., "The Bureau of Public Roads 'Criteria for Prestressed Concrete Bridges' (A9-1-A9-8)," *Proceedings*, World Conference on Prestressed Concrete, University of California at Berkeley, San Francisco, CA.
- Fang *et al.* (1990): Fang, I.-K., Worley, J., Burns, N. H., and Klingner, R. E., "Behavior or Isotropic R/C Bridge Decks on Steel Girders," *Journal of Structural Engineering*, American Society of Civil Engineers, Reston, VA, V. 116, No. 3, Mar., pp. 659-678.
- FIB (2007): *Treatment of Imperfections in Precast Structural Elements*, International Federation for Structural Concrete, Lausanne, Switzerland.
- Galvez *et al.* (2009): Galvez, J. C., Benitez, J. M., Tork, B., Casati, M. J., and Cendron, D. A., "Splitting Failure of Precast Prestressed Concrete During the Release of the Prestressing Force," *Engineering Failure Analysis*, Elsevier, Amsterdam, Netherlands.
- Hanson *et al.* (1959): Hanson, N. W., and Kaar, P. R., "Flexural Bond Tests of Pretensioned Prestressed Beams," *ACI Journal*, American Concrete Institute, Farmington Hills, MI, Jan., pp. 783-802.
- Hawkins (1981): Hawkins, N. M., "Impact of Research on Prestressed Concrete Specimens," *ACI Journal*, American Concrete Institute, Farmington Hills, MI, pp. 163-176.

- Homayoun *et al.* (1993): Homayoun, H. A., and Mitchell, D., "Bond Characteristics of Pretensioned Strand," *ACI Materials Journal*, American Concrete Institute, Farmington Hills, MI, May-June, pp. 228-235.
- Janney (1954): Janney, J. R., "Nature of Bond in Pretensioned Prestressed Concrete," *ACI Journal*, American Concrete Institute, Farmington Hills, MI, V. 50, No. 9, pp. 717-769.
- Jiang *et al.* (1984): Jiang, D. H., Shah, S. P., and Andonian, A. T., "Study of the Transfer of Tensile Forces by Bond," *ACI Journal*, American Concrete Institute, Farmington Hills, MI, May-June, pp. 251-259.
- Jones *et al.* (1970): Jones, H., and Furr, H., "Development Length of Strands in Prestressed Panel Subdecks," Texas Transportation Institute, College Station, TX.
- Kreisa (2008): Kreisa, A., "Constructibility of Prestressed Concrete Panels for Use at Skewed," Thesis, The University of Texas at Austin, Austin, TX.
- Lin (1981): Lin, T. Y., and Burns, N. H., *Design of Prestressed Concrete Structures*, John Wiley & Sons Inc., New York, NY.
- Mallela *et al.* (2005): Mallela, J., Abbas, A., Harman, T., Rao, C., Liu, R., and Darter, M. I., "Measurement and Significance of the Coefficient of Thermal Expansion of Concrete in Rigid Pavement Design." *Journal of Transportation Research Board*, Transportation Research Board, Washington, D. C., pp. 38-46.
- Martin *et al.* (1976): Martin, L. D., and Scott, N. L., "Development of Prestressing Strand in Pretensioned Members," *ACI Journal*, American Concrete Institute, Farmington Hills, MI, Aug., pp. 453-456.
- Marti-Vargas *et al.* (2007): Marti-Vargas, J. R., Arbelaez, C. A., Serna-Ros, P., and Castro-Bugallo, C., "Reliability of Transfer Length Estimation from Strand End Slip," *ACI Structural Journal*, American Concrete Institute, Farmington Hills, MI, July-Aug., pp. 487-494.
- Merrill (2002): Merrill, B. D., "Texas' Use of Precast Concrete Stay-In-Place Forms for Bridge Decks," *Proceedings*, Concrete Bridge Conference, National Concrete Bridge Council, Skokie, IL.
- Mitchell *et al.* (1993): Mitchell, D., Cook, W. D., Khan, A. A., and Tham, T., "Influence of High Strength Concrete on Transfer and Development Length of Pretensioning Strands," *PCI Journal*, Precast/Prestressed Concrete Institute, Chicago, IL, May-June, pp. 52-66.

- Over *et al.* (1965): Over, R. S., and Au, T., "Prestress Transfer Bond of Pretensioned Strands in Concrete," *ACI Journal*, American Concrete Institute, Farmington Hills, MI, Nov. 1, pp. 1451-1460.
- PCI Bridge Committee (1978): "Tentative Design and Construction Specifications for Bridge Deck Panels," *PCI Journal*, Precast/Prestressed Concrete Institute, Chicago, IL, V. 23, No. 1, pp. 32-39.
- PCI (2006): *Manual for the Evaluation and Repair of Precast, Prestressed Concrete Bridge Products*, Precast/Prestressed Concrete Institute, Chicago, IL.
- Ross Bryan Associates, Inc. (1988): "Recommended Practice for Precast Prestressed Concrete Composite Bridge Deck Panels," *PCI Journal*, Precast/Prestressed Concrete Institute, Chicago, IL, pp. 67-109.
- Stocker *et al.* (1970): Stocker, M. F., and Sozen, M. A., "Investigation of Prestressed Concrete for Highway Bridges, Part V: Bond Characteristics of Prestressing Strand," The University of Illinois, Champaign, IL.
- Tadros *et al.* (2003): Tadros, M. K., Nabil, A., Seguirant, A. J., and Gallt, J. G., *NCHRP Report 496: Prestress Losses in Pretensioned High-Strength Concrete Bridge Girders*, Transportation Research Board, Washington, D.C.
- Tepfers (1973): Tepfers, R., "A Theory of Bond applied to Overlapped Tensile Reinforcement Splices for Deformed Bars," Chalmers University of Technology, Gotenborg, Sweden.
- Texas Transportation Institute, and Texas Highway Department (1975): "Investigation to Determine Feasibility of Using In-Place Precast Prestressed Form Panels for Highway Bridge Decks," *PCI Journal*, Precast/Prestressed Concrete Institute, Chicago, IL, V. 20, No. 3, May-June, pp. 62-67.
- TxDOT (2004): *Standard Specifications for Construction and Maintenance of Highways, Streets, and Bridges*, Texas Department of Transportation, Austin, TX.
- Tuchscherer (2009): Tuchscherer, R. G., and Bayrak, O., "Tensile Stress Limit for Prestressed Concrete at Release: ACI 318-08," *ACI Structural Journal*, American Concrete Institute, Farmington Hills, MI, May-June., pp. 279-287.
- Zia *et al.* (1977): Zia, P., and Mostafa, T., "Development Length of Prestressing Strands," *PCI Journal*, Precast/Prestressed Concrete Institute, Chicago, IL, V. 22, No. 5, Sep.-Oct., pp. 54-65.

Zia *et al.* (1979): Zia, P., Preston, H. K., Scott, N. L., and Workman, E. B., "Estimating Prestress Loss," *Concrete International Design and Construction*, American Concrete Institute, Farmington Hills, MI, V. 1, No. 6, June, pp. 32-38.

VITA

James Michael Foreman Jr. was born in Thornton, Colorado on December 27, 1985 to Jim and Mary Jo Foreman. He and his younger brother, Michael, were each raised in Las Vegas, Nevada. In May 2004, James graduated from the Applied Math, Science, and Technology program at Clark High School. He went on to study civil engineering at Colorado State University from 2004 to 2008. He graduated with a Bachelor of Science in 2008. Following an interest to specialize in structural engineering, James attended The University of Texas at Austin from 2008 to 2010, and graduated with a Master of Science in Engineering on May 21, 2010.

Permanent Address: 3605 Steck Avenue, Apt. 1011
Austin TX, 78759

This thesis was typed by the author